

https://dspace.org/

A thermo-responsive scleral device for the management of ocular tumours

Abdalla, Yosra Mahjoub Ahmed

2024
University of the Witwatersrand, Johannesburg
https://hdl.handle.net/10539/43509
Abdalla, Yosra Mahjoub Ahmed . (2024). A thermo-responsive scleral device for the management of ocular tumours [PhD thesis, University of the Witwatersrand, Johannesburg]. WireDSpace. https://hdl.handle.net/10539/43509

Downloaded from a DSpace repository. https://dspace.org/

A THERMO-RESPONSIVE SCLERAL DEVICE FOR THE MANAGEMENT OF OCULAR TUMOURS

Yosra Mahjoub Ahmed Abdalla

A thesis submitted to the Faculty of Health Science, University of the Witwatersrand, in fulfilment of the requirements for the degree of Doctor of Philosophy



Supervisors

Prof. Yahya E Choonara, Prof. Lisa C. du Toit, Prof. Pierre P.D. Kondiah

Wits Advanced Drug Delivery Platform Research Unit, Department of Pharmacy and Pharmacology, School of Therapeutic Science, Faculty of Health Science, University of the Witwatersrand, South Africa

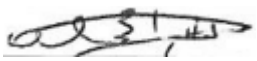
Dr. Naseer Ally

Department of Neurosciences, Division of Ophthalmology, Faculty of Health Science University of the Witwatersrand, South Africa

February 2024

DECLARATION

I, Yosra Mahjoub Ahmed Abdalla, declare that this thesis is my own, unaided work. It is being submitted for the degree of Doctor of Philosophy in the Faculty of Health Science at the University of the Witwatersrand, Johannesburg, South Africa. It has not been submitted before for any degree or examination at any other University.



17th day of February 2024 in Johannesburg, Gauteng, South Africa

RESEARCH OUTPUTS

Research presentations:

1. Yosra Mahjoub Abdalla, Lisa C. du Toit, Pierre P.D Kondiah, Naseer Ally and Yahya E Choonara. Development of an injectable thermo-responsive PEG-PCL-PEG hydrogel for ocular drug delivery. Wits Faculty of Health Sciences Biennial research day, 15th of September 2022. (**Appendix D**)

Publication articles and potential journals for submission:

1. Yosra Mahjoub Abdalla, Lisa C. du Toit, Philemon Ubanako, Pierre P.D. Kondiah, and Yahya E Choonara. A pH-responsive poly beta-amino ester nanoparticulate thermo-responsive PEG-PCL-PEG hydrogel for the delivery of interferon alpha to the ocular surface. Targeted journal; Polymers.
2. Yosra Mahjoub Abdalla, Lisa C. du Toit, Philemon Ubanako, Pierre P.D. Kondiah, Naseer Ally Yahya E Choonara. Ocular pharmacokinetics of IFN-α2b from a single subconjunctival administration of IFN-α2b nanoparticles-loaded thermo-responsive hydrogel. Targeted journal; Pharmaceutics.

ABSTRACT

Several ocular diseases that lead to blindness could benefit from effective treatment delivery to the site of action. Efficacy, however, remains restricted due to the multiple static and dynamic barriers present in the eye, despite substantial study into administration procedures and delivery vehicle. Ocular tumours are a broad group of diseases that range from benign to malignant and that occur in different anatomical regions within the eye. Ocular surface tumours are tumours of the conjunctiva of the eye and are therefore readily accessible for drug delivery. The management of ocular tumours is faced with the challenge of developing a suitable treatment strategy that meets individual patient needs, considering their anatomical location. Foremost is the need to develop strategies with high benefit to risk ratios. This is closely followed by the need to develop therapies that improve patient compliance while limiting the need for frequent hospital visits. Thirdly, the high cost of immune-therapeutic agents currently used for the management such as interferon demands sustained release strategies that deliver the same efficacy from much lower doses. Interferon alpha has been used to treat patients with ocular tumours for decades; however, its short half-life and poor tolerability necessitate frequent administration. This novel study employed a pH responsive/protective nanoparticle embedded into a thermo-responsive hydrogel for site-specific IFN-α2b delivery in the treatment of ocular tumours. Loading the IFN-α2b in a hydrogel isolates the drug from the releasing medium; the inclusion of core-shell nanoparticles increases the loading capacity of the drug and provided pH-responsiveness to the acidic tumour microenvironment, protecting the entrapped drug. As a result, the concentration gradient is reduced and the release pathway extended, furthermore, shielding the IFN-α2b against rapid clearance, and degradation at lower pH of the tumour microenvironment. Nano-embedded thermo-responsive hydrogel were prepared and their physiochemical properties, thermo-responsive behaviour, pH-responsiveness*, in vitro* and *in vivo* release and toxicity were evaluated. Fourier transform infrared (FTIR), 1H–nuclear magnetic resonance (1H-NMR), and X-ray powder diffraction (XRPD) analysis confirmed the synthesis of the copolymer. The rheological analysis revealed a sol-gel transition temperature in the range of 26-45°C which was concentration–dependent. A concentration of 20% w/v was selected based on suitability for *in vivo* application. The surface morphology of the hydrogel was evaluated using scanning electron microscopy (SEM) and porositometric analyser, the SEM images revealed the presence of a mesh-like structure on the surface of the hydrogel. The presence of the pores was further confirm by porositometric analysis. The presence of pores is critical for the diffusion of liquid within the hydrogel, which allows the NP to diffuse out of the hydrogel and release the loaded drug. The formed nanoparticles had particle sizes ranging from 137.1 to 230.6 nm (PDI 0.27–0.137) and zeta potentials ranging from -23.9 to -3.36 mV, demonstrating a pH-responsive controlled

release in an acidic medium simulating the tumour environment, with an entrapment efficiency of 89%. The in vitro release studies demonstrated a two-phase release pattern of IFN-α2b and stability of the released IFN-α2b from IFN-α2b nano-embedded PECE hydrogel (IFNPH) for the duration of the study; thus, the IFNPH exhibits pH-protective and temperature-responsive properties. In vitro biocompatibility findings on the human retinal pigment epithelial cell line highlighted that the IFNPH is safe within the tested range of 5000 to 0.625 µg/mL and does not pose any adverse cytotoxic effects. The in vivo studies were performed by administering a single subconjunctival injection of the IFNPH to New Zealand albino rabbits. The pharmacokinetic data revealed that the Cmax of 129.7 pg/mL was reached after 24 hrs (Tmax) in the vitreous humour. The IFNPH delivered biological active IFN-α2b in a sustained manner, compared to eye drops and subconjunctival injection of IFN-α2b solution, thus limiting dosing frequency and enhancing patient compliance. This investigation highlights that the IFNPH is a potential suitable candidate for ocular delivery of IFN-α2b.

ACKNOWLEDGEMENTS

Praise be to Allah for the many wonderful and blessed grants that make life enjoyable. Praise be to Allah until praise runs out.

I am grateful that Allah has blessed me with my wonderful family. My heartfelt appreciation goes to my father, Mr. Mahjoub A. Sharfy, and my mother, Mrs. Mariam Osman, for their endless support. My siblings, Mohammed, Mazin, and Enas I wouldn't have done it without you.

My sincere appreciation goes to my supervisors Prof. Y.E. Choonara; Prof. L.C. Du Toit; Prof. Pierre P.D. Kondiah; and Dr. N Ally, for their supervision and assistance during my study. This endeavour would not have been possible without your insightful guidance.

My appreciation goes to Ms Tshegofatso Makoba and Dr. Onynye Uwaezuoke for their selfless acts of kindness toward me and my family. May Allah bless and protect you and your families.

Words cannot express my gratitude to my friends and colleges whom all become family, Mrs Ranya Mukhtar, Mr. Ahmed Bakhet, Mrs. Amani Algid, Mr. Magdy Alzubair, Ms. Aysha Suliman, Mr. Leon Koza, Dr. Alex Adekiya, Dr. Hillary Mndlovu and Ms. Alexis Schwuls. I will always remember your kindness, generosity and endless support.

I would like to extend my sincere thanks to members of wits advance drug delivery platform (WADDP) Mr. Kleinbooi Mohlabi, Ms. Busi Nompumelelo, Mr. Bafana Tema, Mrs. Tshidi Mosete, Dr. Philemon Ubanako and Dr. S Adeyemi, for their assistance and patience during our research.

DEDICATION

I dedicate this work to my beautiful daughters Alaa and Razan; I am grateful for having both by my side throughout my journey.

TABLE OF CONTENTS

DECLARATION ii
RESEARCH OUTPUTS iii
ABSTRACT iv
ACKNOWLEDGEMENTS vi
DEDICATION vii
TABLE OF CONTENTS viii
LIST OF TABLES xii
LIST OF FIGURES xiii
LIST OF EQUATIONS xvi
LIST OF ABBREVIATIONS xvii
Chapter one 1
Introduction and overview of the study 1
1.1. Introduction 1
1.2. Rationale and motivation 3
1.3. Aim and bjectives 5
1.4. Novelty of the study 6
1.5. Overview of the thesis 7
1.6. References 8
Chapter Two 11
Advancing the treatment of ocular tumours through smart nanocarriers 11
2.1. Introduction 11
2.2. Barriers to ocular delivery and routes of delivery in ocular tumours 12
2.3. Ocular toxicity of chemotherapeutic agents 15
2.4. Nanotechnologies for potential application in the management of ocular tumours 18
2.4.1. Passive targeting 20
2.4.2. Active targeting 21
2.4.3. Liposomes 22
2.4.4. Lipid Nanoparticles 23
2.4.5. Polymer-based nanoparticles 24
2.4.6. Dendrimers 25
2.5. Potential targets in ocular tumours for active targeting 26
2.5.1. Transferrin as potential molecule target for nano-carrier systems 27

2.5.2. Hyaluronan (HA), Hyaluronate receptor (CD44), and HA-CD44 interaction as possible targets for nano-carrier systems 27
2.6. Stimuli–Responsive Approach 28
2.6.1. pH–Responsive Drug Delivery 28
2.6.2. Temperature-Responsive Drug Delivery 29
2.6.3. Enzyme- responsive drug delivery 30
2.6.4. ROS- responsive drug delivery 31
2.7. Future recommendations and conclusion 32
2.8. References 33
Chapter Three 48
A pH-responsive poly beta-amino ester nanoparticulate thermo-responsive PEG-PCL-PEG hydrogel for the delivery of interferon alpha to the ocular surface 48
3.1. Introduction 48
3.2. Materials and methods 50
3.2.1. Materials 50
3.2.2. Methods 51
3.2.2.1. Synthesis and purification of PEG-PCL-PEG triblock copolymer 51
3.2.2.2. Synthesis of poly (beta-amino ester) copolymer 51
3.2.2.3. Preparation of nanoparticles via the solvent evaporation method 52
3.2.2.4. Preparation of the PECE hydrogel and NP loaded /PECE hydrogel 53
3.2.2.5. Fourier transform infrared spectroscopy (FTIR) 53
3.2.2.6. ^{1}H-Nuclear Magnetic Resonance analysis 53
3.2.2.7. X-ray powder diffraction (XRPD) analysis 53
3.2.2.8. Differential scanning calorimetry (DSC) 53
3.2.2.9. Thermogravimetric (TGA) analysis 54
3.2.2.10. Particle size distribution, polydispersity index (PDI), and zeta potential analysis 54
3.2.2.11. Evaluation of drug entrapment efficiency of IFN-α2b loaded nanoparticles 54
3.2.2.12. Morphological analysis 55
Transmission electron microscopy 55

Scanning electron microscopy (SEM) 55
3.2.2.13. Porositometric and surface topography analysis 55
3.2.2.14. Rheological characterisation of the hydrogels 55
3.2.2.15. Syringeability of the hydrogels 56
3.2.2.16. *In vitro* release analysis of IFN-α2b from IFNPs and IFNPH 56
3.2.2.17. Degradation analysis of formulations 57
3.2.2.18. *In vitro* cytotoxicity analysis 57
3.2.2.19. Assessment of bioactivity of the released IFNα-2b from IFNPH 58
3.2.2.20. Statistical analysis 58
3.3. Results 59
3.3.1. Assessment of the structural modification and integrity 59
3.3.2. Evaluation of the thermal behaviour of the hydrogels 61
3.3.3. Particle size and distribution, zeta potential and entrapment efficiency of the nanoparticles 64
3.3.4. Assessment of surface morphology of the hydrogels 66
3.3.5. Assessment of the porosity profile of the hydrogels and NP-loaded hydrogels 67
3.3.6. Assessment of rheological properties of the hydrogels 69
3.3.7. Assessment of the syringeability of the hydrogels 71
3.3.8. *In vitro* release analysis of IFN-α2b from IFNPs and IFNPH 72
3.3.9. Degradation analysis of the formulations 75
3.3.10. Biocompatibility evaluation of the formulations 75
3.3.11. Assessment of the stability of the released IFN-α2b from the IFNPH 77
3.4. Discussion 78
3.5. Conclusions 81
3.6. References 82
Chapter Four 88
Ocular pharmacokinetics of IFN-α2b from a single subconjunctival administration of IFN-α2b nanoparticles-loaded thermo-responsive hydrogel 88
4.1. Introduction 88

4.2. Materials and Methods 90
4.2.1. Materials 90
4.2.2. Methods 90
4.2.2.1. Preparation of the IFNα nano-embedded PECE hydrogels 90
4.2.2.2. Transcorneal permeability of IFNPH 91
4.2.2.3. Cellular uptake and internalization 92
4.2.2.4. Animal experiments 92
4.2.2.5. Pharmacokinetics studies 93
4.2.2.6. *In vivo* toxicity and histopathological examination 93
4.3. Results 94
4.3.1. Transcorneal permeability of IFNPH across rabbit cornea 94
4.3.2. Assessment of the cellular uptake of the IFNPs 96
4.3.3. *In vivo* toxicity analysis 97
4.3.4. Histopathological analysis 98
4.3.5. Intraocular pharmacokinetics 99
4.4. Discussion 101
4.5. Conclusion 104
4.6. References 105
Chapter Five 112
Conclusions, recommendations, and future prospects 112
5.1. Conclusions 112
5.2. Recommendation and future perspective 113
Appendix A 115
Appendix B 116
Appendix C 117
Appendix D 118
Appendix E 119
Appendix F 120
Appendix G 121

LIST OF TABLES

Table 2.1 Indication of local chemotherapeutic agents, route of application and ocular surface toxicity. 17
Table 2.2 Examples of nanotechnology applied for the management of ocular tumours. 20

Table 3.1 Particle size, PDI and zeta potential of unloaded and loaded nanoparticles and drug entrapment efficacy of loaded nanoparticles. 64
Table 3.2 Effect of pH of the medium on the size, PDI and zeta potential of the drug free NPs. 65
Table 3.3 Porositometric analysis of lyophilised PECE hydrogels and nanoparticulate-loaded PECE hydrogels. 68

Table 4.1 Pharmacokinetic parameters of IFN-α2b (0.6 μg per rabbit eye) following subconjunctival injection of IFNPH. 100

LIST OF FIGURES

Figure 1.1 Standard signalling pathway of IFN 4
Figure 1.2 Flowchart of experimental procedures for the design and evaluation of the thermo-responsive nano-embedded hydrogel system: 1) synthesis of the PBAE polymer and the preparation of IFNα-2b loaded nanoparticles IFNPs; 2) synthesis of the PECE copolymer and preparation of the PECE hydrogel; and 3) the preparation of the IFNPH through loading of the IFNPs into the PECE hydrogels. 6

Figure 2.1 Schematic illustration of the eye and physiological barriers to ocular delivery (Image obtained with permission from Huang et al., 2018). 15
Figure 2.2 Schematic illustration of various nanocarriers and their targeting capabilities. The symbols adjacent to the nanocarriers in each layer of the eye represent the nanocarriers' capacity to target or permeate following topical application (Gorantla *et al.*, 2020). 19
Figure 2.3 Graphic illustration of passive and active drug targeting strategies (Image obtained with permission from (Navya *et al.*, 2019). 21
Figure 2.4 5-FU levels in the aqueous humour and vitreous humour after instillation of a solution, PLA nanoparticles (PLA NPS), and chitosan-coated PLA nanoparticles (CH-PLA NPS) (Image obtained and adapted with permission from (Nagarwal *et al.*, 2012). 25
Figure 2.5 In-vitro levels of 5-FU in the aqueous humour following administration of the MNS, PLA nanoparticles and 5-FU solution (Image obtained with permission from (Nagarwal *et al.*, 2011). 30

Figure 3.1 Synthetic scheme of PEG-PCL-PEG triblock copolymer. 51
Figure 3.2 Synthetic scheme of PBAE copolymer. 52
Figure 3.3 A) FTIR of PECE; B) H-NMR of PECE. 60
Figure 3.4 A) FTIR of PECE, PECE-1 and PECE-2; B) XRPD images of PECE, PECE-1 and PECE-2. 61
Figure 3.5 DSC thermograms of the PECE copolymer, PECE-1 and PECE-2. 63
Figure 3.6 TGA thermograms of PECE, PECE-1 and PECE-2. 63

Figure 3.7 TEM images of PBAE nanoparticles. The scale bar for (a) and (b) is 100 nm, for (c) 500 nm and for (d) 2 µm of the drug free NPs. 65
Figure 3.8 SEM images of PECE-1 (a) and (b) at 10 µm, PECE-2 (c) and (d) at 20 µm. 66
Figure 3.9 Photographic images of the sol-gel transition of hydrogels at room and body temperature (a) solution of PECE-1, (b) gel of PECE-1 and (c) solution of PECE-2, (d) gel of PECE-2. 70
Figure 3.10 a) Temperature ramp of PECE-1 and PECE- 2; (b) Temperature ramp of PECE hydrogel at different concentrations (15%, 20%, 25% and 30% $^{w}/_{v}$); (c) Stress sweep of PECE-1 and PECE-2 at 25°C; (d) Viscosity of PECE-1 and PECE-2 and (e) Viscosity of PECE hydrogel. 71
Figure 3.11 Required force to inject PECE hydrogel at different concentration from 1 mL syringes equipped with 27 G needle, PECE-1 (25% $^{w}/_{v}$ hydrogel), PECE-2 (25% $^{w}/_{v}$ NP-loaded hydrogel), PECE-3 (20% $^{w}/_{v}$ hydrogel) and PECE-4 (20% $^{w}/_{v}$ NP-loaded hydrogel). 72
Figure 3.12 *In vitro* release profiles of immunoenzymatically detected IFN-α2b from IFNP at 37°C at different pH values. 74
Figure 3.13 *In vitro* release profiles of immunoenzymatically detected IFN-α2b from IFNPH at 37°C at different pH values. 74
Figure 3.14. Biodegradation behaviour of the NPH in PBS solution (pH 6.6 and 7.4) at 37°C. The error bars were small, indicating that the data obtained did not differ among themselves the standard deviation ranged is (0-4.62×10^{-15}). 75
Figure 3.15. MTT assay measurement of viability of HRPE cells following 24 and 48 hrs treatment with A) PECE hydrogel, B) PBAE-NP, C) IFN-α2b, and D) IFNPH at different concentrations (Data represents n = 3, mean ± SD). ** Indicates p<0.01, *** indicates p<0.001, and (ns) indicates no significant difference when compared to negative control. 5% $^{v}/_{v}$ DMSO and culture medium were used as positive and negative controls, respectively, indicated by the patterned columns. 77
Figure 3.16. *In vitro* antiproliferative activity on A172 cells of IFN-α2b released from the IFNPH formulation at different pH values. 5% $^{v}/_{v}$ DMSO and culture medium were used as positive control and as negative control, respectively (Data represent n = 3, mean ± SD). * Indicates p<0.05, ** indicates p<0.01, *** indicates p<0.001 when compared to negative control. NS indicates no significant difference when compared to standard IFN-α2b. 78

Figure 4.1 Schematic illustration of IFNPH formulation process from IFN- α2b loaded NPs and PECE precursor solution. 91
Figure 4.2 The barriers encountered by drug carriers following topical application onto the ocular surface..... 95
Figure 4.3 Corneal permeability of the IFNPH across the rabbit's cornea. 96
Figure 4.4 Fluorescence microscope images of cellular uptake of NP (control) and FITC-loaded NP at (10X magnification)..... 97
Figure 4.5 IFNPH formation in vivo following subconjunctival injection in a rabbit eye model: (a) at 0 days and (b) at 14 days post application. 98
Figure 4.6 Histopathological sections of eyes following subconjunctival application. Control; untreated eyes, Group I; termination after one day, Group II; termination after 3 days, Group III; termination after 7days, and Group IV; termination after 14 days.99
Figure 4.7 The intraocular pharmacokinetic profile of IFN-α2b following subconjunctival application of IFNPH in rabbits (n =5, mean± SD). 101

LIST OF EQUATIONS

Equation 3.1 percentage encapsulation efficiency 54
Equation 3.2 percentage degradation 57
Equation 3.3 percentage cell viability 58

LIST OF ABBREVIATIONS

APNPs	Activatable protein nanoparticles
3AP	3-Amino-1-propanol
ANOVA	Analysis of variance
AREC	Animal Research Ethics Committee
ATF	Artificial tear fluid
BJH	Barrett, Joyner and Halenda model
BDDA	1,4-Butanediol diacrylate
BRB	Blood-retinal barrier
BSA	Bovine serum albumin
BCRP	Breast cancer resistance protein
BET	Brunauer–Emmett–Teller
G5 PAMAM	Conjugated 5 polyamidoamine
CGC	Critical gelling concentration
$CDCl_3$	Deuterated chloroform
DSC	Differential scanning calorimetry
DOX	Doxorubicin
DMEM F12	Dulbecco's modified Eagle medium mixture with Ham's F12
DLS	Dynamic light scattering
TPGS	D-α-tocopheryl polyethylene glycol 1000 succinate
EE	Encapsulation efficiency
EPR	Enhanced permeation and retention
ELISA	Enzyme-linked immunosorbent assay kit
ECM	Extracellular matrix
Ɛ-CL	Ɛ-caprolactone
FBS	Fetal bovine serum albumin
FITC	Fluorescein isothiocyanate
5-FU	5- Fluorouracil
FTIR	Fourier transform infrared
HMDI	1,6-hexamethylene diisocyanate
^{1}H-NMR	^{1}H-nuclear magnetic resonance
HaCaT	Human immortalized keratinocytes
HRPE	Human retinal pigment epithelial cells
HA	Hyaluronan
H_2O_2	Hydrogen peroxide
•OH	Hydroxyl radical
IFN-α2b	Interferon-alpha2b
IFNPs	Interferon-alpha2b loaded PBAE-NPs
IFNPH	Interferon-alpha2b nano-embedded PECE hydrogel
IFN-β	Interferon beta
LNPs	Lipid nanoparticles

(G")	Loss modulus
LCST	Lower critical solution temperature
MMPs	Matrix metalloproteinase
Mel	Melittin
MTX	Methotrexate
MMC	Mitomycin C
MNS	Modified nano *in-situ* gel
MRP	Multidrug resistance protein
MTT	3-(4, 5-dimethylthiazol-2-yl)-2,5-diphenyl tetrazolium bromide
NPs	Nanoparticles
NPH	Nano-embedded PECE hydrogel
NLC	Nanostructured lipid carrier
NZWA	New-Zealand White Albino rabbits
OSSN	Ocular surface squamous neoplasia
PECE	Poly (ethylene glycol)-poly (caprolactone)-poly (ethylene glycol)
PEG-PCL-PEG	Poly (ethylene glycol)-poly (caprolactone)-poly (ethylene glycol)
PECE-1	25% w/v PECE hydrogel
PECE-2	NPs-embedded into 25% $^{w}/_{v}$ PECE hydrogel
PECE-3	30% w/v PECE hydrogel
PECE-4	NPs-embedded into 30% $^{w}/_{v}$ PECE hydrogel
PEGIFN-α2b	Pegylated interferon- alpha2b
P-gp	P-glycoprotein
PBS	Phosphate buffer saline
PBAE	Poly (beta-amino ester)
PBAE-NPs	Poly (beta-amino ester) nanoparticles
PLGA	Poly (D, L-lactide-co-glycolic acid)
PEG	Poly (ethelyene glycol)
PLA	Poly (lactide)
PCL	Poly (caprolactone)
mPEG	Poly(ethylene glycol) methyl ether
mPEGA	Poly(ethylene glycol) methyl ether acrylate
PAMAM	Polyamidoamine
PDI	Polydispersity index
ROS	Reactive oxygen species
RES	Reticuloendothelial system
RPE	Retinal pigment epithelium
RP	Rhodamine phalloidin
SEM	Scanning electron microscopy
($^{1}O_2$)	Singlet oxygen
SLN	Solid lipid nanoparticles
SD	Standard deviation
$Sn(Oct)_2$	Stannous octoate
(G')	Storage modulus
($O_2^{\bullet -}$)	Superoxide

(Cmax)	The maximum concentration
TGA	Thermogravimetric analysis
(W_{NPs} + W_{PECE})	Total mass of the solid component
(Tf)	Transferrin
(TfRs)	Transferrin receptors
TEM	Transmission Electron Microscopy
UCST	Upper critical solution temperature
W_{NPs}	Mass ratio of the NPs
W_{PECE}	Mass ratio of the PECE hydrogel
XRPD	X-ray powder diffraction

Chapter one

Introduction and overview of the study

1.1. Introduction

Tumours of the ocular surface include a wide array of slowly progressive epithelial lesions of the conjunctiva and/or cornea ranging from benign to pre-malignant and malignant (Alkatan and Alzahem, 2018). Corneal and conjunctival intraepithelial neoplasia, as well as conjunctival squamous cell carcinoma, are the most prevalent non-pigmented ocular surface cancers (Sayed-Ahmed *et al.*, 2017). Patients may be asymptomatic or exhibit symptoms such as pain, redness, and vision loss, especially with more advanced disease. Signs include a solitary or diffuse mass on the bulbar conjunctiva, which can occasionally become inflamed. Solitary lesions may appear fleshy, viscous, or papillomatous, and may have a plaque-like appearance (Gichuhi and Irlam, 2007). Tumours may have feeder vessels or appear avascular. There are no pathognomonic clinical signs that correlate well with histological diagnosis. Most tend to develop within the interpalpebral fissure, predominantly at the limbus, although any part of the conjunctiva or cornea may be involved (Alkatan and Alzahem, 2018). Ocular surface squamous neoplasia (OSSN) is usually uncommon in moderate climates, often detected in old males and is a slow growing tumour. In Africa, OSSN is more frequently and destructive affecting young people, in particular women. This is attributed to the concurrence of the human papillomavirus, human immunodeficiency virus and ultraviolet radiation from the sun. In Africa, reports from South Africa, Zimbabwe, Uganda, Nigeria and Malawi indicate that most patients were HIV-positive. Ophthalmologists regard OSSN in young Africans as an indicator of human immunodeficiency virus infection (Gichuhi *et al.*, 2013). Meanwhile, reports from Australia and Britain were of mature males above 60 years (Gichuhi and Irlam, 2007). Studies within Africa clearly indicated that the epidemiology of ocular surface tumours is distorted.

Treatment strategies vary but usually involve excision with 2–4 mm margins with or without intra-operative or postoperative radiotherapy, cryotherapy, chemotherapy (Gichuhi *et al.*, 2016). Extensive surgical excision may result in corneal epithelial stem cell deficits, scarring, and conjunctival adhesion. Complete histological excision is

associated with recurrence in 43% of the case frequently within two years of treatment (Gichuhi and Irlam, 2007). Chemotherapeutic agents used include: Mitomycin C is an alkylating agent applied as first line of treatment in non-invasive tumours (Hirst, 2007), preoperatively, intra-operatively, or postoperatively depending on the tumour size (Gupta and Muecke, 2010). 5-fluorouracil is an analogue of thymine, applied as the first line of therapy or as an adjunct to surgery (Midena *et al.*, 2000; Parrozzani *et al.*, 2017). Additionally, immunotherapy using interferon-alpha2b (IFN-α2b) which is a natural glycoprotein secreted in the body secondary to tumours or viral infections, is applied as subconjunctival/perilesional injection or as topical drops (Galor *et al.*, 2010; Karp *et al.*, 2001).

The unique intrinsic barriers of the eye, such as the cornea barrier, tear film barrier, enzyme degradation, the blood-aqueous barrier and the retinal barrier hinders the delivery of sufficient quantities of ocular medication (Lynch *et al.*, 2020). Topically applied drugs, such as eye drops, are cleared out of the eye shortly after application due to the clearing out by tears. On average, only 2–7% of the drug reaches the intraocular tissue due to the brief contact between the drug and the ocular surface and the low diffusion rate (Diebold and Calonge, 2010). Ophthalmic in-situ gels are stimuli-responsive formulations that are a glutinous liquid at room temperature and transform into a gel when exposed to an increase in temperature, in this case the physiological temperature of the eye (Makwana *et al.*, 2016). The bioavailability of the administered drug is enhanced due to an increase in the mucoadhesive properties which extends the ocular surface contact time of the drug (Geethalakshmia *et al.*, 2013).

Nanoparticles are drug delivery systems with a size range between 10 to 1000nm used for delivery of drugs and bioactive agents. They increase the availability of ophthalmic therapeutics by extending ocular retention time (Meng *et al.*, 2019). Nevertheless, nanoparticles are rapidly cleared out of the eyes, due to their lack of mucoadhesive property (Gupta *et al.*, 2010). The inclusion of nanoparticles in an *in-situ* gel may overcome this shortcoming as the gel would act as a mucoadhesive matrix, while the nanocarriers would enhance the drug loading capacity of the in-situ gel. Hence, nanocarriers delivered within an *in situ* gel could have a synergistic effect in the delivery of the drug (Pitorre *et al.*, 2017).

Several studies have demonstrated the application of nanoparticles in the delivery of IFN-α, but none for ocular delivery. PEGylated interferon (PEGIFN)-α2b has been investigated as an approach in the management of ocular tumours (Karp *et al.*, 2010b). PEGylation, is the covalent binding of a drug or protein to polyethylene glycol, to reduce the clearance, extend the half-life and overall improve the bioavailability (Turecek *et al.*, 2016). However, PEGylation causes steric hindrance and reduces the specific activity of PEG-IFN as compared to native IFN (Caliceti, 2004). The current study discusses the design and assessment of an ocular delivery system based on the concept of an injectable thermo-responsive *in situ* gelling system containing IFN-α2b encapsulated within nanoparticles. This system is proposed to overcome the challenges of available delivery systems, enhance the bioavailability of IFN-α2b, and provide sustained/controlled release in an acidic microenvironment.

1.2. Rationale and motivation

Interferons are natural cytokines with antiviral, antiproliferative, antitumor, and immunomodulatory activities and have been used in the management of several types of cancer. Type 1 IFN standard signalling consists of the activation of the Janus kinases (JAK-STAT) pathway, as shown in **Figure 1.1**. The IFNs binds to the heterodimeric receptors with high affinity to IFN receptor2 (IFNAR2) followed by the low affinity IFN receptor1 (IFNAR1) dimerization is then induced. The Janus kinases (JAKs) are activated and phosphorylates the signal transducers and activators of transcriptions (STATs). The IFNAR1 binds to tyrosine kinase 2 (TYK2) and IFNAR2 binds to JAK1 during the activation. The binding activates the phosphorylation of STAT1 and STAT2 binds them to interferon regulatory factor 9 (IRF9). They form a heterotrimeric transcriptional complex named IFN-stimulated gene factor 3 (ISGF3). The activated ISGF3 binds to IFN-stimulated response elements (ISREs) and regulates the transcription of IFN-stimulated genes (ISGs) to trigger IFN responses (Lazear *et al.*, 2019). Intralesional injections of IFN-α2b has been used as a first line of therapy for extensive tumours (Kim *et al.*, 2012; Shields *et al.*, 2013). Notable benefits were recorded for this treatment, as there is a significant reduction of tumour size, especially in immune-suppressed patients with OSSN, and its prolonged use prevents tumour recurrence through immunomodulation (Kim *et al.*, 2012). However, despite the effectiveness of IFNα-2b, their instability due to their complex structure, immunogenicity, susceptibility to enzymatic degradation, and short half-life, restricts

its application (Nie *et al.*, 2021). Furthermore, the drug dosages employed in the management of ocular tumours are high and can lead to toxicity and persistent flu-like symptoms in patients (Karp *et al.*, 2010a). Thus, a method that would be non-invasive, reduce drug concentration, increase bioavailability to the tumour, release the drug in a controlled and sustainable manner and assist with patient compliance would be an improved approach for the management of the ocular malignancies. The proposed design of a system would be responsiveness to the tumour microenvironment, thereby shielding the IFN-α2b from the cursive acidic tumour microenvironment while providing controlled release of effective drug levels.

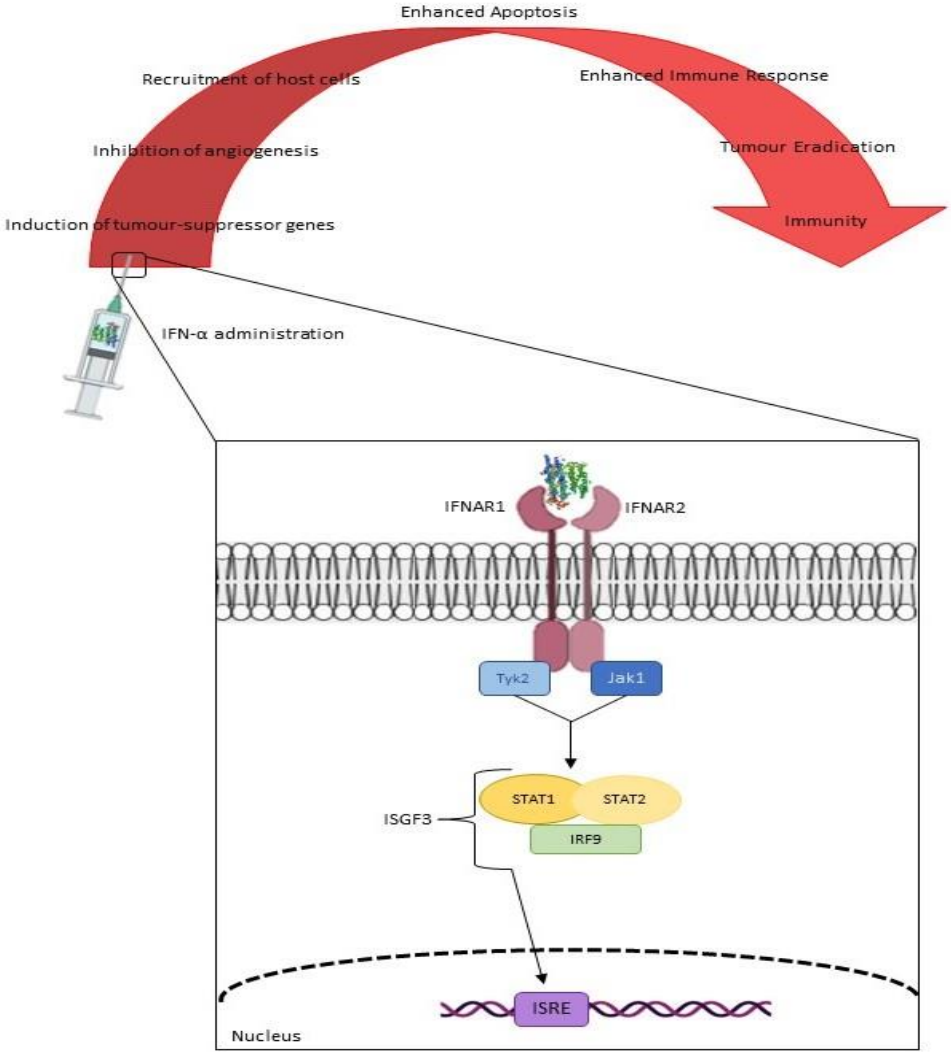


Figure 1.1 Standard signalling pathway of IFN

1.3. Aim and bjectives

The aim of the study was to design an injectable thermo-responsive nano-enabled gel formulation for the delivery of IFN-α2b for the enhanced management of ocular tumours. This aim was proposed to be attained through the following objectives:

1. Development of a novel IFN-α2b loaded into poly(beta-aminoester) nanoparticles (PBAE-NPs) embedded in a thermo-responsive and pH-protective poly(ethylene glycol)-poly(caprolactone)-poly(ethylene glycol) (PECE) hydrogel (IFN-α2b nano-embedded PECE hydrogel) (IFNPH) for enhancing the stability and therapeutic efficacy of IFN-α2b.
2. Determination of the physiochemical (FTIR, ^{1}H-NMR, XRPD, DSC, DLS, TEM, SEM, and porosity analysis) and physiomechanical (rheology, and syringability) properties of the IFNPH to ensure optimal properties for ocular delivery.
3. Evaluation of the *in vitro* release profile of IFN-α2b from IFNPs and IFNPH, and *ex vivo* permeation of IFN-α2b across the corneas of New Zealand white albino rabbits (NZWA).
4. Investigation of the *in vitro* cytotoxicity of the IFNPH as compared to the native IFN-α2b in primary Human retinal pigment epithelial cell line (HRPE).
5. Evaluation of the *in vivo* toxicity, histopathological analysis of the IFNPH in NZWA rabbits, following injection into the subconjunctival space around the sclera, to assess the safety and efficacy of the formulation.

Figure 1.2 provides a schematic summary of the formulation and characterisation of the thermo-responsive nano-embedded hydrogel system.

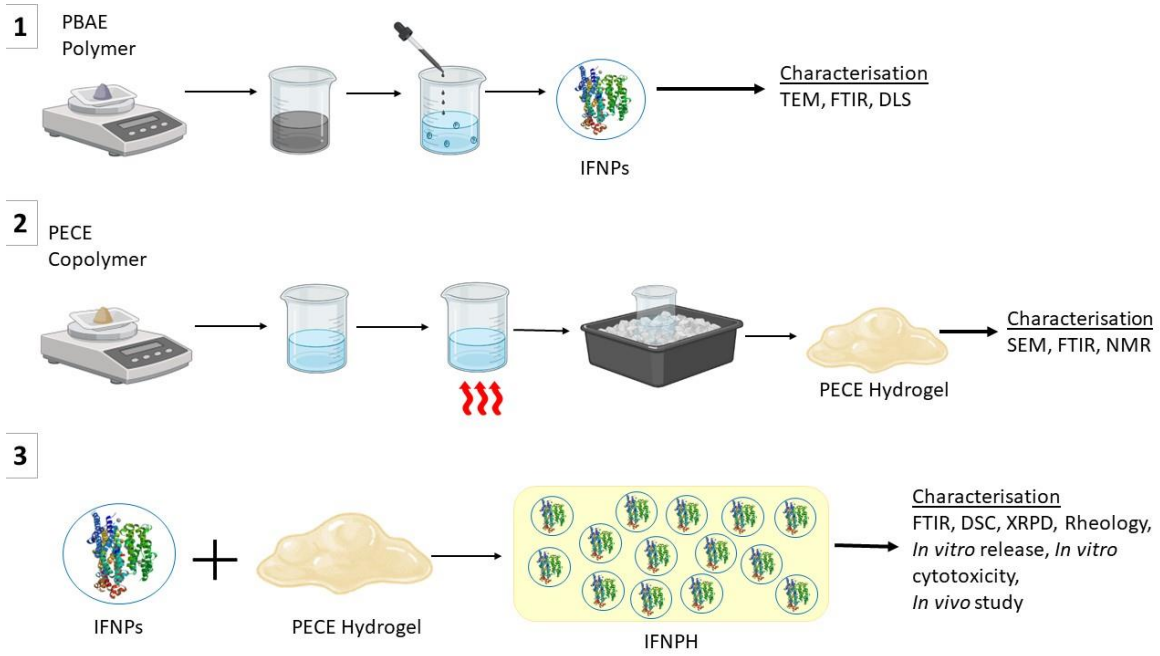


Figure 1.2 Flowchart of experimental procedures for the design and evaluation of the thermo-responsive nano-embedded hydrogel system: 1) synthesis of the PBAE polymer and the preparation of IFNα-2b loaded nanoparticles IFNPs; 2) synthesis of the PECE copolymer and preparation of the PECE hydrogel; and 3) the preparation of the IFNPH through loading of the IFNPs into the PECE hydrogels.

1.4. Novelty of the study

A novel drug delivery system containing IFNα-2b loaded into poly(beta-aminoester) nanoparticles embedded into poly(ethylene glycol)- poly(caprolactone)-poly(ethelyene glycol) (PECE) hydrogel would be developed. This system was proposed to serve as a site-specific drug delivery system to the conjunctiva via a subconjunctival injection for controlled and sustained drug release into the tumorigenic tissue. This system is purportedly an advancement for the treatment of ocular surface tumours, and upon application it is proposed to provide a notable enhancement in the delivery of IFN-α2b compared to conventional intralesional injections and topical administration of IFN-α2b, by providing controlled, site-specific release, with the potential for reduced dosing frequency.

1.5. Overview of the thesis

Chapter 1: In this chapter, the overview and context of the current study were introduced. The rationale and motivation for the study were provided, and the aims and objectives for undertaking the study were detailed. Further, the novelty of this study was presented.

Chapter 2: This chapter provides an overview of ocular tumours, and the current available management strategies. It also provides insight into ophthalmic routes of delivery, and more so the use of nano- delivery systems that can be employed for potential advancement in managing of ocular diseases. Furthermore, the chapter provides an insight on the use of tumour hallmarks as an approaches to achieve site-specific and responsive therapy, and highlights the potential targets found on ocular tumours, for effective specific interaction with receptors for more efficacious therapy.

Chapter 3: In this chapter, the chemical synthesis of the PECE copolymer and poly (beta amino ester) copolymer for IFN-α2b delivery in the treatment of ocular tumours was presented. The nano-embedded/PECE hydrogel was prepared and their physiochemical properties using Fourier transform infrared (FTIR), thermal behaviour, X-ray powder diffraction (XRPD), scanning electron microscopy (SEM), and transmission electron microscopy (TEM) analysis, porosity analysis and temperature-transition behaviour. *In vitro* toxicity, drug entrapment efficiency, drug release were also evaluated.

Chapter 4: This chapter presents the development and evaluation of the long term stability of the IFN-α2b nano-embedded PECE hydrogel (IFNPH). The IFNPH was designed to extend the release profile and overcome the challenges of rapid clearance and sensitivity of interferon to degradation, investigate its toxicity, and improve the immunotherapy efficacy of IFN-α2b. The aim was pursued using a subconjunctival injection of the fabricated IFNPH delivery system for site-specific delivery to the sclera. The long term release and stability of the IFNα-2b was evaluated via an enzyme-linked immunosorbent assay kit (ELISA).

Chapter 5: The IFNPH delivery system developed fulfilled the aims and objectives of this study. The physiochemical parameters, *in vitro* and *in vivo* evaluations of the developed system produced favourable results. In this chapter, the concluding

remarks of the thesis were provided, as well as the recommendations and future perspectives.

1.6. References

1. Alkatan, H. & Alzahem, T. 2018. Histopathology of the Ocular Surface. *Histopathology-An Update.* IntechOpen, 67,2018.
2. Caliceti, P. 2004. Pharmacokinetics of pegylated interferons: what is misleading? *Digestive and Liver Disease,* 36**,** S334-S339.
3. Diebold, Y. & Calonge, M. 2010. Applications of nanoparticles in ophthalmology. *Progress in Retinal and Eye Research,* 29**,** 596-609.
4. Galor, A., Karp, C. L., Chhabra, S., Barnes, S. & Alfonso, E. C. 2010. Topical interferon alpha 2b eye-drops for treatment of ocular surface squamous neoplasia: a dose comparison study. *British journal of ophthalmology,* 94**,** 551-554.
5. Geethalakshmia, A., Karkib, R., Sagib, P. & Jhac, S. K. 2013. Temperature triggered in situ gelling system for betaxolol in glaucoma. *Journal of applied pharmaceutical science,* 3**,** 153-159.
6. Gichuhi, S. & Irlam, J. H. 2007. Interventions for squamous cell carcinoma of the conjunctiva in HIV-infected individuals. *Cochrane Database of Systematic Reviews*.
7. Gichuhi, S., Macharia, E., Kabiru, J., Zindamoyen, A. M. b., Rono, H., Ollando, E., Wachira, J., Munene, R., Maina, J. & Onyuma, T. 2016. Topical fluorouracil after surgery for ocular surface squamous neoplasia in Kenya: a randomised, double-blind, placebo-controlled trial. *The Lancet Global Health,* 4**,** e378-e385.
8. Gichuhi, S., Sagoo, M. S., Weiss, H. A. & Burton, M. J. 2013. Epidemiology of ocular surface squamous neoplasia in A frica. *Tropical medicine & international health,* 18**,** 1424-1443.
9. Gupta, A. & Muecke, J. 2010. Treatment of ocular surface squamous neoplasia with Mitomycin C. *British Journal of Ophthalmology,* 94**,** 555-558.
10. Gupta, H., Aqil, M., Khar, R. K., Ali, A., Bhatnagar, A. & Mittal, G. 2010. Sparfloxacin-loaded PLGA nanoparticles for sustained ocular drug delivery. *Nanomedicine: nanotechnology, biology and medicine,* 6**,** 324-333.
11. Hirst, L. W. 2007. Randomized controlled trial of topical mitomycin C for ocular surface squamous neoplasia: early resolution. *Ophthalmology,* 114**,** 976-982.

12. Karp, C. L., Galor, A., Chhabra, S., Barnes, S. D. & Alfonso, E. C. 2010a. Subconjunctival/perilesional recombinant interferon α2b for ocular surface squamous neoplasia: a 10-year review. *Ophthalmology,* 117**,** 2241-2246.
13. Karp, C. L., Galor, A., Lee, Y. & Yoo, S. H. 2010b. Pegylated interferon alpha 2b for treatment of ocular surface squamous neoplasia: a pilot study. *Ocular immunology and inflammation,* 18**,** 254-260.
14. Karp, C. L., Moore, J. K. & Rosa Jr, R. H. 2001. Treatment of conjunctival and corneal intraepithelial neoplasia with topical interferon α-2b. *Ophthalmology,* 108**,** 1093-1098.
15. Kim, H. J., Shields, C. L., Shah, S. U., Kaliki, S. & Lally, S. E. 2012. Giant ocular surface squamous neoplasia managed with interferon alpha-2b as immunotherapy or immunoreduction. *Ophthalmology,* 119**,** 938-944.
16. Lazear, H. M., Schoggins, J. W. & Diamond, M. S. 2019. Shared and distinct functions of type I and type III interferons. *Immunity,* 50**,** 907-923.
17. Lynch, C. R., Kondiah, P. P., Choonara, Y. E., Du Toit, L. C., Ally, N. & Pillay, V. 2020. Hydrogel biomaterials for application in ocular drug delivery. *Frontiers in Bioengineering and Biotechnology,* 8**,** 228.
18. Makwana, S., Patel, V. & Parmar, S. 2016. Development and characterization of in-situ gel for ophthalmic formulation containing ciprofloxacin hydrochloride. *Results in pharma sciences,* 6**,** 1-6.
19. Meng, T., Kulkarni, V., Simmers, R., Brar, V. & Xu, Q. 2019. Therapeutic implications of nanomedicine for ocular drug delivery. *Drug discovery today,* 24**,** 1524-1538.
20. Midena, E., Degli Angeli, C., Valenti, M., De Belvis, V. & Boccato, P. 2000. Treatment of conjunctival squamous cell carcinoma with topical 5-fluorouracil. *British Journal of Ophthalmology,* 84**,** 268-272.
21. Nie, T., Wang, W., Liu, X., Wang, Y., Li, K., Song, X., Zhang, J., Yu, L. & He, Z. 2021. Sustained Release Systems for Delivery of Therapeutic Peptide/Protein. *Biomacromolecules,* 22**,** 2299-2324.
22. Parrozzani, R., Frizziero, L., Trainiti, S., Testi, I., Miglionico, G., Pilotto, E., Blandamura, S., Fassina, A. & Midena, E. 2017. Topical 1% 5-fluoruracil as a sole treatment of corneoconjunctival ocular surface squamous neoplasia: long-term study. *British Journal of Ophthalmology,* 101**,** 1094-1099.

23. Pitorre, M., Gondé, H., Haury, C., Messous, M., Poilane, J., Boudaud, D., Kanber, E., Ndombina, G. A. R., Benoit, J.-P. & Bastiat, G. 2017. Recent advances in nanocarrier-loaded gels: Which drug delivery technologies against which diseases? *Journal of Controlled Release,* 266**,** 140-155.
24. Sayed-Ahmed, I. O., Palioura, S., Galor, A. & Karp, C. L. 2017. Diagnosis and medical management of ocular surface squamous neoplasia. *Expert review of ophthalmology,* 12**,** 11-19.
25. Shields, C. L., Kaliki, S., Kim, H. J., Al-Dahmash, S., Shah, S. U., Lally, S. E. & Shields, J. A. 2013. Interferon for ocular surface squamous neoplasia in 81 cases: outcomes based on the American Joint Committee on Cancer classification. *Cornea,* 32**,** 248-256.
26. Turecek, P. L., Bossard, M. J., Schoetens, F. & Ivens, I. A. 2016. PEGylation of biopharmaceuticals: a review of chemistry and nonclinical safety information of approved drugs. *Journal of pharmaceutical sciences,* 105**,** 460-475.

Chapter Two

Advancing the treatment of ocular tumours through smart nanocarriers

2.1. Introduction

The eye is a complex organ composed of multiple structures; working in concert to enable vision. The impairment in any part of the eye can lead to serious complications and eventual vision loss. Ocular tumours are one such impairment that are unique and considered a threat to both vision and eventually life if left untreated. The tumours can develop primarily from ocular tissues or affect ocular structures as a result of metastatic propagation from cancer elsewhere in the body (Williams and Di Nicola, 2021). The most common ocular tumours of the anterior and posterior segment, include basal cell carcinoma of the eyelid, ocular surface squamous neoplasia, retinoblastoma, choroidal melanoma, ocular adnexal lymphoma and metastatic orbital tumours (Maheshwari and Finger, 2018; Moon *et al.*, 2021; Williams and Di Nicola, 2021). The strategies used for management of ocular tumours include surgery excision, chemotherapy (topical, subconjunctival, intravenous and intravitreal) and radiation (Chiu-Tsao *et al.*, 2012; Fung *et al.*, 2003; Pe'er, 2015; Shields *et al.*, 2013). Failure in treatment might have catastrophic consequences, where preservation of life may necessitate removal of the entire orbital contents (exenteration) as the last resort.

The high recurrence rate associated with surgical excision underscores the need for improved treatment strategies. A shift to the application of chemotherapeutic agents as an adjuvant to surgery or as monotherapy has been reported in the last decade amongst ophthalmologists (Adler *et al.*, 2013; Moon *et al.*, 2021). Most chemotherapy agents are cytotoxic and are not targeted or specific to the cancer site; hence, they are hazardous to healthy tissues. The limited retention time of chemotherapeutics in the tumour causes damage to normal tissue and lowers therapeutic efficacy (Moon *et al.*, 2021). Generally, delivery of therapeutics to the eye, specifically the ocular surface, is challenged by the anatomical and physiological barriers of the eye. These ocular barriers protect the eyes from invasion by foreign substances, namely the static and dynamic barriers, and efflux pump in ocular tissue. The diffusion and permeability of therapeutics (that are also detected as foreign by the eye) to the ocular tissue are therefore hindered, resulting in reduced bioavailability (Huang *et al.*, 2018). The static barriers include the cornea, sclera and the retinal pigment epithelia (including the

blood-aqueous barrier and the blood retinal barrier). The lymphatic flow in the choroid and conjunctiva blood flow represents the dynamic barriers (Gaudana *et al.*, 2010; Patel *et al.*, 2013b). Efflux pumps or transporters expressed on plasma membrane of ocular tissues are another barrier to drug perfusion to ocular tissues. Prominent efflux transporters identified on ocular tissues are P-glycoprotein (P-gp), multidrug resistance protein (MRP), and breast cancer resistance protein (BCRP). They lower the permeability to the dugs by effluxing the drug molecules out of the cytoplasm and cell membrane resulting in limited drug bioavailability (Gaudana *et al.*, 2010; Patel *et al.*, 2013a).

The management of ocular tumours is further faced with the challenge of developing a suitable treatment strategy that meets individual patient needs. Foremost is the requirement to develop strategies with high benefit-to-risk ratios. This is closely followed by the goal to develop therapies that improve patient compliance while limiting the need for frequent hospital visits. The high cost of immunotherapeutic agents currently used for the management of tumours, such as interferons, demands sustained release strategies that deliver the same efficacy from much lower doses. Thus, this review chapter explored the current routes of delivery and their shortcomings; and further investigated most recent nano-technological advancements that may resolve or minimize these shortcomings.

2.2. Barriers to ocular delivery and routes of delivery in ocular tumours

Following application to the ocular surface the precorneal barrier that naturally protects the cornea and conjunctiva represents the first obstacle faced by topical applications. The rapid turnover rate of tears, reflex blinking and nasolacrimal drainage result in rapid removal of the applied drugs (Lynch *et al.*, 2020; Weng *et al.*, 2017). The cornea is the second anatomical barrier with different layers bound by intracellular tight junctions. These layers of cornea are the epithelium, the Bowman’s layer, the Descemet's membrane, the stroma, and the endothelium (DelMonte and Kim, 2011). The corneal epithelium is hydrophobic and the presence of the tight junction restricts the permeability of hydrophilic drugs to the aqueous humour. The stroma on the other hand, is a hydrophilic layer limiting the penetration of hydrophobic drugs. The endothelium is the innermost layer of the cornea and is permeable, hence permitting the movement of macromolecules between the stroma and aqueous humour

(Imperiale *et al.*, 2018). The third barrier is the conjunctiva, it shields the anterior surface of the sclera and the inner eyelid lining (Nishida *et al.*, 2011). The conjunctiva is a thin transparent vascularized mucus membrane, containing nerves, lymphatic and blood vessels, an outer epithelium and underlying stroma. The conjunctiva has a larger surface area and wide epithelial intracellular spacing when compared to the cornea, hence drug permeability though it is higher (Huang *et al.*, 2018). However, the conjunctival capillary and lymphatic vessels results in the drainage of topical applications to systemic circulation minimizing the absorption of the therapeutics (Huang *et al.*, 2018).

The ocular barriers in the posterior segment of the eye are the sclera, choroidal, retinal pigment epithelial and blood-retinal barrier. The sclera connects the anterior and posterior segments of the eye, has a large and permeable surface area as well as a high degree of hydration, making it accessible to hydrophilic molecules. Because of these characteristics, transscleral administration is a promising approach for intraocular macromolecule delivery (Uwaezuoke *et al.*, 2022). The choroid is a highly vascular barrier, which supplies blood to the retina and impedes delivery through the transscleral pathway (Tsai *et al.*, 2018). The retina is a transparent tissue that is considered a significant barrier to the diffusion of large macromolecules (Jackson *et al.*, 2003). Choriocapillaries and retinal pigment epithelium (RPE) together generate Bruch's membrane. Changes in the choroid and Bruch's membrane thickness with age affect drug transport from the sclera into the inner ocular tissues. Furthermore, highly hydrophobic drugs may be drained through the choroidal systemic circulation (Cholkar *et al.*, 2012). The blood-retinal barrier (BRB), is composed of an inner BRB composed of retinal capillary endothelial cells and outer BRB composed of RPE. The BRB act as barrier for diffusion between systemic circulation and the retina. The BRB is a tight monolayer that limits diffusion of therapeutic molecules (Gote *et al.*, 2019). **Figure 2.1** is a schematic illustration of ocular barriers in both the anterior and posterior segments.

Topical applications to the ocular surface through conventional formulations such as solutions, suspensions and ointments, comprise up to 90% of the marketed ocular formulations (Bachu *et al.*, 2018; Jumelle *et al.*, 2020). Their attractiveness arises from their non-invasiveness, and ease of administration that often promotes patient compliance. Nevertheless, topical applications comes with several limitations such as

reduced therapeutic level of the drug at the site of action, and the propensity to elicit systemic effects due to the naso-lacrimal drainage and these manages to limit the amount of drug that reaches the target site to about 5% (Diebold and Calonge, 2010). The value of topically applied chemotherapeutic agents in the management of multifocal, recurring lesions and microscopic subclinical disease is due to fact that topical agents provide coverage to the whole ocular surface (Venkateswaran *et al.*, 2019). For systemic administration, the blood-ocular barriers, which include the blood-retinal and blood-aqueous barriers, limit drug molecule penetration to the posterior segment of the eye. The choroidal capillaries provide ocular delivery via the systemic route, mainly by oral or intravenous methods (Kim and Woo, 2021). The systemic route has limitations, including the necessity for a high dose to achieve therapeutic efficacy due to limited permeability across the blood-ocular barrier and systemic metabolism. Furthermore, non-site-specific exposure may result in systemic toxicity and adverse outcomes (Shastri *et al.*, 2023; Tian *et al.*, 2022).

Subconjunctival injections are considered relatively easy to administer with the need for only topical anaesthesia. The drug is administered into the subconjunctival space around the sclera, crossing through the sclera to the anterior chamber, escaping the cornea and blood aqueous barriers (Janagam *et al.*, 2017). The route provides site specific targeting of the drug in a non-invasive manner to overcome blood-ocular barriers and enhanced bioavailability (Chaw *et al.*, 2021). In a study evaluated the subconjunctival route for the delivery of dexamethasone, the route proved its efficiency in delivering the drug to both ocular segments (Weijtens *et al.*, 1999). The intravitreal route delivers the drug directly to the posterior segment of the eye by injecting it into the vitreous cavity, bypassing various ocular barriers (Shastri *et al.*, 2023). However, intravitreal injection is an invasive operation that might result in retinal detachment, vitreous haemorrhage, and cataracts, among other complications (Sampat and Garg, 2010).

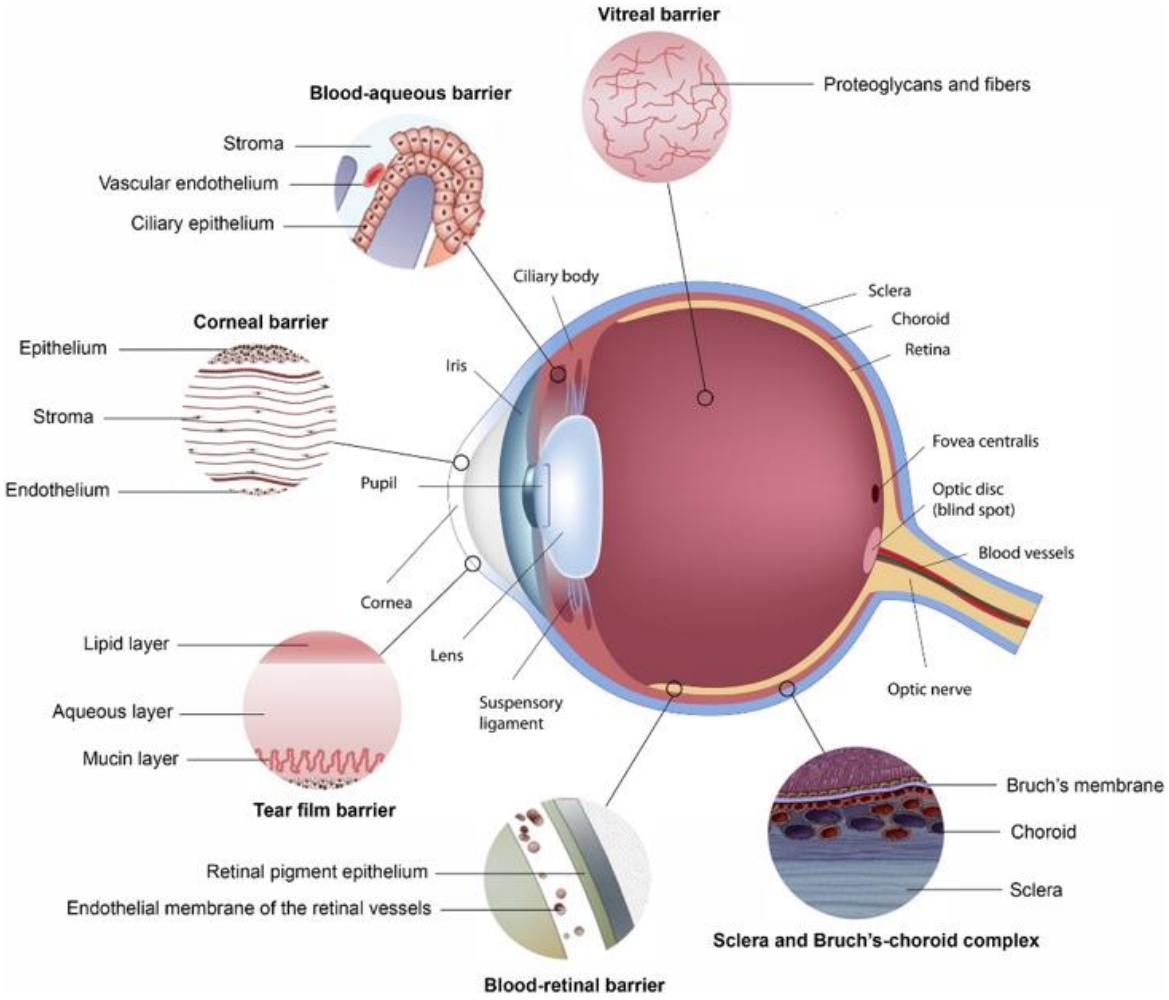


Figure 2.1 Schematic illustration of the eye and physiological barriers to ocular delivery (Image obtained with permission from Huang et al., 2018).

2.3. Ocular toxicity of chemotherapeutic agents

Table 2.1 provides the indications of local chemotherapy, the route of administration, and the ocular surface complications caused by exemplary anticancer agents used in ocular cancers. The physiological differentiating features of cancer cells that cause them to proliferate more than normal cells are used as targets by chemotherapeutic agents. The majority of chemotherapeutic drugs break down DNA, resulting in cell cycle arrest and/or apoptosis (Alimbetov *et al.*, 2018). Antimetabolite agents, such as 5- Fluorouracil (5-FU) and Methotrexate (MTX) exert their anticancer effect through the blockage of fundamental cellar processes through the inhibition of DNA synthesis. Due to their inherited antimetabolite activity, they block the proliferation of rapidly dividing cancer cells. They also affect the proliferation of normal cells that display the same feature, such as corneal and limbal epithelium on the ocular surface, causing

corneal epitheliopathy (Alimbetov *et al.*, 2018). The alkylating agent Mitomycin C (MMC) has anticancer properties that are due to the inhibition of cell proliferation and DNA replication (Greer *et al.*, 2018). However, there is a danger of ocular damage from topical MMC treatment because it is thought to suppress proliferation and induce apoptosis in normal cells (e.g., corneal epithelium and endothelium cells, retinal epithelial cells) (Kang *et al.*, 2001; Mladenov *et al.*, 2007; Netto *et al.*, 2006). Immunotherapeutic drugs, such as imiquimod and IFN-α2b exert anticancer action by activating the immune system. As a result, immunocompromised patients with OSSN are unlikely to respond to topical IFN-α2b treatment; other non-immune-modifying agents may be more successful. (Ashkenazy, 2017). One of the reasons for inflammatory effects such as conjunctivitis, keratitis, and blepharitis is due to activated immune cells and an elevated level of inflammatory cytokines on the ocular surface following local chemotherapy (Moon *et al.*, 2021).

Several strategies have been implemented to reduce the ocular toxicity of chemotherapeutic agent. One strategy is through the adjustment of the dosing regimen; for example, MMC is applied as a 0.02%–0.04% eye drop four times daily for one week for 1–5 cycles with treatment-free intervals to reduce the toxic effects of MMC on healthy ocular tissue (Gupta and Muecke, 2010; Kusumesh *et al.*, 2017). A second strategy involves the use of punctual plugs after topical administration of MMC to increase retention time on the ocular surface, allowing for improved drug delivery to the targeted tissue while decreasing systemic absorption by the nasal mucosa (Sepulveda *et al.*, 2010). They have been shown to minimise the punctual stenosis caused by MMC application (Nanji *et al.*, 2013). For IFN-α2b eye drops the toxicities resolved after cessation of treatment (Kunkler *et al.*, 2019), while subconjunctival injections are generally well tolerated, they are associated with transient systemic flu-like symptoms, which can be easily treated with an oral antipyretic such as acetaminophen (Antonietta Blasi *et al.*, 2018; Kaliki *et al.*, 2016; Kim *et al.*, 2012). Similarly, 5-FU symptoms normally subside once treatment ceases; topical corticosteroids can be used to minimise side effects (Schmid *et al.*, 2006). Another strategy is the use of nanocarrier for delivery of chemotherapeutic agent. Nanocarriers offer several advantages compared to conventional chemotherapeutic agents namely, the nanoscale size offers high surface area, the enhance permeability and retention effect in tumour cells allows selective delivery and accumulation of the drug in the

tumour site (Cryer and Thorley, 2019). Furthermore, the possibility of surface modification of nanocarriers with either hydrophilic polymers (such as poly ethylene glycol) to prolongs circulation time or the use of ligands for active targeting of tumour cells reduces non-targeted toxicity, and thus enhances tolerance to local chemotherapy (ud Din *et al.*, 2017).

Table 2.1 Indication of local chemotherapeutic agents, route of application and ocular surface toxicity.

Indication	Chemotherapeutic (mechanism of action)	Application	Shortcoming	Reference
OSSN	Mitomycin C (DNA crosslinking)	Topical	Punctual stenosis, discomfort, hyperemia, chemosis, keratopathy.	(Antonietta Blasi *et al.*, 2018; Kusumesh *et al.*, 2017)
OSSN	5- Fluorouracil (DNA alkylating agent)	Topical	Hyperemia, blepharitis keratopathy, pain, epiphora.	(Gichuhi *et al.*, 2016; Venkateswaran *et al.*, 2019)
OSSN	IFN-α2b (Immunotherapeutic agent)	Topical	Pain, epiphora, blurred vision, hyperemia.	(Kaliki *et al.*, 2019; Venkateswaran *et al.*, 2019)
OSSN	IFN-α2b	Subconjunctival	Flu-like symptoms.	(Kaliki *et al.*, 2019; Nanji *et al.*, 2014)
BCC	Imiquimod (Immunotherapeutic agent)	Topical	Conjunctivitis, keratitis foreign body sensation, discomfort, irritation.	(Garcia-Martin *et al.*, 2011; Macedo *et al.*, 2015)
VRL	Methotrexate (folate antimetabolite)	Intravitreal	Keratopathy.	(Kvopka *et al.*, 2020; Vishnevskia-Dai *et al.*, 2020)

OSSN: ocular surface squamous neoplasia, BCC: basal cell carcinoma, RB: retinoblastoma, VRL: vitreoretinal lymphoma.

2.4. Nanotechnologies for potential application in the management of ocular tumours

Nanomedicine defines the employment of nanotechnology in the delivery of medicines or therapeutics for the prevention, treatment, or imaging. Nano-based drug delivery systems offer several attractive features namely, enhanced drug solubility and stability, reduced toxicity, enhanced bioavailability, and ultimately enhance therapeutic efficacy (Meng *et al.*, 2019; Parhi *et al.*, 2012). Furthermore, they protect the contained drug cargo from degradation, while improving site specific targeting through the manipulation of size, payload, shape and surface topographies (Longmire *et al.*, 2011; Ogier *et al.*, 2009). For instance, size and surface charge of nanoparticles (NPs) play a key role in their penetration through ocular barriers. To avoid the foreign body sensation of topically applied NPs the size of the drug loaded NPs should be less than 10 µm (Imperiale *et al.*, 2018). The cornea and conjunctiva are negatively charged, topical applied cationic NPs will penetrate the ocular surface effectively due to the electrical attraction allowing a longer residence time of the NPs loaded drug (Akhter *et al.*, 2016). Chaw *et al.* (2021) examined the effect of size and charge on the accumulation of liposomes in different ocular tissue following subconjunctival injection. Cationic liposomes with micro-size act as a depot at subconjunctival space/conjunctiva/sclera providing sustain release; whereas negatively charged, neutral and small liposomes (≤ 250 nm) were detected in the corneal periphery/limbus prior to their clearance (Chaw *et al.*, 2021). Ban *et al*. (2017) proved that lipid NPs modified with positively charged chitosan increased the bioavailability of dexamethasone, through enhancement of the retention and permeability into the cornea, compared to the unmodified lipid NPs (Ban *et al.*, 2017). Similarly, Tseng *et al*. (2013) demonstrated that positively charged gelatine NPs, of zeta potential about +33 mV and size around 180 nm, can be efficiently retained on the cornea for a prolonged time. The NPs showed wide distribution in rabbit corneal cryosection, compared to free-drug formulation (Tseng *et al.*, 2013). Additionally, molecules such as folate (Suen and Chau, 2014) and hyaluronic acid (De la Fuente *et al.*, 2008a) can be attached to the surface of the NPs for targeted delivery. Nanocarriers can therefore, be designed for target delivery of chemotherapeutics to the tumour, to achieve the required therapeutic efficacy at the tumour site and cause less adverse effect to the surrounding healthy tissues (Kanapathipillai *et al.*, 2014). Nanocarriers that are

commonly used in cancer treatment include carbon nanotubes, quantum dots, micelles, nanoparticles, dendrimers (Nikzamir *et al.*, 2021) and liposomes (Huang *et al.*, 2020; Jin *et al.*, 2020). **Figure 2.2** illustrates various nanocarriers available for ocular delivery and their targeting ability. Advancements in the field of nanomedicine present an opportunity to develop a nano-based delivery system to ensure the site-specific targeting of ocular tumours. **Table 2.2** summarises representative examples of nanotechnology employed in the treatment of ocular tumours and their benefits indicated.

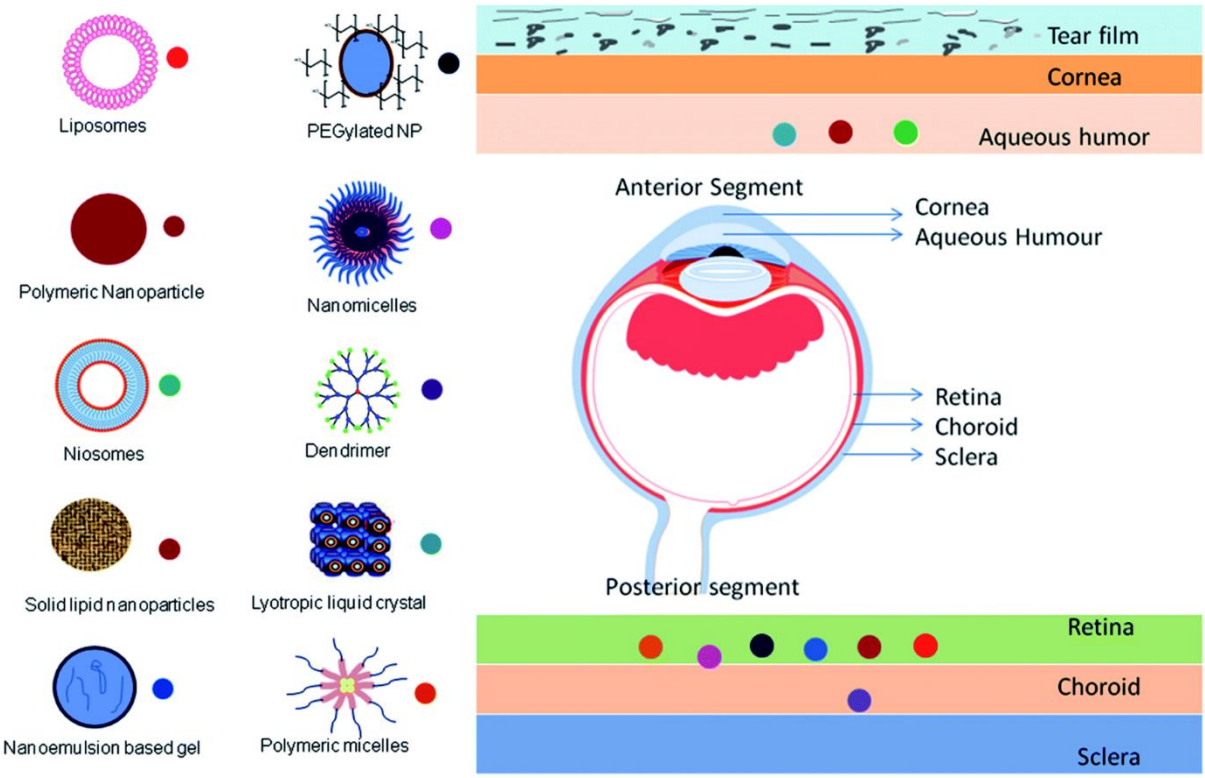


Figure 2.2 Schematic illustration of various nanocarriers and their targeting capabilities. The symbols adjacent to the nanocarriers in each layer of the eye represent the nanocarriers' capacity to target or permeate following topical application (Gorantla *et al.*, 2020).

Table 2.2 Examples of nanotechnology applied for the management of ocular tumours.

Formulation	Polymeric material	Payload	Target	Function	Reference
Nanoparticles	PLA	5-FU	OSSN	Increased corneal residence & drug bioavailability	(Nagarwal *et al.*, 2012)
Nanoparticle *in-situ* gel	PLA/MNS	5-FU	OSSN	Increased retention, sustain release & increased bioavailability	(Nagarwal *et al.*, 2011)
Dendrimer	PAMAM	Carboplatin	Retinoblastoma	Increased half-life & drug bioavailability reduced drug toxicity & tumour mas	(Kang *et al.*, 2009)
Dendrimer	Porphyrin-glycodendrimers	Concanavalin A	Intraocular tumours & retinoblastoma	Effective & enhanced targeting reduced toxicity	(Makky *et al.*, 2011)

OSSN: ocular surface squamous neoplasia.

2.4.1. Passive targeting

Tumours and inflamed areas possess vasculatures that are characterized by enhanced permeability and are leaky. This characteristic provides the means of passage and accumulation of nanocarriers through the tumour tissue and internalization under the influence of enhanced permeation effect (Siegler *et al.*, 2016). The enhanced permeability is further accompanied by the poor lymphatic drainage around the tissue leading to enhanced retention of nanocarriers in the tumour cells. The two phenomena are known collectively as the enhanced permeation and retention (EPR) effect (Platt and Szoka, 2008). The process is referred to as “passive targeting or accumulation’’ due to the lack of specific targeting ligand with the tumour cells (Bozzuto and Molinari, 2015). The size of the nanocarriers contributes to the internalization, whereby nanocarriers in the size range of 100-200nm will passively target the sites. Nanocarriers with certain cut-off size will allow for long-circulation of the carrier in blood circulation (Siegler *et al.*, 2016). Achieving long-circulation times using nanocarrier is attractive for attaining a high level of the drug in the blood for

extended durations. Furthermore, the nanocarrier can gradually accumulate at pathological tissue due to EPR effect or accumulate via a compromised filtration mechanism enhancing drug's delivery to the targeted area (Torchilin, 2007). However, as the size increases, the recognition and clearance by the reticuloendothelial system becomes easier (Bozzuto and Molinari, 2015).

2.4.2. Active targeting

Active targeting is the modification of a nanocarrier with specific ligands for targeting tumour site. The targeting ligands selectively binds to receptors overexpressed on cancer cells to improve the therapeutic index of chemotherapeutic agents. The active targeting will increase the selectivity of the agents to the cancer cells and reduce their distribution and toxicity to healthy tissues (Jose *et al.*, 2019). The nanocarriers are conjugated with different ligands, for example, peptides, aptamers, antibodies and folic acid (Tang *et al.*, 2022). **Figure 2.3** is an Illustration of passive and active targeting delivery techniques into tumour cells.

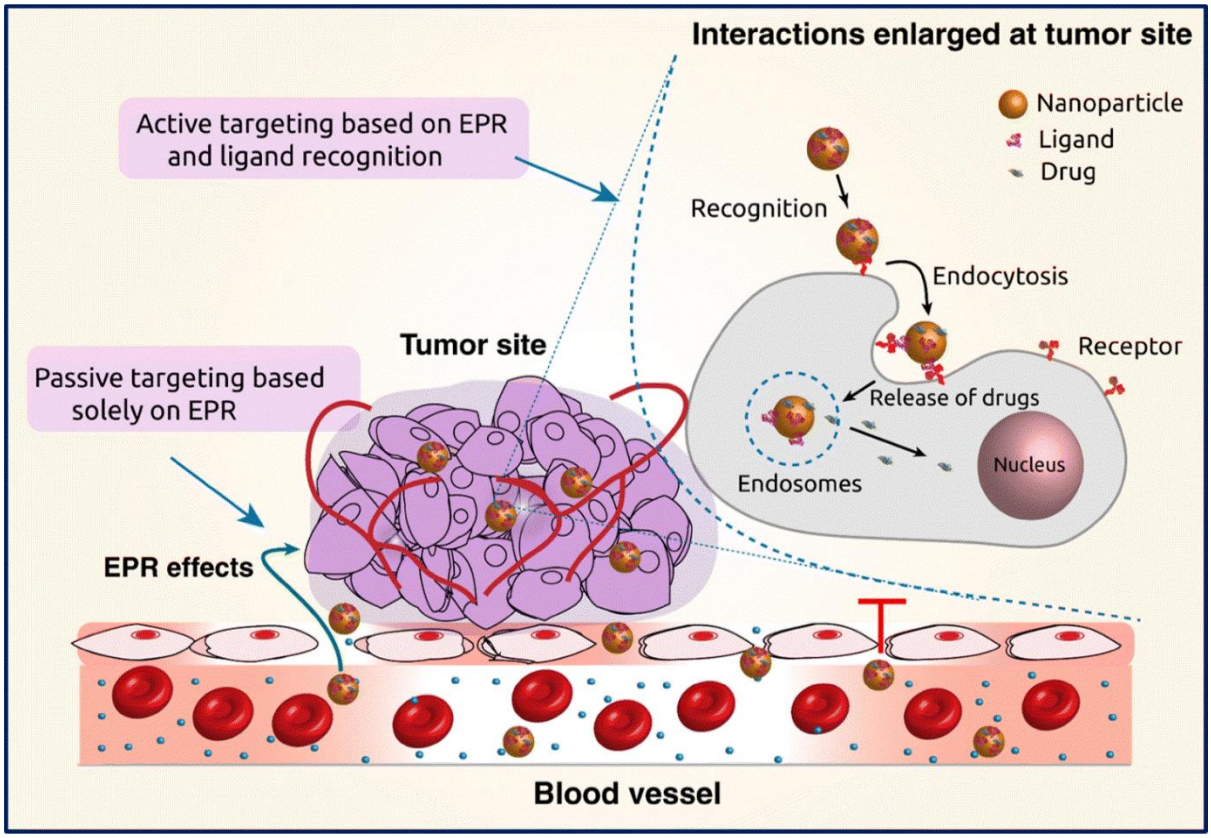


Figure 2.3 Graphic illustration of passive and active drug targeting strategies (Image obtained with permission from (Navya *et al.*, 2019).

2.4.3. Liposomes

Liposomes are vesicular lipid-based drug delivery systems with sizes that range from 10 nm to 1 µm, and contains an internal aqueous core surrounded by lipid bilayer. They have shown characteristics that renders them suitable for ocular drug delivery namely, biodegradability and biocompatibility, and ability to entrap both lipophilic and hydrophilic molecules. Additionally, liposomes enables the possibility of surface modification for targeted delivery (Campardelli *et al.*, 2018; Danaei *et al.*, 2018). Despite these laudable achievements, liposomes exhibit several limitations that include their low encapsulation efficiency and drug loading, fast drug release, instability of the final product, and sterilization difficulties (Hossen *et al.*, 2019; Zhang and Wang, 2009) Coating of liposomes with hydrophilic polymers such as polyethylene glycol reduced opsonization and recognition by the reticuloendothelial system. The use of antibodies and specific ligands on the surface of liposomes can be used for targeted delivery to cancer cell. They have been employed for delivery to the anterior and posterior segments of the eye. Wong *et al*. (2018) demonstrated that PEGylated liposomal of triamcinolone acetonide phosphate formulation (applied as a single subconjunctival injection) in comparison with steroidal eye drops prepared as suspensions (applied four times per day). The subconjunctival formulation sustained the anti-inflammatory response in the eye for at least one month. Additionally, suppression of initial inflammation as a result of rapid build-up of therapeutic level (Wong *et al.*, 2018). Likewise, Feghhi *et al*. (2020) prepared a ciprofloxacin loaded liposomal formulations with and without carbomer coating that were applied as eye drops (Feghhi *et al.*, 2020). The results demonstrated increased ciprofloxacin concentration in the aqueous humor and vitreous after both liposomal applications. The carbomer coating showed enhanced mucoadhesive properties and a higher drug concentration in the aqueous and vitreous homers especially six hrs after administration (Feghhi *et al.*, 2020). Liposomal formulations in ocular delivery have demonstrated their capacity to improve corneal retention and permeability, as well as overall therapeutic efficacy. Furthermore, there is no evidence of ocular tissue inflammation or toxicity.

To maximize the efficacy of liposomes for the delivery of chemotherapeutic in cancer treatment, various challenges and restrictions must be overcome. Biological barriers; liposome-related barriers (size, surface charge, morphology, payload design, and drug

release); immune system barriers (liposomes-immune system interaction) (Beltrán-Gracia *et al.*, 2019); tumour-related barriers (tumour interstitial fluid pressure); vascular-related barriers EPR effect; and preclinical study challenges all play a critical role in their in vivo performance (Moosavian *et al.*, 2021). In preclinical studies, an appropriate experimental model is crucial to establishing the efficacy of liposomal formulations. It is advised to choose a suitable animal model, or better yet, models. Despite the fact that mice models, subcutaneous models, and xenograft models have been used in the preclinical evaluation of liposomes, they overestimate the EPR effect in humans and are unable to effectively assess immune system reactions against cancer cells or liposomal formulations. Allograft models may be a better option for evaluating the efficacy of nanocarriers. These challenges have led to the failure of various liposomal formulations in clinical trials, despite promising preclinical results (Moosavian *et al.*, 2021).

2.4.4. Lipid Nanoparticles

Lipid nanoparticles (LNPs) are classified as solid lipid nanoparticles (SLN), nanostructured lipid carrier (NLC), lipid drug conjugate, and polymer-lipid hybrid nanoparticles. They are colloidal carriers in the submicron size range composed of lipid matrix in an aqueous phase which is stabilized by surfactants (Doktorovova *et al.*, 2016). These colloidal carriers offer several advantages such as stability in the reticuloendothelial system, sustained and/or controlled drug release, biocompatibility, biodegradability, low toxicity, high drug loading capacity, and efficient targeting (Ahmad *et al.*, 2019; Wang *et al.*, 2018). As ocular drug delivery systems they enhanced pre-corneal residence time due to their mucoadhesive properties, and increased bioavailability (Li *et al.*, 2014). Additionally, LNPs offer the possibility for large-scale production and the ease of sterilization by autoclaving (for heat stable payloads) (Khames *et al.*, 2019). In a recent study, Yavda *et al*. (2020) prepared Atorvastatin loaded SLNs that were applied as eye drops. The formulation showed higher levels of the drug in both the aqueous and vitreous humour. Evidence of intact fluorescein labelled SLN were detected in the intraocular tissue, possibly demonstrating improved permeability and delivery. The formulation demonstrated *in-vitro*, *ex vivo* and *in vivo* ocular safety, improved stability including photo stability, and higher corneal flux 2.5-fold greater than free Atorvastatin (Yadav *et al.*, 2020).

The quick elimination of SLN by the reticuloendothelial system (RES) is one of its limitations; another key concern during storage is the polymorphic transition of the crystal structure, which leads to drug removal and decreased loading efficiency. Furthermore, the transition generates a change in nanoparticle size and shape, which triggers SLN destabilization and nanocarrier aggregation. To address these issues, solid and liquid lipids have been used for the manufacture of NLCs in order to limit polymorphic transitions and improve loading efficiency (Bayón-Cordero *et al.*, 2019). In cancer chemotherapy, the EPR effect varies depending on tumour type and status. As a result, the use of active targeting in cancer therapy appears to be more prevalent than passive targeting.

2.4.5. Polymer-based nanoparticles

Polymeric nanoparticles are colloidal particles with sizes ranging from10-1000 nm. Drug can be loaded by attachment to matrix or dissolved within, encapsulated and entrapped giving rise to adaptable drug delivery systems namely, nanoparticles, nanospheres or nanocapsules (Nagarwal *et al.*, 2009). Many of the polymers used are biodegradable and biocompatible ranging from synthetic polymers such as poly (D, L-lactide-co-glycolic acid) PLGA, poly (lactide) (PLA) to natural polymers such as chitosan, alginate, and albumin (Tang *et al.*, 2016; Vaneev *et al.*, 2021). Polymeric nanoparticles when compared to other nanocarriers are more stable, with tuneable physiochemical properties, offering uniform particle size distribution, more controllable and sustained drug release profile, and with higher encapsulation efficiency. These unique features of polymeric nanoparticles make them highly desirable in cancer therapy (Hu *et al.*, 2010). Nagarwal *et al.* (2012*)* prepared 5-FU loaded in PLA nanoparticles for topical application. **Figure 2.4** displays the *in-vivo* release of 5-FU following application in an animal model (Nagarwal *et al.*, 2012). The release of 5-FU from the PLA nanoparticles and chitosan-coated PLA nanoparticles showed a higher aqueous humour levels when compared to the free drug solution. The findings demonstrated that the chitosan-coated nanoparticles maintained 5-FU release due to chitosan's mucoadhesion capabilities arising from the interaction of the positively charged chitosan and the negatively charged corneal surface. The formulation, according to the findings, could be used to treat carcinoma of conjunctival/ corneal squamous cells (Nagarwal *et al.*, 2012).

The primary concerns with polymeric nanoparticles are related to nanoecotoxicology, which refers to nanoparticle toxicity. First, the physiochemical properties of the nanoparticles must be assessed before, during, and after biological experiments. The second challenge is to provide an approach to test the toxicity of synthetic nanoparticles induced on humans and other organisms upon consumption of food, water, or air contaminated with nanomaterials. The third challenge is to select relevant organisms that can be used in experiments (Zielińska *et al.*, 2020).

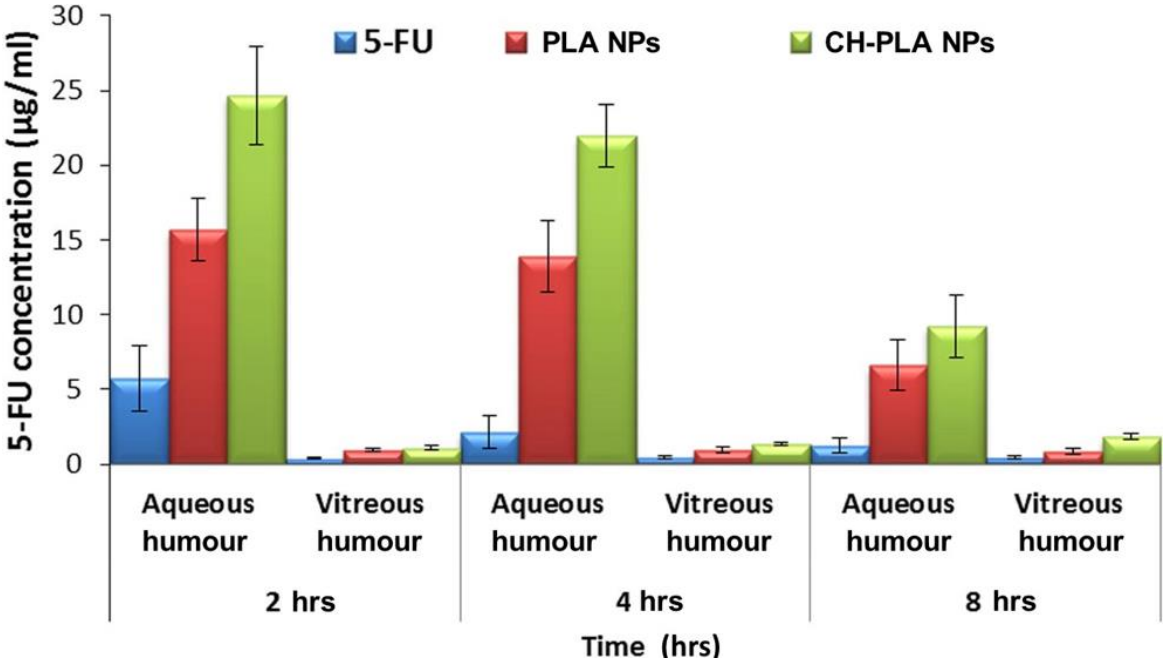


Figure 2.4 5-FU levels in the aqueous humour and vitreous humour after instillation of a solution, PLA nanoparticles (PLA NPS), and chitosan-coated PLA nanoparticles (CH-PLA NPS) (Image obtained and adapted with permission from (Nagarwal *et al.*, 2012).

2.4.6. Dendrimers

Dendrimers are monodispersed macromolecules with tree-like structures composed of three parts: the central core, the branching units, and functional groups situated at the surface of the dendritic structure (Kalomiraki *et al.*, 2016). Dendrimers, as drug delivery systems, offer unique characteristics due to their structure. They increase the solubility of hydrophobic drugs, provide targeted and sustained delivery to the retina, enhance corneal residence time, and act as effective as cornea adhesives following cornea surgeries (Yavuz *et al.*, 2013). Additionally, their amenability to chemical conjugation or physical entrapment of drugs increases dug stability, and reduces drug

toxicity (Huang and Wu, 2018). The dendrimer polyamidoamine (PAMAM) with -OH and -COOH terminal functional groups is the most commonly used in ocular drug delivery (Gote *et al.*, 2019; Rodríguez Villanueva *et al.*, 2016). PAMAM demonstrated enhance corneal permeability, extended the residence time, and overall enhanced the bioavailability of the dexamethasone (Souza *et al.*, 2015). Dendrimer nanoparticles have been reported to effectively deliver carboplatin in the management of murine transgenic retinoblastoma. A single subconjunctival injection decreased the tumour burden with no toxic effects (Kang *et al.*, 2009).

Dendrimers as drug delivery vehicles are challenged by safety concerns, and the mechanisms underlying their toxicity are unknown. The cytotoxicity and hemolytic toxicity of dendrimers are associated with their chemical composition, production, concentration, surface functionality, exposure period, cell type, and cell medium composition (Wu *et al.*, 2015). The highest toxicity have been proven to impart by cationic dendrimers (Chis *et al.*, 2020). Dendrimers are rapidly cleared by the reticuloendothelial system, hence lowering the uptake of chemotherapeutic agents. Chemical modification with linear polymers and surface modification techniques are utilised to reduce the toxicity associated with dendrimers and actively target cancer cells (Santos *et al.*, 2019). In a study Choi and co-workers prepared a conjugated 5 polyamidoamine (G5 PAMAM) dendrimers with fluorescein and folic acid creating clustered molecules by linking them together using complementary DNA oligonucleotides. The dendrimers were utilized to target cancer cells that over-express the high-affinity folate receptor. *In-vitro* studies showed that the DNA-linked clusters binds specifically to the human epidermoid carcinoma cell line that overexpresses folate receptors and might be applied for cancer imaging and therapeutics (Choi *et al.*, 2005).

2.5. Potential targets in ocular tumours for active targeting

The fabrication or modification of nanocarriers with specific ligands to target ocular tumour cells warrants further investigation, as various studies in the field of oncology have proven efficacy in adopting an active targeting method. Transferrin, folate, and peptide and protein receptors are all overexpressed in ocular malignancies.

2.5.1. Transferrin as potential molecule target for nano-carrier systems

The single chain glycoprotein, transferrin (Tf), is widely used as a ligand in targeting tumours expressing transferrin receptors. Transferrin receptors (TfRs) are overexpressed in cancer cell as opposed to normal cells, and their expression can be associated to the stage of tumour progression. The cellular uptake of Tf is receptor-mediated endocytosis rendering this a potential pathway for targeted delivery of therapeutic genes, anticancer agents, and protein delivery to cancer cells (Akhtar *et al.*, 2014). Several nanocarriers such as liposomes, nanoparticles (Kompella *et al.*, 2006), and dendrimers were used as transferrin conjugates and the end results showed enhancement in the drug targeting selectivity and reduced toxicity (Qian *et al.*, 2002). Asasutjarit *et al*. (2020) designed a transferrin (Tf)-conjugated liposomes loaded with ganciclovir for targeted delivery to the retina (Asasutjarit *et al.*, 2020). The retinal epithelial cells express transferrin receptors, and coupling transferrin to liposomes increased Tf receptor-mediated endocytosis of ganciclovir-loaded liposomes. The optimized Tf conjugated liposomes showed cell viability of 80-100% against human retinal epithelial cells (Asasutjarit *et al.*, 2020).

2.5.2. Hyaluronan (HA), Hyaluronate receptor (CD44), and HA-CD44 interaction as possible targets for nano-carrier systems

Hyaluronan (HA) is a glycosaminoglycan, a structural component of extracellular matrix (ECM). HA is an essential constituent of the cornea, and acts through its receptor (CD44) in corneal and conjunctival epithelial cell regeneration (de la Fuente *et al.*, 2008b). CD44 is a trans-membrane glycoprotein involved in lymphocyte homing and activation, cell migration, and tumour growth and metastasis. Immunostaining revealed high density of the CD44 receptors in the corneal epithelium and endothelium. Destructive processes distressing the corneal lead to an overexpression of the receptor CD44 isotype arising from alternate splicing (Guter and Breunig, 2017). Binding of HA to the CD44 receptor activates the cytoplasmic domain of CD44 which recruits and activates several proteins signalling events such as ankyrin and merlin. HA interaction with CD44 receptor activates several signalling pathways. This pathways regulate cell survival, growth, migration and metastasis as well as promoting chemo resistance (Chaudhry *et al.*, 2021; Kesharwani *et al.*, 2021). Targeting HA in the matrix, targeting CD44 expressed on cancer cells, and interfering with HA-CD44 interaction are potential strategies for targeted delivery to cancer cells (Platt and

Szoka, 2008). Strategies employed for HA targeting include the use of HA-based drug, HA inhibitors, apoptosis induced by HA oligosaccharides, and hyaluronidases along with chemotherapeutics (Akim *et al.*, 2021). CD44 targeting strategies include pharmacological and natural inhibitors, siRNAs, peptides, antibodies and HA-modified nanocarriers (Hassn Mesrati *et al.*, 2021). Radwan *et al*. (2021) designed a HA-coated, Apatinib-loaded bovine serum albumin nanoparticle. The topically applied nanoparticles were tested as a potential therapy for diabetic retinopathy. The mucoadhesive properties of the HA and its binding to hyaluronan receptors on the corneal epithelium extended the retention duration of the HA-coated nanoparticles. Furthermore, the HA actively targeted the CD44 receptor on retinal cells, improving Apatinib delivery (Radwan *et al.*, 2021).

2.6. Stimuli–Responsive Approach

Polymeric materials have gained momentum in the field of drug delivery due to their excellent properties (Besford *et al.*, 2020). Most of the biomaterials used in drug delivery systems are in “static regimens”, meaning a trigger is required for the drug to be released from the system. The development of stimuli-responsive polymeric systems for drug delivery derives from this concept. Stimuli-responsive polymers respond to a slight change in the environment such as pH, temperature, and electrolytes, etc. (Nguyen and Lai, 2020). The model of stimuli-sensitive platforms can be exploited in cancer treatment in light of the biological difference between tumour and normal cells (Torchilin, 2007). These stimulus-responsive platforms can be exploited to initiate medication release and accumulation at the site of action, boosting therapeutic efficacy while decreasing toxicity to healthy tissues.

2.6.1. pH–Responsive Drug Delivery

As a result of the high proliferation rates in cancer cells, there is a lack of oxygen and nourishment, and the metabolism is shifted to anaerobic settings. Lactic acid is created as a result of the acidic pH in the extracellular and intracellular environments caused by adaptation. The acidic environment can be problematic for drug permeability, but it can also be exploited for chemotherapeutic agent delivery using carriers activated in an acidic environment (Tian and Bae, 2012). The targeting can be to extracellular tumour tissues with a pH of 6.5-7, which is lower than healthy tissue with a pH of 7.4, or to lysosomes upon drug carrier internalisation, which has a pH of 4.5–5 (Bawa *et*

al., 2009). The acidic pH of tumours can be used to induce pH-dependent drug release from the nanocarriers by either: (a) stimulating the internalization of nanocarrier by the tumour cells or (b) destabilizing the structure of nanocarrier (Pérez-Herrero and Fernández-Medarde, 2021). Noreen *et al*. (2020) prepared a pH responsive *in-situ* gel from sodium alginate and *Terminalia arjuna* gum for the delivery of moxifloxacin HCl (Noreen *et al.*, 2020). The optimized formulation provided sustained ocular release through the enhancement of corneal retention and permeability resulting in an overall enhanced bioavailability of the moxifloxacin hydro chloride. Alruwaili *et al*. (2020) prepared a stimulus-responsive chitosan nanoparticles loaded with gentamycin. The optimized chitosan NPs were further converted into a pH-sensitive *in-situ* gel using Carbopol®. The system provided a sustained release profile, enhanced corneal permeation, and displayed higher antimicrobial activity compared to the marketed eye drop (Alruwaili *et al.*, 2020). Poly(beta-aminoesters) are pH-responsive polymers that have been used for protein, peptide, antimicrobial, and chemotherapeutic drug delivery. Nanocarriers derived from PBAE extend the circulation of chemotherapeutic drugs, restrict their exposure to normal cells, and release their payload in a controlled manner in the acidic tumour microenvironment.

2.6.2. Temperature-Responsive Drug Delivery

The tumour microenvironment is slightly hyperthermic, 1-2°C greater than healthy tissue (Taghizadeh *et al.*, 2015). This feature can be exploited for tumour targeting through the use of thermo-responsive polymers. Thermo-responsive polymers transition to a soluble or insoluble state depending on the temperature to which they are subjected. The polymers transition to an insoluble state at the lower critical solution temperature (LCST), whereas they shift to a soluble state at the upper critical solution temperature (UCST) (Bawa *et al.*, 2009). *In situ* hydrogels are an example of stimuli-responsive systems that remain as solutions at room temperatures but rapidly transition to gels in the cul-de-sac of the eye (at body temperature) enabling a gradual release of the drug from the hydrogel (Lynch *et al.*, 2020; Makwana *et al.*, 2016). The ocular bioavailability is consequently enhanced, with the concomitant attendant reduction in dosing frequency and side effects ultimately improving patient compliance (Wu *et al.*, 2019). Notwithstanding these advantages, hydrogels are limited by low drug loading capacity especially for hydrophobic drugs, early dissolution of the hydrogel and subsequent rapid drug release (Hoare and Kohane, 2008). The inclusion of

nanoparticles into the *in situ* hydrogel may solve some of these shortcomings. The combination of these two platforms can act in the delivery of the payload to the intended site efficiently, whereby the hydrogel acts as a mucoadhesive matrix for the nanocarriers reducing their rapid clearance from the eyes and the nanocarriers enhances the drug loading capacity. The nanocarrier *in-situ* hydrogel composite will therefore offer a synergistic effect in the delivery of therapeutics (Wu *et al.*, 2019). Nagarwal and colleagues reported the loading of 5-FU into a modified nano *in-situ* gel (MNS) (Nagarwal *et al.*, 2011). The MNS demonstrated a diffusion-controlled release with an initial burst release and the potential for usage in ocular tumours. **Figure 2.5** displays the *in vivo* release from 5-FU solution, PLA nanoparticles, and the MNS. In aqueous humour, the MNS resulted in a greater maximum concentration and area under the curve. The MNS's higher retention time was responsible for the high 5-FU levels in the aqueous humour, which corresponded to a sustained release and improved bioavailability. The system proved its potential as a candidate for the delivery of 5-FU in conjunctival/corneal squamous cell carcinoma (Nagarwal *et al.*, 2011).

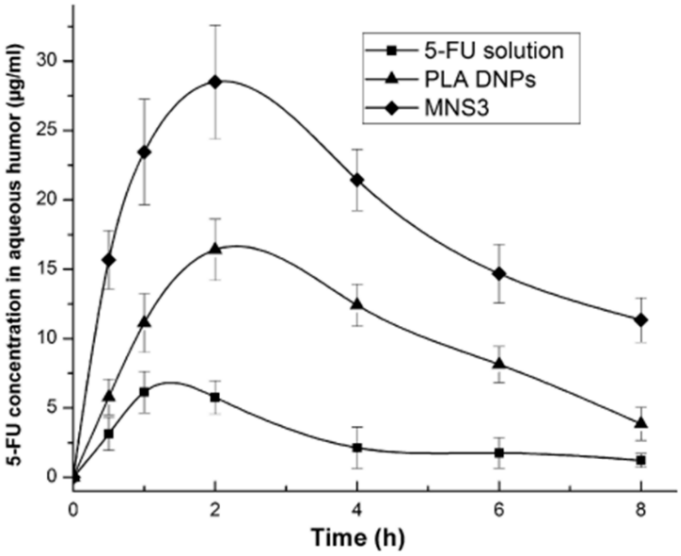


Figure 2.5 In-vitro levels of 5-FU in the aqueous humour following administration of the MNS, PLA nanoparticles and 5-FU solution (Image obtained with permission from (Nagarwal *et al.*, 2011).

2.6.3. Enzyme- responsive drug delivery

The tumour microenvironment is characterized by the change in enzyme regulation and expression, some ocular enzymes include hyaluronidase, lysozymes and

esterase and matrix metalloproteinase (MMPs) (Dludla *et al.*, 2022). Enzyme-responsive drug delivery systems are based on smart polymers that are triggered by enzymes present in the tumour extracellular environment resulting in drug release (Taghizadeh *et al.*, 2015). The enzyme-responsive release employs two techniques. The first is based on a polymer that is an enzyme substrate and experiences physical and chemical changes in the tumour microenvironment due to the catalytic action of a specific enzyme. The second method employs a polymer that experiences an internal macroscopic transition, causing the carrier to become unstable and the loaded medicine to be released (Karimi *et al.*, 2016). Grimaudo *et al*. 2018, created mixed micelles based on poloxamer 407/D-α-tocopheryl polyethylene glycol 1000 succinate (TPGS) for the administration of cyclosporine for the therapy of dry eye disease, uveitis, and other ocular disorders (Grimaudo *et al.*, 2018). Poloxamer and TPGS improved cyclosporine solubility and permeability and lengthened the retention time on the ocular surface. TPGS is a substrate of the esterase enzyme reported to be prevalent in ocular tissues. The enzyme-stimulated release was mediated by TPGS hydrolysis, resulting in the dissolution of the self-assembled micelles and the release of cyclosporine. TPGS is hydrolysed into vitamin E and vitamin E succinate, which are advantageous antioxidants for ocular disorders and support the therapeutic efficacy of cyclosporine (Grimaudo *et al.*, 2018). Yu and colleagues developed activatable protein nanoparticles (APNPs) to enhance the transport of the therapeutic peptide Melittin (Mel) (Yu *et al.*, 2018). The APNPs are composed of three polypeptides that self-assemble and are activated by protease, which is overexpressed in the tumour microenvironment. APNPs allowed for targeted delivery, extended circulation, and lower systemic toxicity. Mel-APNPs were created using a substrate of MMP. The Mel-APNPs were tested in tumour-bearing mice. When compared to free Mel, the Mel-APNPs suppressed cancer progress with less toxicity. A transferrin receptor target, was also built on Mel-APNPs and tagged as TfR-Mel-APNPs. The in vivo studies concluded that targeted delivery improves Mel's anticancer efficacy (Yu *et al.*, 2018).

2.6.4. ROS- responsive drug delivery

Reactive oxygen species (ROS) are oxygen-containing molecular species essential for biological functions. The ROS include hydroxyl radical (•OH), hydrogen peroxide (H_2O_2), singlet oxygen ($^1O_2$) and superoxide ($O_2^{\bullet-}$), etc. (Trachootham *et al.*, 2009). The cancer cells increased oxidative stress modifies ROS generation, resulting in

significantly higher levels in the intracellular and tissue milieu of tumour cells than in healthy tissues (Pelicano *et al.*, 2004; Xu *et al.*, 2017). As a result, ROS-responsive polymers can be employed for site-specific delivery in the cancer microenvironment. Among the ROS-sensitive polymers used for therapeutic delivery are selenium, thioether, thioketal, boronic acid, etc. (Liang and Liu, 2016; Lin *et al.*, 2021). The mechanism of drug release from ROS-responsive carriers includes ROS-induced carrier cleavage or induction of carrier disintegration by modifying the solubility and induction of cleavage of the carrier-drug linker (Liang and Liu, 2016). Tavazzi and colleagues created an H_2O_2-responsive contact lens designed for prolonged delivery (Tavazzi *et al.*, 2014). The induction of H_2O_2 was not caused by a pathophysiological state but rather by the conversion of mechanical energy to chemical energy. When the siloxane-hydrogel contact lenses were subjected to the pressure created by eyelid movement, the mechanical energy cleaved of the siloxane bonds, resulting in the formation of H_2O_2. The hydrogen peroxide concentration produced was biocompatible and suitable to trigger the drug release from the H_2O_2-responsive platform (Tavazzi *et al.*, 2014). As an example for the use in cancer treatment, Du et al. (2019) created a range of novel liposomes based on thioether phosphatidylcholines for ROS-responsive drug release in tumour cells. Doxorubicin (DOX) was used as a model drug; when exposed to ROS, the hydrophobic thioethers transform into hydrophilic sulfones or sulfoxides (Du *et al.*, 2019). The transition breaks the structure of the liposomes, causing the loaded DOX to be released. In vitro and in vivo anticancer activity assays show that ROS-responsive liposomes have higher therapeutic efficacy than free DOX and standard liposomes. The elevated ROS levels in the tumour microenvironment caused the carrier to degrade quickly, triggering the DOX release (Du *et al.*, 2019). Further research into ROS-responsive drug delivery systems in the field of ocular delivery is required. Du et al.'s findings could be used as a starting point since tumour microenvironments are comparable with high ROS and enhanced permeation and retention effects. Furthermore, liposomes have been used successfully for ocular delivery, implying that ROS-responsive platforms could be used for ocular tumour administration.

2.7. Future recommendations and conclusion

The current challenge in ocular drug delivery is the design of a system that encloses and carries the drug load through multiple physiological barriers to the targeted site

and achieve the desired therapeutic effect. The field of nanomedicine has developed significantly in the last decade, and research into the management of ocular tumours is not as sparse. The development of nanotechnology for ocular delivery is showing potential as site specific drug delivery systems, particularly when combined with bio-adhesive materials. The available technologies and overabundance of polymeric materials renders it a possibility to produce an ocular drug delivery system that is site-specific, stable, and safe for the management of ocular tumours. Strategies for improving therapeutic targeting rely heavily on an in-depth knowledge of the biochemical variations between cancer and healthy cells, as well as the availability of therapeutic drugs that target cell processes that are critical for cancer cells but not necessary for normal cells. The design and development of drug delivery systems triggered by the local microenvironment is a cutting-edge approach increasingly being employed in nanomedicine. Intracellular tumour biomarkers could be used to identify disease locations and trigger a controlled drug release, resulting in improved therapeutic efficacy and reduced toxicity. A better understanding of the ocular tumour microenvironment and their specific biomarker is expected to further enhance the targeting. The major limitation of the use of nanocarriers is their quick elimination by the reticuloendothelial system, the biological barriers, and nanoecotoxicology. The use of antibodies and specific ligands on the surface of nanocarriers can be used for targeted delivery to cancer cell. Furthermore, the loading of nanocarriers into *in situ* gelling systems that act as matrix for the nanocarriers will reduce their rapid clearance and upon their diffusion the active targeting ligands will release the payload in a site-specific manner. Future research might focus on ligand coupling of multiple types for higher-sensitivity malignant lesion detection.

2.8. References

1. Adler, E., Turner, J. R. & Stone, D. U. 2013. Ocular surface squamous neoplasia: a survey of changes in the standard of care from 2003 to 2012. *Cornea,* 32**,** 1558-1561.
2. Ahmad, I., Pandit, J., Sultana, Y., Mishra, A. K., Hazari, P. P. & Aqil, M. 2019. Optimization by design of etoposide loaded solid lipid nanoparticles for ocular delivery: Characterization, pharmacokinetic and deposition study. *Materials Science and Engineering: C,* 100**,** 959-970.

3. Akhtar, M. J., Ahamed, M., Alhadlaq, H. A., Alrokayan, S. A. & Kumar, S. 2014. Targeted anticancer therapy: Overexpressed receptors and nanotechnology. *Clinica Chimica Acta,* 436**,** 78-92.
4. Akhter, S., Anwar, M., Siddiqui, M. A., Ahmad, I., Ahmad, J., Ahmad, M. Z., Bhatnagar, A. & Ahmad, F. J. 2016. Improving the topical ocular pharmacokinetics of an immunosuppressant agent with mucoadhesive nanoemulsions: Formulation development, in-vitro and in-vivo studies. *Colloids and Surfaces B: Biointerfaces,* 148**,** 19-29.
5. Akim, A., Zafar, M. N., Safdar, N., Sung, Y. Y. & Muhammad, T. S. T. 2021. Understanding Hyaluronan Receptor (CD44) Interaction, HA-CD44 Activated Potential Targets in Cancer Therapeutics. *Advanced Pharmaceutical Bulletin,* 11**,** 426.
6. Alimbetov, D., Askarova, S., Umbayev, B., Davis, T. & Kipling, D. 2018. Pharmacological targeting of cell cycle, apoptotic and cell adhesion signaling pathways implicated in chemoresistance of cancer cells. *International journal of molecular sciences,* 19**,** 1690.
7. Alruwaili, N. K., Zafar, A., Imam, S. S., Alharbi, K. S., Alotaibi, N. H., Alshehri, S., Alhakamy, N. A., Alzarea, A. I., Afzal, M. & Elmowafy, M. 2020. Stimulus responsive ocular gentamycin-ferrying chitosan nanoparticles hydrogel: formulation optimization, ocular safety and antibacterial assessment. *International Journal of Nanomedicine,* 15**,** 4717.
8. Antonietta Blasi, M., Maceroni, M., Grazia Sammarco, M. & Pagliara, M. M. 2018. Mitomycin C or interferon as adjuvant therapy to surgery for ocular surface squamous neoplasia: comparative study. *European journal of ophthalmology,* 28**,** 204-209.
9. Asasutjarit, R., Managit, C., Phanaksri, T., Treesuppharat, W. & Fuongfuchat, A. 2020. Formulation development and in vitro evaluation of transferrin-conjugated liposomes as a carrier of ganciclovir targeting the retina. *International Journal of Pharmaceutics,* 577**,** 119084.
10. Ashkenazy 2017. Immunosuppression as a possible risk factor for interferon non-response in ocular surface squamous neoplasia. *Investigative ophthalmology & visual science,* 58.

11. Bachu, R. D., Chowdhury, P., Al-Saedi, Z. H., Karla, P. K. & Boddu, S. H. 2018. Ocular drug delivery barriers—role of nanocarriers in the treatment of anterior segment ocular diseases. *Pharmaceutics,* 10**,** 28.
12. Ban, J., Zhang, Y., Huang, X., Deng, G., Hou, D., Chen, Y. & Lu, Z. 2017. Corneal permeation properties of a charged lipid nanoparticle carrier containing dexamethasone. *International Journal of Nanomedicine,* 12**,** 1329.
13. Bawa, P., Pillay, V., Choonara, Y. E. & Du Toit, L. C. 2009. Stimuli-responsive polymers and their applications in drug delivery. *Biomedical materials,* 4**,** 022001.
14. Bayón-Cordero, L., Alkorta, I. & Arana, L. 2019. Application of solid lipid nanoparticles to improve the efficiency of anticancer drugs. *Nanomaterials,* 9**,** 474.
15. Beltrán-Gracia, E., López-Camacho, A., Higuera-Ciapara, I., Velázquez-Fernández, J. B. & Vallejo-Cardona, A. A. 2019. Nanomedicine review: Clinical developments in liposomal applications. *Cancer Nanotechnology,* 10**,** 1-40.
16. Besford, Q. A., Cavalieri, F. & Caruso, F. 2020. Glycogen as a building block for advanced biological materials. *Advanced Materials,* 32**,** 1904625.
17. Bozzuto, G. & Molinari, A. 2015. Liposomes as nanomedical devices. *International journal of nanomedicine,* 10**,** 975.
18. Campardelli, R., Trucillo, P. & Reverchon, E. 2018. Supercritical assisted process for the efficient production of liposomes containing antibiotics for ocular delivery. *Journal of CO2 Utilization,* 25**,** 235-241.
19. Chaudhry, G. E., Akim, A., Naveed Zafar, M., Safdar, N., Sung, Y. Y. & Muhammad, T. S. T. 2021. Understanding Hyaluronan Receptor (CD44) Interaction, HA-CD44 Activated Potential Targets in Cancer Therapeutics. *Advanced Pharmaceutical Bulletin,* 11**,** 426-438.
20. Chaw, S. Y., Novera, W., Chacko, A.-M., Wong, T. T. L. & Venkatraman, S. 2021. In vivo fate of liposomes after subconjunctival ocular delivery. *Journal of Controlled Release,* 329**,** 162-174.
21. Chis, A. A., Dobrea, C., Morgovan, C., Arseniu, A. M., Rus, L. L., Butuca, A., Juncan, A. M., Totan, M., Vonica-Tincu, A. L., Cormos, G., Muntean, A. C., Muresan, M. L., Gligor, F. G. & Frum, A. 2020. Applications and Limitations of Dendrimers in Biomedicine. *Molecules,* 25**,** 3982.

22. Chiu-Tsao, S. T., Astrahan, M. A., Finger, P. T., Followill, D. S., Meigooni, A. S., Melhus, C. S., Mourtada, F., Napolitano, M. E., Nath, R. & Rivard, M. J. 2012. Dosimetry of 125I and 103Pd COMS eye plaques for intraocular tumors: Report of Task Group 129 by the AAPM and ABS. *Medical physics,* 39**,** 6161-6184.
23. Choi, Y., Thomas, T., Kotlyar, A., Islam, M. T. & Baker, J. R. 2005. Synthesis and Functional Evaluation of DNA-Assembled Polyamidoamine Dendrimer Clusters for Cancer Cell-Specific Targeting. *Chemistry & Biology,* 12**,** 35-43.
24. Cholkar, K., Patel, A., Dutt Vadlapudi, A. & K Mitra, A. 2012. Novel nanomicellar formulation approaches for anterior and posterior segment ocular drug delivery. *Recent patents on nanomedicine,* 2**,** 82-95.
25. Cryer, A. M. & Thorley, A. J. 2019. Nanotechnology in the diagnosis and treatment of lung cancer. *Pharmacology & therapeutics,* 198**,** 189-205.
26. Danaei, M., Dehghankhold, M., Ataei, S., Hasanzadeh Davarani, F., Javanmard, R., Dokhani, A., Khorasani, S. & Mozafari, M. 2018. Impact of particle size and polydispersity index on the clinical applications of lipidic nanocarrier systems. *Pharmaceutics,* 10**,** 57.
27. De la Fuente, M., Seijo, B. & Alonso, M. J. 2008a. Novel hyaluronic acid-chitosan nanoparticles for ocular gene therapy. *Investigative ophthalmology & visual science,* 49**,** 2016-2024.
28. de la Fuente, M., Seijo, B. a. & Alonso, M. J. 2008b. Novel Hyaluronic Acid-Chitosan Nanoparticles for Ocular Gene Therapy. *Investigative Ophthalmology & Visual Science,* 49**,** 2016-2024.
29. DelMonte, D. W. & Kim, T. 2011. Anatomy and physiology of the cornea. *Journal of Cataract & Refractive Surgery,* 37**,** 588-598.
30. Diebold, Y. & Calonge, M. 2010. Applications of nanoparticles in ophthalmology. *Progress in Retinal and Eye Research,* 29**,** 596-609.
31. Dludla, S. B. K., Mashabela, L. T., Ng'andwe, B., Makoni, P. A. & Witika, B. A. 2022. Current Advances in Nano-Based and Polymeric Stimuli-Responsive Drug Delivery Targeting the Ocular Microenvironment: A Review and Envisaged Future Perspectives. *Polymers,* 14**,** 3580.
32. Doktorovova, S., Kovačević, A. B., Garcia, M. L. & Souto, E. B. 2016. Preclinical safety of solid lipid nanoparticles and nanostructured lipid carriers: Current

evidence from in vitro and in vivo evaluation. *European Journal of Pharmaceutics and Biopharmaceutics,* 108**,** 235-252.

33. Du, Y., He, W., Xia, Q., Zhou, W., Yao, C. & Li, X. 2019. Thioether phosphatidylcholine liposomes: a novel ROS-responsive platform for drug delivery. *ACS applied materials & interfaces,* 11**,** 37411-37420.
34. Feghhi, M., Sharif Makhmalzadeh, B., Farrahi, F., Akmali, M. & Hasanvand, N. 2020. Anti-microbial effect and in vivo ocular delivery of ciprofloxacin-loaded liposome through rabbit's eye. *Current eye research,* 45**,** 1245-1251.
35. Fung, C. Y., Tarbell, N. J., Lucarelli, M. J., Goldberg, S. I., Linggood, R. M., Harris, N. L. & Ferry, J. A. 2003. Ocular adnexal lymphoma: Clinical behavior of distinct World Health Organization classification subtypes. *International Journal of Radiation Oncology*Biology*Physics,* 57**,** 1382-1391.
36. Garcia-Martin, E., Gil-Arribas, L., Idoipe, M., Alfaro, J., Pueyo, V., Pablo, L. & Fernandez, F. 2011. Comparison of imiquimod 5% cream versus radiotherapy as treatment for eyelid basal cell carcinoma. *British journal of ophthalmology,* 95**,** 1393-1396.
37. Gaudana, R., Ananthula, H. K., Parenky, A. & Mitra, A. K. 2010. Ocular drug delivery. *The AAPS journal,* 12**,** 348-360.
38. Gichuhi, S., Macharia, E., Kabiru, J., Zindamoyen, A. M. b., Rono, H., Ollando, E., Wachira, J., Munene, R., Maina, J. & Onyuma, T. 2016. Topical fluorouracil after surgery for ocular surface squamous neoplasia in Kenya: a randomised, double-blind, placebo-controlled trial. *The Lancet Global Health,* 4**,** e378-e385.
39. Gorantla, S., Rapalli, V. K., Waghule, T., Singh, P. P., Dubey, S. K., Saha, R. N. & Singhvi, G. 2020. Nanocarriers for ocular drug delivery: current status and translational opportunity. *Royal Society of Chemistry Advances,* 10**,** 27835 - 27855.
40. Gote, V., Sikder, S., Sicotte, J. & Pal, D. 2019. Ocular drug delivery: Present innovations and future challenges. *Journal of Pharmacology and Experimental Therapeutics,* 370**,** 602-624.
41. Greer, C., Polski, A. & Berry, J. L. 2018. Topical chemotherapy and the evolving role of the biopsy for ocular surface squamous neoplasia. *Advances in Ophthalmology and Optometry,* 3**,** 115-137.
42. Grimaudo, M. A., Pescina, S., Padula, C., Santi, P., Concheiro, A., Alvarez-Lorenzo, C. & Nicoli, S. 2018. Poloxamer 407/TPGS mixed micelles as

promising carriers for cyclosporine ocular delivery. *Molecular pharmaceutics,* 15**,** 571-584.

43. Gupta, A. & Muecke, J. 2010. Treatment of ocular surface squamous neoplasia with Mitomycin C. *British Journal of Ophthalmology,* 94**,** 555-558.
44. Guter, M. & Breunig, M. 2017. Hyaluronan as a promising excipient for ocular drug delivery. *European Journal of Pharmaceutics and Biopharmaceutics,* 113**,** 34-49.
45. Hassn Mesrati, M., Syafruddin, S. E., Mohtar, M. A. & Syahir, A. 2021. CD44: A Multifunctional Mediator of Cancer Progression. *Biomolecules,* 11.
46. Hoare, T. R. & Kohane, D. S. 2008. Hydrogels in drug delivery: Progress and challenges. *polymer,* 49**,** 1993-2007.
47. Hossen, S., Hossain, M. K., Basher, M., Mia, M., Rahman, M. & Uddin, M. J. 2019. Smart nanocarrier-based drug delivery systems for cancer therapy and toxicity studies: A review. *Journal of advanced research,* 15**,** 1-18.
48. Hu, C.-M. J., Aryal, S. & Zhang, L. 2010. Nanoparticle-assisted combination therapies for effective cancer treatment. *Therapeutic delivery,* 1**,** 323-334.
49. Huang, D., Chen, Y.-S. & Rupenthal, I. D. 2018. Overcoming ocular drug delivery barriers through the use of physical forces. *Advanced drug delivery reviews,* 126**,** 96-112.
50. Huang, D. & Wu, D. 2018. Biodegradable dendrimers for drug delivery. *Materials Science and Engineering: C,* 90**,** 713-727.
51. Huang, H., Yang, X., Li, H., Lu, H., Oswald, J., Liu, Y., Zeng, J., Jin, C., Peng, X. & Liu, J. 2020. iRGD decorated liposomes: A novel actively penetrating topical ocular drug delivery strategy. *Nano Research,* 13**,** 3105-3109.
52. Imperiale, J. C., Acosta, G. B. & Sosnik, A. 2018. Polymer-based carriers for ophthalmic drug delivery. *Journal of controlled release,* 285**,** 106-141.
53. Jackson, T. L., Antcliff, R. J., Hillenkamp, J. & Marshall, J. 2003. Human retinal molecular weight exclusion limit and estimate of species variation. *Investigative ophthalmology & visual science,* 44**,** 2141-2146.
54. Janagam, D. R., Wu, L. & Lowe, T. L. 2017. Nanoparticles for drug delivery to the anterior segment of the eye. *Advanced drug delivery reviews,* 122**,** 31-64.
55. Jin, C., Wang, K., Oppong-Gyebi, A. & Hu, J. 2020. Application of nanotechnology in cancer diagnosis and therapy-a mini-review. *International Journal of Medical Sciences,* 17**,** 2964.

56. Jose, S., Cinu, T. A., Sebastian, R., Shoja, M., Aleykutty, N., Durazzo, A., Lucarini, M., Santini, A. & Souto, E. B. 2019. Transferrin-conjugated docetaxel–PLGA nanoparticles for tumor targeting: influence on MCF-7 cell cycle. *Polymers,* 11**,** 1905.
57. Jumelle, C., Gholizadeh, S., Annabi, N. & Dana, R. 2020. Advances and limitations of drug delivery systems formulated as eye drops. *Journal of Controlled Release,* 321**,** 1-22.
58. Kaliki, S., Bejjanki, K. M., Desai, A. & Mohamed, A. 2019. Interferon Alfa 2b for Ocular Surface Squamous Neoplasia: Factors Influencing the Treatment Response. *Seminars in Ophthalmology,* 34**,** 465-472.
59. Kaliki, S., Singh, S., Iram, S. & Tripuraneni, D. 2016. Recombinant interferon alpha 2b for ocular surface squamous neoplasia: an efficient and cost-effective treatment modality in Asian Indian patients. *Indian Journal of Ophthalmology,* 64**,** 702.
60. Kalomiraki, M., Thermos, K. & Chaniotakis, N. A. 2016. Dendrimers as tunable vectors of drug delivery systems and biomedical and ocular applications. *International journal of nanomedicine,* 11**,** 1.
61. Kanapathipillai, M., Brock, A. & Ingber, D. E. 2014. Nanoparticle targeting of anti-cancer drugs that alter intracellular signaling or influence the tumor microenvironment. *Advanced Drug Delivery Reviews,* 79-80**,** 107-118.
62. Kang, S. G., Chung, H., Yoo, Y. D., Lee, J. G., Choi, Y. I. & Yu, Y. S. 2001. Mechanism of growth inhibitory effect of Mitomycin-C on cultured human retinal pigment epithelial cells: apoptosis and cell cycle arrest. *Current eye research,* 22**,** 174-181.
63. Kang, S. J., Durairaj, C., Kompella, U. B., O'Brien, J. M. & Grossniklaus, H. E. 2009. Subconjunctival Nanoparticle Carboplatin in the Treatment of Murine Retinoblastoma. *Archives of Ophthalmology,* 127**,** 1043-1047.
64. Karimi, M., Ghasemi, A., Zangabad, P. S., Rahighi, R., Basri, S. M. M., Mirshekari, H., Amiri, M., Pishabad, Z. S., Aslani, A. & Bozorgomid, M. 2016. Smart micro/nanoparticles in stimulus-responsive drug/gene delivery systems. *Chemical Society Reviews,* 45**,** 1457-1501.
65. Kesharwani, P., Chadar, R., Sheikh, A., Rizg, W. Y. & Safhi, A. Y. 2021. CD44-Targeted Nanocarrier for Cancer Therapy. *Front Pharmacol,* 12**,** 800481.

66. Khames, A., Khaleel, M. A., El-Badawy, M. F. & El-Nezhawy, A. O. 2019. Natamycin solid lipid nanoparticles–sustained ocular delivery system of higher corneal penetration against deep fungal keratitis: preparation and optimization. *International Journal of Nanomedicine,* 14**,** 2515.
67. Kim, H. J., Shields, C. L., Shah, S. U., Kaliki, S. & Lally, S. E. 2012. Giant ocular surface squamous neoplasia managed with interferon alpha-2b as immunotherapy or immunoreduction. *Ophthalmology,* 119**,** 938-944.
68. Kim, H. M. & Woo, S. J. 2021. Ocular Drug Delivery to the Retina: Current Innovations and Future Perspectives. *Pharmaceutics,* 13.
69. Kompella, U. B., Sundaram, S., Raghava, S. & Escobar, E. R. 2006. Luteinizing hormone-releasing hormone agonist and transferrin functionalizations enhance nanoparticle delivery in a novel bovine ex vivo eye model. *Molecular Vision,* 12**,** 1185-98.
70. Kunkler, A. L., Binkley, E. M., Mantopoulos, D., Hendershot, A. J., Ohr, M. P., Kendra, K. L., Davidorf, F. H. & Cebulla, C. M. 2019. Known and novel ocular toxicities of biologics, targeted agents, and traditional chemotherapeutics. *Graefe's Archive for Clinical and Experimental Ophthalmology,* 257**,** 1771-1781.
71. Kusumesh, R., Ambastha, A., Kumar, S., Sinha, B. P. & Imam, N. 2017. Retrospective Comparative Study of Topical Interferon a2b Versus Mitomycin C for Primary Ocular Surface Squamous Neoplasia. *Cornea,* 36**,** 327-331.
72. Kvopka, M., Lake, S. R. & Smith, J. R. 2020. Intraocular chemotherapy for vitreoretinal lymphoma: a review. *Clinical & Experimental Ophthalmology,* 48**,** 240-248.
73. Li, J., Guo, X., Liu, Z., Okeke, C. I., Li, N., Zhao, H., Aggrey, M. O., Pan, W. & Wu, T. 2014. Preparation and evaluation of charged solid lipid nanoparticles of tetrandrine for ocular drug delivery system: pharmacokinetics, cytotoxicity and cellular uptake studies. *Drug development and industrial pharmacy,* 40**,** 980-987.
74. Liang, J. & Liu, B. 2016. ROS-responsive drug delivery systems. *Bioengineering & translational medicine,* 1**,** 239-251.
75. Lin, X., Wu, X., Chen, X., Wang, B. & Xu, W. 2021. Intellective and stimuli-responsive drug delivery systems in eyes. *International Journal of Pharmaceutics,* 602**,** 120591.

76. Longmire, M. R., Ogawa, M., Choyke, P. L. & Kobayashi, H. 2011. Biologically Optimized Nanosized Molecules and Particles: More than Just Size. *Bioconjugate Chemistry,* 22**,** 993-1000.
77. Lynch, C. R., Kondiah, P. P., Choonara, Y. E., Du Toit, L. C., Ally, N. & Pillay, V. 2020. Hydrogel biomaterials for application in ocular drug delivery. *Frontiers in Bioengineering and Biotechnology,* 8**,** 228.
78. Macedo, E. M. S. d., Carneiro, R. C., de Lima, P. P., Silva, B. G. & Matayoshi, S. 2015. Imiquimod cream efficacy in the treatment of periocular nodular basal cell carcinoma: a non-randomized trial. *BMC ophthalmology,* 15**,** 1-7.
79. Maheshwari, A. & Finger, P. T. 2018. Cancers of the eye. *Cancer and Metastasis Reviews,* 37**,** 677-690.
80. Makky, A., Michel, J., Maillard, P. & Rosilio, V. 2011. Biomimetic liposomes and planar supported bilayers for the assessment of glycodendrimeric porphyrins interaction with an immobilized lectin. *Biochimica et Biophysica Acta (BBA)-Biomembranes,* 1808**,** 656-666.
81. Makwana, S., Patel, V. & Parmar, S. 2016. Development and characterization of in-situ gel for ophthalmic formulation containing ciprofloxacin hydrochloride. *Results in pharma sciences,* 6**,** 1-6.
82. Meng, T., Kulkarni, V., Simmers, R., Brar, V. & Xu, Q. 2019. Therapeutic implications of nanomedicine for ocular drug delivery. *Drug discovery today,* 24**,** 1524-1538.
83. Mladenov, E., Tsaneva, I. & Anachkova, B. 2007. Activation of the S phase DNA damage checkpoint by mitomycin C. *Journal of Cellular Physiology,* 211**,** 468-476.
84. Moon, J., Choi, S. H., Lee, M. J., Jo, D. H., Park, U. C., Yoon, S.-O., Woo, S. J. & Oh, J. Y. 2021. Ocular surface complications of local anticancer drugs for treatment of ocular tumors. *The Ocular Surface,* 19**,** 16-30.
85. Moosavian, S. A., Bianconi, V., Pirro, M. & Sahebkar, A. Challenges and pitfalls in the development of liposomal delivery systems for cancer therapy. Seminars in Cancer Biology, 2021. Elsevier, 337-348.
86. Nagarwal, R. C., Kant, S., Singh, P., Maiti, P. & Pandit, J. 2009. Polymeric nanoparticulate system: a potential approach for ocular drug delivery. *Journal of controlled release,* 136**,** 2-13.

87. Nagarwal, R. C., Kumar, R., Dhanawat, M. & Pandit, J. K. 2011. Modified PLA nano in situ gel: a potential ophthalmic drug delivery system. *Colloids and surfaces. B, Biointerfaces,* 86 1**,** 28-34.
88. Nagarwal, R. C., Kumar, R. & Pandit, J. 2012. Chitosan coated sodium alginate–chitosan nanoparticles loaded with 5-FU for ocular delivery: In vitro characterization and in vivo study in rabbit eye. *European Journal of Pharmaceutical Sciences,* 47**,** 678-685.
89. Nanji, A. A., Moon, C. S., Galor, A., Sein, J., Oellers, P. & Karp, C. L. 2014. Surgical versus medical treatment of ocular surface squamous neoplasia: a comparison of recurrences and complications. *Ophthalmology,* 121**,** 994-1000.
90. Nanji, A. A., Sayyad, F. E. & Karp, C. L. 2013. Topical chemotherapy for ocular surface squamous neoplasia. *Current opinion in ophthalmology,* 24**,** 336-342.
91. Navya, P., Kaphle, A., Srinivas, S., Bhargava, S. K., Rotello, V. M. & Daima, H. K. 2019. Current trends and challenges in cancer management and therapy using designer nanomaterials. *Nano convergence,* 6**,** 1-30.
92. Netto, M. V., Mohan, R. R., Sinha, S., Sharma, A., Gupta, P. C. & Wilson, S. E. 2006. Effect of prophylactic and therapeutic mitomycin C on corneal apoptosis, cellular proliferation, haze, and long-term keratocyte density in rabbits. *Journal of Refractive Surgery*, *22*, 562-574.
93. Nguyen, D. D. & Lai, J.-Y. 2020. Advancing the stimuli response of polymer-based drug delivery systems for ocular disease treatment. *Polymer Chemistry,* 11**,** 6988-7008.
94. Nikzamir, M., Hanifehpour, Y., Akbarzadeh, A. & Panahi, Y. 2021. Applications of dendrimers in nanomedicine and drug delivery: A review. *Journal of Inorganic and Organometallic Polymers and Materials,* 31**,** 2246-2261.
95. Nishida, T., Saika, S. & Morishige, N. 2011. Cornea and sclera: anatomy and physiology. *Cornea,* 1**,** 1-22.
96. Noreen, S., Ghumman, S. A., Batool, F., Ijaz, B., Basharat, M., Noureen, S., Kausar, T. & Iqbal, S. 2020. Terminalia arjuna gum/alginate in situ gel system with prolonged retention time for ophthalmic drug delivery. *International Journal of Biological Macromolecules,* 152**,** 1056-1067.
97. Ogier, J., Arnauld, T. & Doris, E. 2009. Recent advances in the field of nanometric drug carriers. *Future medicinal chemistry,* 1**,** 693-711.

98. Parhi, P., Mohanty, C. & Sahoo, S. K. 2012. Nanotechnology-based combinational drug delivery: an emerging approach for cancer therapy. *Drug Discovery Today,* 17**,** 1044-1052.
99. Patel, A., Cholkar, K., Agrahari, V. & Mitra, A. K. 2013a. Ocular drug delivery systems: An overview. *World journal of pharmacology,* 2**,** 47.
100. Patel, A. D., Cholkar, K., Agrahari, V. & Mitra, A. K. 2013b. Ocular drug delivery systems: An overview. *World journal of pharmacology,* 2 2**,** 47-64.
101. Pe'er, J. 2015. Ocular surface squamous neoplasia: evidence for topical chemotherapy. *International ophthalmology clinics,* 55**,** 9-21.
102. Pelicano, H., Carney, D. & Huang, P. 2004. ROS stress in cancer cells and therapeutic implications. *Drug resistance updates,* 7**,** 97-110.
103. Pérez-Herrero, E. & Fernández-Medarde, A. 2021. The reversed intra- and extracellular pH in tumors as a unified strategy to chemotherapeutic delivery using targeted nanocarriers. *Acta Pharmaceutica Sinica B,* 11**,** 2243-2264.
104. Platt, V. M. & Szoka, F. C., Jr. 2008. Anticancer therapeutics: targeting macromolecules and nanocarriers to hyaluronan or CD44, a hyaluronan receptor. *Molecular Pharmaceutics,* 5**,** 474-86.
105. Qian, Z. M., Li, H., Sun, H. & Ho, K. 2002. Targeted drug delivery via the transferrin receptor-mediated endocytosis pathway. *Pharmacological reviews,* 54**,** 561-587.
106. Radwan, S. E.-S., El-Kamel, A., Zaki, E. I., Burgalassi, S., Zucchetti, E. & El-Moslemany, R. M. 2021. Hyaluronic-coated albumin nanoparticles for the non-invasive delivery of apatinib in diabetic retinopathy. *International Journal of Nanomedicine,* 16**,** 4481.
107. Rodríguez Villanueva, J., Navarro, M. G. & Rodríguez Villanueva, L. 2016. Dendrimers as a promising tool in ocular therapeutics: Latest advances and perspectives. *International Journal of Pharmaceutics,* 511**,** 359-366.
108. Sampat, K. M. & Garg, S. J. 2010. Complications of intravitreal injections. *Current opinion in ophthalmology,* 21**,** 178-183.
109. Santos, A., Veiga, F. & Figueiras, A. 2019. Dendrimers as pharmaceutical excipients: synthesis, properties, toxicity and biomedical applications. *Materials,* 13**,** 65.

110. Schmid, K. E., Kornek, G. V., Scheithauer, W. & Binder, S. 2006. Update on Ocular Complications of Systemic Cancer Chemotherapy. *Survey of Ophthalmology,* 51**,** 19-40.
111. Sepulveda, R., Pe'er, J., Midena, E., Seregard, S., Dua, H. S. & Singh, A. D. 2010. Topical chemotherapy for ocular surface squamous neoplasia: current status. *British journal of ophthalmology,* 94**,** 532-535.
112. Shastri, D. H., Silva, A. C. & Almeida, H. 2023. Ocular Delivery of Therapeutic Proteins: A Review. *Pharmaceutics,* 15**,** 205.
113. Shields, C. L., Kaliki, S., Kim, H. J., Al-Dahmash, S., Shah, S. U., Lally, S. E. & Shields, J. A. 2013. Interferon for ocular surface squamous neoplasia in 81 cases: outcomes based on the American Joint Committee on Cancer classification. *Cornea,* 32**,** 248-256.
114. Siegler, E. L., Kim, Y. J. & Wang, P. 2016. Nanomedicine targeting the tumor microenvironment: Therapeutic strategies to inhibit angiogenesis, remodel matrix, and modulate immune responses. *Journal of Cellular Immunotherapy,* 2**,** 69-78.
115. Souza, J. G., Dias, K., Silva, S. A., de Rezende, L. C., Rocha, E. M., Emery, F. S. & Lopez, R. F. 2015. Transcorneal iontophoresis of dendrimers: PAMAM corneal penetration and dexamethasone delivery. *Journal of Controlled Release,* 200**,** 115-124.
116. Suen, W.-L. L. & Chau, Y. 2014. Size-dependent internalisation of folate-decorated nanoparticles via the pathways of clathrin and caveolae-mediated endocytosis in ARPE-19 cells. *Journal of Pharmacy and Pharmacology,* 66**,** 564-573.
117. Taghizadeh, B., Taranejoo, S., Monemian, S. A., Salehi Moghaddam, Z., Daliri, K., Derakhshankhah, H. & Derakhshani, Z. 2015. Classification of stimuli–responsive polymers as anticancer drug delivery systems. *Drug Delivery,* 22**,** 145-155.
118. Tang, Z., Fan, X., Chen, Y. & Gu, P. 2022. Ocular Nanomedicine. *Advanced Science***,** 2003699.
119. Tang, Z., He, C., Tian, H., Ding, J., Hsiao, B. S., Chu, B. & Chen, X. 2016. Polymeric nanostructured materials for biomedical applications. *Progress in Polymer Science,* 60**,** 86-128.

120. Tavazzi, S., Ferraro, L., Cozza, F., Pastori, V., Lecchi, M., Farris, S. & Borghesi, A. 2014. Hydrogen peroxide mechanosynthesis in siloxane-hydrogel contact lenses. *ACS Applied Materials & Interfaces,* 6**,** 19606-19612.
121. Tian, B., Bilsbury, E., Doherty, S., Teebagy, S., Wood, E., Su, W., Gao, G. & Lin, H. 2022. Ocular Drug Delivery: Advancements and Innovations. *Pharmaceutics,* 14**,** 1931.
122. Tian, L. & Bae, Y. H. 2012. Cancer nanomedicines targeting tumor extracellular pH. *Colloids and Surfaces B: Biointerfaces,* 99**,** 116-126.
123. Torchilin, V. P. 2007. Targeted pharmaceutical nanocarriers for cancer therapy and imaging. *The AAPS journal,* 9**,** E128-E147.
124. Trachootham, D., Alexandre, J. & Huang, P. 2009. Targeting cancer cells by ROS-mediated mechanisms: a radical therapeutic approach? *Nature reviews Drug discovery,* 8**,** 579-591.
125. Tsai, C.-H., Wang, P.-Y., Lin, I.-C., Huang, H., Liu, G.-S. & Tseng, C.-L. 2018. Ocular drug delivery: Role of degradable polymeric nanocarriers for ophthalmic application. *International journal of molecular sciences,* 19**,** 2830.
126. Tseng, C.-L., Chen, K.-H., Su, W.-Y., Lee, Y.-H., Wu, C.-C. & Lin, F.-H. 2013. Cationic gelatin nanoparticles for drug delivery to the ocular surface: in vitro and in vivo evaluation. *Journal of Nanomaterials,* 2013.
127. ud Din, F., Aman, W., Ullah, I., Qureshi, O. S., Mustapha, O., Shafique, S. & Zeb, A. 2017. Effective use of nanocarriers as drug delivery systems for the treatment of selected tumors. *International journal of nanomedicine,* 12**,** 7291.
128. Uwaezuoke, O., Du Toit, L. C., Kumar, P., Ally, N. & Choonara, Y. E. 2022. Linoleic Acid-Based Transferosomes for Topical Ocular Delivery of Cyclosporine A. *Pharmaceutics,* 14**,** 1695.
129. Vaneev, A., Tikhomirova, V., Chesnokova, N., Popova, E., Beznos, O., Kost, O. & Klyachko, N. 2021. Nanotechnology for topical drug delivery to the anterior segment of the eye. *International Journal of Molecular Sciences,* 22**,** 12368.
130. Venkateswaran, N., Mercado, C., Galor, A. & Karp, C. L. 2019. Comparison of topical 5-fluorouracil and interferon alfa-2b as primary treatment modalities for ocular surface squamous neoplasia. *American journal of ophthalmology,* 199**,** 216-222.

131. Vishnevskia-Dai, V., Sella King, S., Lekach, R., Fabian, I. D. & Zloto, O. 2020. Ocular manifestations of leukemia and results of treatment with intravitreal methotrexate. *Scientific reports,* 10**,** 1-7.

132. Wang, F.-z., Zhang, M.-w., Zhang, D.-s., Huang, Y., Chen, L., Jiang, S.-m., Shi, K. & Li, R. 2018. Preparation, optimization, and characterization of chitosan-coated solid lipid nanoparticles for ocular drug delivery. *Journal of Biomedical Research,* 32**,** 411.

133. Weijtens, O., Feron, E. J., Schoemaker, R. C., Cohen, A. F., Lentjes, E. G. W. M., Romijn, F. P. H. T. M. & van Meurs, J. C. 1999. High concentration of dexamethasone in aqueous and vitreous after subconjunctival injection. *American Journal of Ophthalmology,* 128**,** 192-197.

134. Weng, Y., Liu, J., Jin, S., Guo, W., Liang, X. & Hu, Z. 2017. Nanotechnology-based strategies for treatment of ocular disease. *Acta pharmaceutica sinica B,* 7**,** 281-291.

135. Williams, B. K., Jr. & Di Nicola, M. 2021. Ocular Oncology-Primary and Metastatic Malignancies. *Medical Clinics,* 105**,** 531-550.

136. Wong, C. W., Czarny, B., Metselaar, J. M., Ho, C., Ng, S. R., Barathi, A. V., Storm, G. & Wong, T. T. 2018. Evaluation of subconjunctival liposomal steroids for the treatment of experimental uveitis. *Scientific reports,* 8**,** 1-11.

137. Wu, L.-p., Ficker, M., Christensen, J. B., Trohopoulos, P. N. & Moghimi, S. M. 2015. Dendrimers in medicine: therapeutic concepts and pharmaceutical challenges. *Bioconjugate chemistry,* 26**,** 1198-1211.

138. Wu, Y., Liu, Y., Li, X., Kebebe, D., Zhang, B., Ren, J., Lu, J., Li, J., Du, S. & Liu, Z. 2019. Research progress of in-situ gelling ophthalmic drug delivery system. *Asian journal of pharmaceutical sciences,* 14**,** 1-15.

139. Xu, X., Saw, P. E., Tao, W., Li, Y., Ji, X., Bhasin, S., Liu, Y., Ayyash, D., Rasmussen, J. & Huo, M. 2017. ROS-responsive polyprodrug nanoparticles for triggered drug delivery and effective cancer therapy. *Advanced Materials,* 29**,** 1700141.

140. Yadav, M., Schiavone, N., Guzman-Aranguez, A., Giansanti, F., Papucci, L., Perez de Lara, M. J., Singh, M. & Kaur, I. P. 2020. Atorvastatin-loaded solid lipid nanoparticles as eye drops: Proposed treatment option for age-related macular degeneration (AMD). *Drug delivery and translational research,* 10**,** 919-944.

141. Yavuz, B., Bozdağ Pehlivan, S. & Ünlü, N. 2013. Dendrimeric systems and their applications in ocular drug delivery. *The Scientific World Journal,* 2013.

142. Yu, X., Gou, X., Wu, P., Han, L., Tian, D., Du, F., Chen, Z., Liu, F., Deng, G. & Chen, A. T. 2018. Activatable protein nanoparticles for targeted delivery of therapeutic peptides. *Advanced Materials,* 30**,** 1705383.

143. Zhang, J. & Wang, S. 2009. Topical use of Coenzyme Q10-loaded liposomes coated with trimethyl chitosan: Tolerance, precorneal retention and anti-cataract effect. *International journal of pharmaceutics,* 372**,** 66-75.

144. Zielińska, A., Carreiró, F., Oliveira, A. M., Neves, A., Pires, B., Venkatesh, D. N., Durazzo, A., Lucarini, M., Eder, P. & Silva, A. M. 2020. Polymeric nanoparticles: production, characterization, toxicology and ecotoxicology. *Molecules,* 25**,** 3731.

Chapter Three

A pH-responsive poly beta-amino ester nanoparticulate thermo-responsive PEG-PCL-PEG hydrogel for the delivery of interferon alpha to the ocular surface

3.1. Introduction

The management of ocular tumours is mainly through surgery, cryotherapy, radiotherapy, chemotherapy, and immunotherapy (Pe'er, 2015). The first line treatment involves surgical excision employing a no-touch technique with adjuvant cryotherapy (Venkateswaran *et al.*, 2019). However, these strategies are fraught with challenges such as high recurrence rate, vision-threatening side effects (limbal stem cells deficiency, corneal oedema etc.) (Nanji *et al.*, 2013). Additionally, topically applied chemotherapy, which is usually presented as eye drops, is faced with decreased patient compliance, due to the dosing regimen. As a result, immunotherapy using IFN-α2b, is important in the management of ocular surface tumours. IFN-α2b is a cytokine produced in the body with antiviral, antiproliferative, antitumour, and immunomodulatory activities and has been used in management of other types of cancer including malignant melanoma, hairy cell leukaemia, follicular non-Hodgkin's lymphoma and AIDS-related sarcoma (Park *et al.*, 2022; Pestka *et al.*, 2004). The antitumor effect of IFN-α2b is mediated by the JAK-STAT and signal transduction pathways. Cancer cell growth suppression is via cell cycle arrest and apoptosis is regulated by this mechanism. Furthermore, IFN-α2b operates by inhibiting angiogenesis, activating immune cells such as T cells and natural killer cells, and inducing cytokines (Asmana Ningrum, 2014). Application of IFNα-2b is through doses of 1-3 million IU/mL as subconjunctival/perilesional injection/s applied at a single or multiple sites, or via topical application (Galor *et al.*, 2010; Karp *et al.*, 2010). Subconjunctival injections can be safely administered with relative ease and without the need for sophisticated equipment in the clinical setting. However, systemic flu-like symptoms including mild fever and myalgia are common in most patients but are considered mild and well tolerated (Karp *et al.*, 2010). Immunotherapy with IFNα-2b is hindered by its macromolecule size, hydrophilicity, rapid clearance, and degradation at low pH in the tumour microenvironment. Rapid clearance necessitates the administration of high doses, resulting in unwanted complications (Beilharz *et al.*, 2010; Feczkó *et al.*, 2016). Multiple approaches have been investigated for the

delivery of interferons, including coupling of proteins or polymers (e.g. PEG), nanoparticles, microspheres, and hydrogels (Fodor-Kardos *et al.*, 2020; Gulia *et al.*, 2014; Kristó *et al.*, 2020). Pegylated interferon (PEGIFN)-α-2b has been investigated as an approach to limit the rapid clearance of IFN-α2b by the reticuloendothelial system (RES) and reduce immunogenicity (Mehvar, 2000); unfortunately, this is very expensive and complex. Therefore, there remains a need for a simple approach for site-specific and sustained delivery of immunotherapy for the management of ocular malignancies.

The design of a delivery system for immunotherapeutic agents can incorporate specific polymers or ligands to target specialized characteristics displayed by the tumour microenvironment and/or cells of interest for directed delivery of therapeutic agents (Navya *et al.*, 2019). These characteristics include enhanced permeation and retention (EPR) effect, acidic pH of tumour cells, and overexpressed receptors, which are identified on the surface of tumours and known as the “hallmark” of tumours (Kakde *et al.*, 2011). The acidic pH of extracellular tumour is an important characteristic that can be employed for controlled delivery; the pH is within a range of 6.0–7.0, whereas the extracellular pH for normal cells is at 7.4 (Dai *et al.*, 2017). These unique features render it possible to design a platform that protects the bioactive at this pH and releases it in a sustained manner at the tumour sites.

PECE is an amphiphilic copolymer, with poly caprolactone (PCL) as the hydrophobic block and polyethylene glycol as the hydrophilic block. Both PCL and PEG are FDA-approved polymers that have been employed in several formulations due to their biodegradability and biocompatibility (Gong *et al.*, 2009b). Poly (beta amino esters) (PBAE) are a class of copolymers that are cationic in nature, therefore considered appropriate for intracellular delivery of therapeutic genes, proteins, peptides, and anticancer drugs. They offer several advantageous characteristics including low toxicity, biodegradability, efficient cell uptake and facilitate the escape of the cargo from the endolysosomal system owing to their high buffer capacity (Song *et al.*, 2012). The highly positive charge of PBAEs leads to rapid hydrolysis in physiological conditions rendering the NPs unstable in blood (An *et al.*, 2016). PBAEs are synthesised through Michael addition polymerisation of diacrylate esters and primary amines monomer. Modification of the polymers through conjugation with poly(ethylene glycol) or surface modification with polyelectrolyte can minimize the poor stability and

enhance functionality. Previous reports have concluded that surface-modification of PBAE-NPs with HA leads to an enhanced cytotoxicity effect of DOX and prolonged *in vivo* circulation and stability of the NPs (An *et al.*, 2016). Gupta and group reported the conjugation of PBAEs with mPEGA, the stability and release were enhanced by the applied modification of the PBAEs polymer (Gupta *et al.*, 2015).

Aiming to overcome the drawbacks of subconjunctival or perilesional injection of IFN-α2b, the present research proposes the preparation of pH-responsive NPs loaded into a thermo-responsive in-situ hydrogel, designed for site-specific ocular delivery of IFN-α2b. The IFN-α2b was encapsulated into poly(beta amino ester) nanoparticles (PBAE-NPs) and suspended in a poly(ethylene glycol)-poly(caprolactone)-poly(ethylene glycol) hydrogel PECE. The nanoparticles embedded PECE hydrogel matrix with its core-shell structure is expected to enclose the bioactive protecting it from the cursive environment and prolong the release pathway. The system is proposed to display both pH- and thermo-responsive behaviour, gelling following injection into the subconjunctival space of the eye, and release of IFNα-2b in a controlled, sustained manner.

3.2. Materials and methods

3.2.1. Materials

1,4-Butanediol diacrylate (BDDA, Mwt=198.22), poly(ethylene glycol) methyl ether acrylate (mPEGA, Mwt=480), 3-Amino-1-propanol (3AP, Mwt=75.11), poly(ethylene glycol) methyl ether (mPEG, Mn=550), Ɛ-caprolactone (Ɛ-CL, Mwt=114.14), stannous octoate (Sn(Oct)2), and 1,6-hexamethylene diisocyanate (HMDI) were purchased from Sigma Aldrich (St Louis, MO, USA). Human retinal pigment epithelial cells (HRPE) were obtained from ATCC (Manassas, VA, USA), 3-(4, 5-dimethylthiazol-2-yl)-2,5-diphenyl tetrazolium bromide (MTT) were purchased from Sigma Aldrich (St Louis, MO, USA). Dulbecco's modified Eagle medium mixture with Ham's (DMEM F12), Rhodamine phalloidin (RP), DAPI stain, and enzyme-linked immunosorbent assay kit (ELISA) catalogue no BMS216 were purchased from Thermofisher (Vienna, Austria). All other reagents and solvents used were of analytical grade and used as received.

3.2.2. Methods

3.2.2.1. Synthesis and purification of PEG-PCL-PEG triblock copolymer

The di-block polymer PEG-PCL was synthesised through ring opening polymerisation of Ɛ-CL using mPEG as a macro-initiator and stannous octoate $Sn(Oct)_2$ as a catalyst while the triblock copolymer PEG-PCL-PEG was synthesis by using HMDI as a coupling agent as shown in **Figure 3.1**, as previously described by Gong *et al*. (2009a). Briefly, 10.67 mL (0.01 mol) of Ɛ-CL, 5 mL (0.01 mol) of mPEG and 0.5% $^{w}/_{w}$ of $Sn(Oct)_2$ were transferred, under nitrogen, to a three necked round bottom flask mounted on a magnetic stirrer. The reaction was allowed to proceed at 130°C for 12 hrs. Thereafter, the HMDI was added to the reaction flask at 80°C and the reaction continued for 6 hrs. The resulting copolymer mixture was cooled to room temperature, dissolved in dichloromethane (DCM), and subsequently precipitated using petroleum ether. The precipitate was dried under vacuum at room temperature to a constant weight (Gong *et al.*, 2009a).

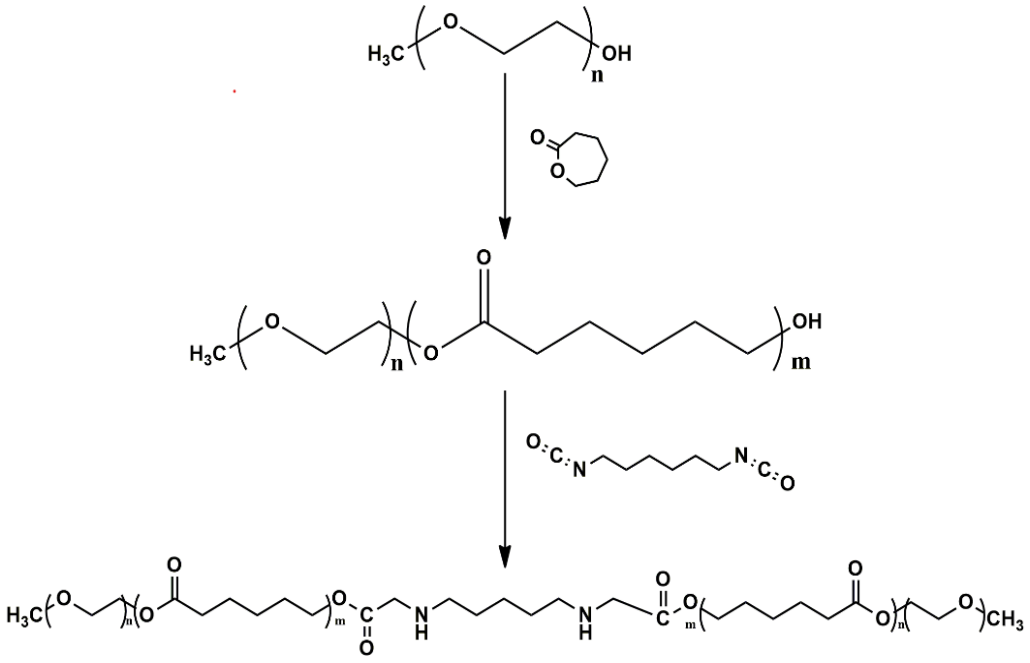


Figure 3.1 Synthetic scheme of PEG-PCL-PEG triblock copolymer.

3.2.2.2. Synthesis of poly (beta-amino ester) copolymer

The poly(beta-amino ester) (PBAE) copolymer was synthesised via Michael addition polymerisation as shown in **Figure 3.2**, from predetermined amounts of 3AP, BDDA, and mPEGA (Liu *et al.*, 2019; Lynn and Langer, 2000). Briefly, predetermined ratios

of 3AP and BDDA were transferred into glass vials containing 5 mL of tetrahydrofuran (THF) to dissolve the mixture. Thereafter, the mixture was transferred to a three-neck round bottom flask containing a solution of mPEGA in 5 mL THF. The reaction flask was mounted on a magnetic stirrer, under nitrogen; the reaction was allowed to proceed at 50°C for 48 hrs. The resulting copolymer mixture was cooled to room temperature, precipitated using a large excess of cold diethyl ether, and dried under vacuum at room temperature to a constant weight.

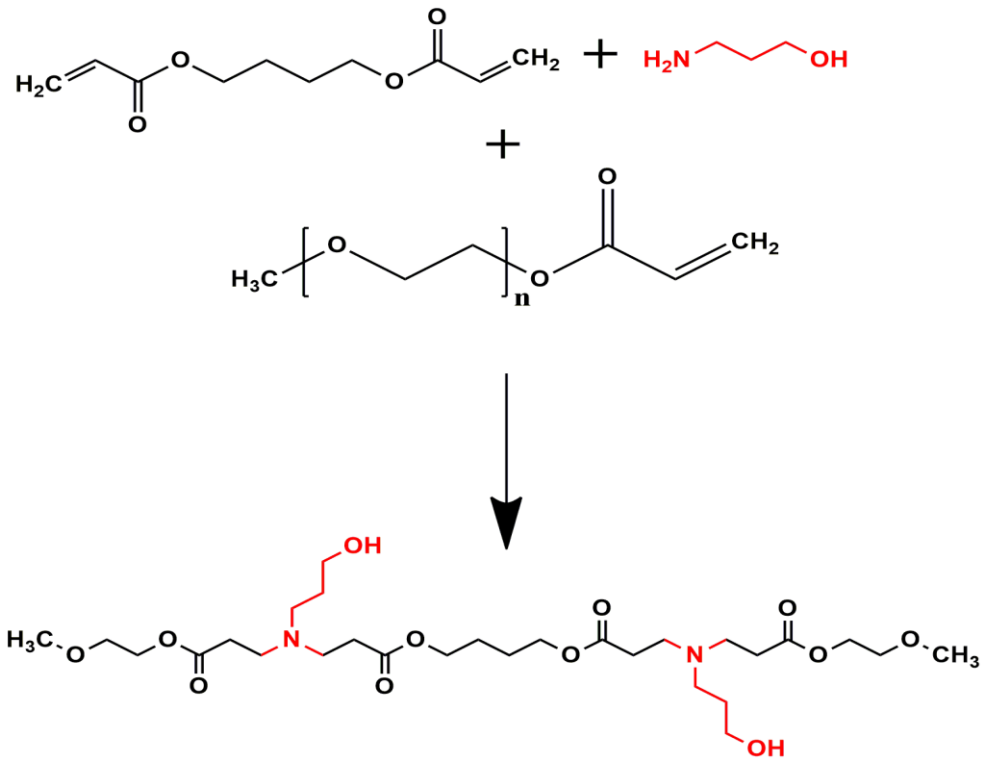


Figure 3.2 Synthetic scheme of PBAE copolymer.

3.2.2.3. Preparation of nanoparticles via the solvent evaporation method

Poly(beta-amino ester) nanoparticles (PBAE-NPs) were prepared using the solvent evaporation approach (Shen *et al.*, 2009). Briefly, 20 mg of the PBAE copolymer was dissolved in 2 mL of acetone. IFN-α2b aqueous solution (200 µL; 1 ng/mL) was added to the organic phase, and the two phases stirred for 30s. This mixture was added dropwise to 5 mL 1% $^{w}/_{w}$ aqueous Span® 20 solution and stirred at 500 rpm for 3 hrs to evaporate the acetone. The dispersed IFN-α2b NPs were stored at -20°C for further analysis. The same procedure applied for preparation of the unloaded PBAE-NPs.

3.2.2.4. Preparation of the PECE hydrogel and NP loaded /PECE hydrogel

The PECE hydrogel was prepared by dissolving the required amount of PECE in deionized water. Thereafter the mixture was heated in a water bath at 55°C for 2 min and cooled, under stirring, in an ice bath to 0°C for 10 min. The NP-loaded PECE hydrogels NP/PECE were prepared by adding the required amount of the NPs into the PECE solution under stirring. The percentage of the NPs in the NP/PECE composite was expressed as the mass ratio of the NPs (W_{NPs}) to the total mass of the solid component ($W_{NPs} + W_{PECE}$).The IFNPH were prepared by adding the IFN-α2b loaded NPs to the PECE hydrogel solution with stirring.

3.2.2.5. Fourier transform infrared spectroscopy (FTIR)

The functional groups appearing as a result of molecular transitions in the structures of the copolymers and their starting materials were recorded using Fourier-transform infrared (FTIR) spectroscopy using a spectrophotometer (PerkinElmer Spectrum 100, Beaconsfield, United Kingdom). FTIR spectra scans were obtained in the region of 4000-650 cm^{-1} with a resolution of 4 cm^{-1}.

3.2.2.6. ^{1}H-Nuclear Magnetic Resonance analysis

^{1}H-nuclear magnetic resonance (^{1}H-NMR) analysis was undertaken using a 400 MHz spectrometer (300, Bruker, Switzerland) and deuterated chloroform ($CDCl_3$) as a solvent to confirm the synthesis of the copolymers.

3.2.2.7. X-ray powder diffraction (XRPD) analysis

The degree of crystallinity of the lyophilized PECE copolymer, PECE-1 and PECE-2 were analyzed using XRPD spectra (Rigaku MiniFlex 600, Tokyo, Japan). The 2θ scan from 30-90°C was selected at a scanning rate of 10°/min to determine the diffractogram of the samples.

3.2.2.8. Differential scanning calorimetry (DSC)

The thermal behaviour of PECE copolymer, PECE-1 and PECE-2 (refers to 25% PECE hydrogel and PBAE-NPs/ 25% PECE, respectively) were analyzed employing a differential scanning calorimeter (DSC) (Mettler Toledo, Greifensee, Switzerland) equipped with STARe SW software. The lyophilised samples were weighed and

placed into aluminium crucibles. The samples were subjected to a heating cycle from 0-70°C and cooled from 70 to 0°C with a heating rate of 3°C/min under the flow of nitrogen.

3.2.2.9. Thermogravimetric (TGA) analysis

The thermal degradation of PECE copolymer, PECE-1 and PECE-2 was analysed using a thermogravimetric analyser (TGA) (PerkinElmer, TGA 4000, Llantrisant, Wales, UK). The lyophilized samples were subjected to a heating gradient from 30-900°C with a heating rate of 10°C/min under the flow of nitrogen.

3.2.2.10. Particle size distribution, polydispersity index (PDI), and zeta potential analysis

The dimensions of the unloaded and loaded NPs were measured by dynamic light scattering (DLS) using a Malvern ZetaSizer Nano ZS (Malvern Instruments Ltd., Worcestershire, UK) at 25°C. The particle size, zeta potential and PDI were measured in disposable cuvettes. Sample measurements were conducted in triplicate, and the mean value was reported accordingly.

3.2.2.11. Evaluation of drug entrapment efficiency of IFN-α2b loaded nanoparticles

The encapsulation efficiency (EE) of IFN-α2b in the nanoparticles was measured indirectly. The loaded nanoparticle suspension (2 mL), were centrifuged for 25 min at 30,000g. The concentration of IFN-α2b in the supernatant was measured using an ELISA kit (catalog no BMS216), the assay was carried out in accordance with the manufacturer's instructions. The absorbance was measured at 450 nm as the primary wavelength, 620 nm as reference wavelength using a Victor 30X plate reader (PerkinElmer, Biocompare, San Francisco, USA). The procedure was conducted to determine the percentage encapsulation efficiency (% EE) via the **Equation 3.1.**

$$\% \text{ EE} = \frac{\text{Total quantity of IFN}\alpha\text{2b} - \text{Quantity of free IFN}-\alpha\text{2b}}{\text{Total quantity of IFN}-\propto\text{2b}} \times 100 \ldots\ldots\ldots\ldots\ldots \textbf{(3.1)}$$

3.2.2.12. Morphological analysis

Transmission electron microscopy

High Resolution Transmission Electron Microscopy (TEM) (version TECNAIF3OST-TEM software) was employed for the imaging of the PBAE-NPs. The nanoparticle suspension was drop-cast on a carbon-coated copper grid. Samples were allowed a 5 min contact time before removing the excess nanoparticles suspension using filter paper. Finally, air-drying of the samples was allowed overnight at 25°C before observation under the microscope.

Scanning electron microscopy (SEM)

The surface morphology of the prepared PBAE-NPs, PECE-1, and PECE-2 were studied using the SEM analysis (SIGMA VP, Zeiss Electron Microscopy, Carl Zeiss Microscopy Ltd; Cambridge, UK). A drop of the samples were placed on aluminium stubs and allowed to dry. These were subsequently sputter-coated with palladium gold prior to SEM imaging.

3.2.2.13. Porositometric and surface topography analysis

The surface area, pore size and pore volume were analysed employing the Brunauer–Emmett–Teller (BET) theory and the Barrett, Joyner and Halenda model (BJH). Lyophilized samples of PECE copolymer, PECE hydrogel and NPs/PECE were analysed using a Porositometric analyzer (Micromeritics ASAP 2020, Norcross, GA, USA). A sample weight of (0.1-0.3 g) was transferred to a sample tube and degassed. Thereafter, the sample tube was transferred to the analysis port for determination of the surface area, pore volume and pore size in accordance with the BET and BJH models. The analysis was conducted under an evacuation rate of 50 mm Hg/s with a temperature rate of 10°C, target temperature of 40°C and hold temperature at 30°C for 900 min under nitrogen.

3.2.2.14. Rheological characterisation of the hydrogels

The physico-mechanical properties of the PECE hydrogel as a function of temperature were evaluated using rheometer (Haake Modular Advanced Rheometer System, Thermo Fisher Scientific, Germany). For each hydrogel sample, an appropriate volume was loaded between the two parallel plates of the Rheometer with steel cone-

plate geometry of (35 mm, with gap distance of 0.052 mm). In oscillatory mode the ($T_{sol-gel}$) of the formulations was measured employing the temperature ramp analysis. The experiment was performed within a range of 20°C to 50°C at a constant frequency of (1.0Hz) and a heating rate of 1°C/m. The storage modulus (G') and the loss modulus (G") were calculated using the RheoWin 480,00 (Haake®) software. The oscillatory stress sweeps were performed at a range from (0,07 to 200 Pa) at a constant frequency of (1.0Hz).

3.2.2.15. Syringeability of the hydrogels

The injectability of the hydrogels was investigated using a texture analyser (Stable Micro System TA-XT2, Surrey, UK). The tests were performed in compression mode using 21 G needles. The syringe was placed in a holder perpendicularly with the needle downward. A cylinder probe (P/50 R) was lined to the surface area of the plunger plate to extrude the hydrogel from the syringe. The test was conducted at a speed of 1 mm/s for a distance of 20 mm. The maximum force used to extrude the content of the syringe out was recorded (Cilurzo *et al.*, 2011; Zhang *et al.*, 2018).

3.2.2.16. *In vitro* release analysis of IFN-α2b from IFNPs and IFNPH

Interferon alpha release from IFN-α2b loaded PBAE-NPs (IFNPs) and IFN-α2b nano-embedded PECE hydrogel (IFNPH) was determined in phosphate buffer saline (PBS) at different pH values (6.6 and 7.4) simulating tumour pH and normal physiological conditions, respectively, with 0.02% Tween 80. The surfactant was added to prevent adsorption of IFN-α2b to the surface of the container. Briefly, the 2 mL of the IFNP suspension was transferred directly into the release medium. At specific time intervals (1, 2, 4, 8, 12 and 24 hrs), a 200 µL sample was withdrawn for analysis and replaced with an equivalent amount of pre-warmed release medium to maintain sink conditions. Release from IFNPH was conducted as follows: 0.5 mL of the precursor polymer solutions was transferred and pre-heated at 37°C for a few minutes for hydrogel formation and immersed thereafter within the release medium. At specific time intervals (1, 3, 7, 12, up to 14 days), 200 µL samples were withdrawn for analysis and replaced with an equivalent amount of pre-warmed release medium to maintain sink conditions. The vials were placed in a thermostatically-controlled orbital shaking incubator (type LM-530, Yihder Technology Co., LTD.) set at 25 rpm at 37 ± 1°C. Samples were centrifuged at 13000 rpm for 10 min, the supernatant was analysed for

IFN-α2b release using an ELISA kit, measured at 450 nm, and reference wavelength of 620 nm using a Victor 30X plate reader (PerkinElmer, Biocompare, San Francisco, USA). The quantity of IFNα-2b release was calculated from a standard linear curve of IFN-α2b in PBS (pH 7.4), refer to Appendix A.

3.2.2.17. Degradation analysis of formulations

Hydrogel degradation studies were performed under simulated in vitro conditions. Samples of PBAE-NP embedded into PECE hydrogels (NPH) were prepared by weighing 6 g of each sample into vials containing 5 mL PBS pH (6.6 and 7.4), which were placed in an orbital shaking incubator maintained at 37°C set at 50 rpm. The degree of degradation was measured at 1, 3, 7 and 14 days via measurement of the transitions in sample mass. Excess fluid was removed, and the samples weighed and left to air dry for 72 hrs to ensure complete removal of moisture before obtaining the second weight to determine the eroded mass. The percentage of degradation was subsequently measured using **Equation 3.2.**

$$\%\, Degradation = \frac{W_i - W_t}{W_i} \times 100 \quad \text{..... (3.2)}$$

Where W_t represents the mass of the dried samples at the different time points, W_i represents the initial mass of the samples at the different time points.

3.2.2.18. *In vitro* cytotoxicity analysis

The cell viability and cyto-compatibility of IFN-α2b, PBAE-NPs, PECE-1 and IFNPH in a primary Human retinal pigment epithelial cell line (HRPE) was evaluated using a 3-(4,5-dimethylthiazol-2-yl)-2,5-diphenyl tetrazolium bromide (MTT) cell viability assay. The cells were maintained in culture medium DMEM/ Hams F12 (1:1) supplemented with 10% fetal bovine serum albumin (FBS) and 1% penicillin-streptomycin, the culturing condition was 95% humidity, 5% CO_2 at 37°C. The growth medium was replaced every 48 hrs with fresh medium until the cells reached ~80-90% confluence. The HRPE were seeded in 96-well plates with a seeding density of 1 x 10^5 cells/well. After 24 hrs, the cells were treated with PECE hydrogel, NPs, IFN-α2b and IFNPH in concentration range of (0-1000 µg/mL) in triplicates. Samples of the IFN-α2b, PBAE-NPs, PECE and IFNPH were sterilized by UV light prior to analysis. The hydrogel samples PECE-1 and IFNPH were placed in 1.5 mL centrifuge tubes covered by the

culture medium and incubated in an orbital shaking incubator-horizontal (type LM-530, Yihder Technology Co., LTD.) set at 25 rpm for 7 days at 37°C. A volume of 200 µL of the medium was sampled and used to treat the cells. Following 24 and 48hrs of treating, 10 µL of MTT reagent (Merck, Darmstadt, Germany) was added, followed by 4hrs incubation at 37°C. Thereafter, 100 µL of the solubilising buffer was added to dissolve the formazan crystals. The culture medium and 5% $^{v}/_{v}$ DMSO served as the negative and positive controls, respectively, and the untreated wells served as the blank. The absorbance of the developed purple crystals was measured at 570 nm using a Victor 30X plate reader (PerkinElmer, Biocompare, San-Francisco, USA). The percentage cell viability was subsequently measured using **Equation 3.3.**

$$\%\, Cell\ viability\ = \frac{A_{sample} - A_{blank}}{A_{control} - A_{blank}} \times 100 \quad \text{..... (3.3)}$$

Where A_{sample} represents the absorbance of the cells incubated with the different samples, A_{blank} absorbance of the cells in the absence of treatment and $A_{control}$ is the absorbance in the cells treated with the culture medium alone.

3.2.2.19. Assessment of bioactivity of the released IFNα-2b from IFNPH

The bioactivity of the released IFNα-2b was determined by the antiproliferative effect on a A172 glioblastoma cell line. The Human cells were maintained in DMEM culture medium supplemented with 10% fetal bovine serum albumin (FBS) and 1% penicillin -streptomycin, the culturing condition was 95% humidity, 5% CO2 at 37°C. The growth medium was replaced every 48 hrs with fresh medium until the cells reached ~80-90% confluence. The A172 were seeded in 96-well plates with a seeding density of 6 x 105 cells/well. After 24 hrs, the cells were treated with the released IFNα-2b in triplicate. The assay was conducted under aseptic conditions the collection of the release samples was conducted under laminar flow. The antiproliferative effect of the released IFNα-2b was measured using an MTT assay.

3.2.2.20. Statistical analysis

All experiments were carried out in triplicates, and the results were expressed as the mean ± standard deviation (SD). The data was analysed using the GraphPad Prism Software (Version 5 for Windows, GraphPad Software, San Diego, California, USA).

The difference between groups was assessed using an analysis of variance (two-way ANOVA) among three groups or a student's t-test between two groups. A p-value of ≤ 0.05 was regarded as statistically significant.

3.3. Results

3.3.1. Assessment of the structural modification and integrity

The chemical characteristics of the native polymers and synthesised products were investigated using FTIR. As shown in **Figure 3.3 A**, the PECE triblock copolymer was characterized by an absorption peak at 1722 cm^{-1}, attributed to the strong C=O stretching band of the ester bond. The absorption peaks at 2940 cm^{-1} and 2865 cm^{-1} represent the C-H stretching vibration. The absorption peak at 1527 cm^{-1} corresponds to the N-H bending vibration, confirming the formation of the PECE triblock copolymer. This is further confirmed by the disappearance of the absorption peak at 2250 cm-^{1} which corresponds to the –NCO groups of HMDI, indicating the coupling of the –OH with the –NCO group, as documented in other studies (Gong *et al.*, 2009a; Gong *et al.*, 2009b). Further, the copolymer was characterised by ^{1}H-NMR to confirm the synthesis of the PEG-PCL-PEG triblock copolymer. As evident in **Figure 3.3 B**, the sharp absorption peaks at 3.6 and 3.38 ppm represent the methylene proton of CH_2CH_2O– and –OCH_3 end groups in PEG blocks, respectively. The peaks at 1.39, 1.65, 2.32, and 4.06 ppm are attributed to the methylene protons of -$(CH_2)_3$, -$OCCH_2$, and -CH_2OOC- in the PCL block, respectively. The methylene protons of -O-CH_2-CH_2- in PEG end blocks linked with the PCL blocks appear as weak peaks at 4.2 and 3.70 ppm. The findings correlate with previous studies signifying the successful synthesis of the PECE triblock copolymer (Gong *et al.*, 2009b).

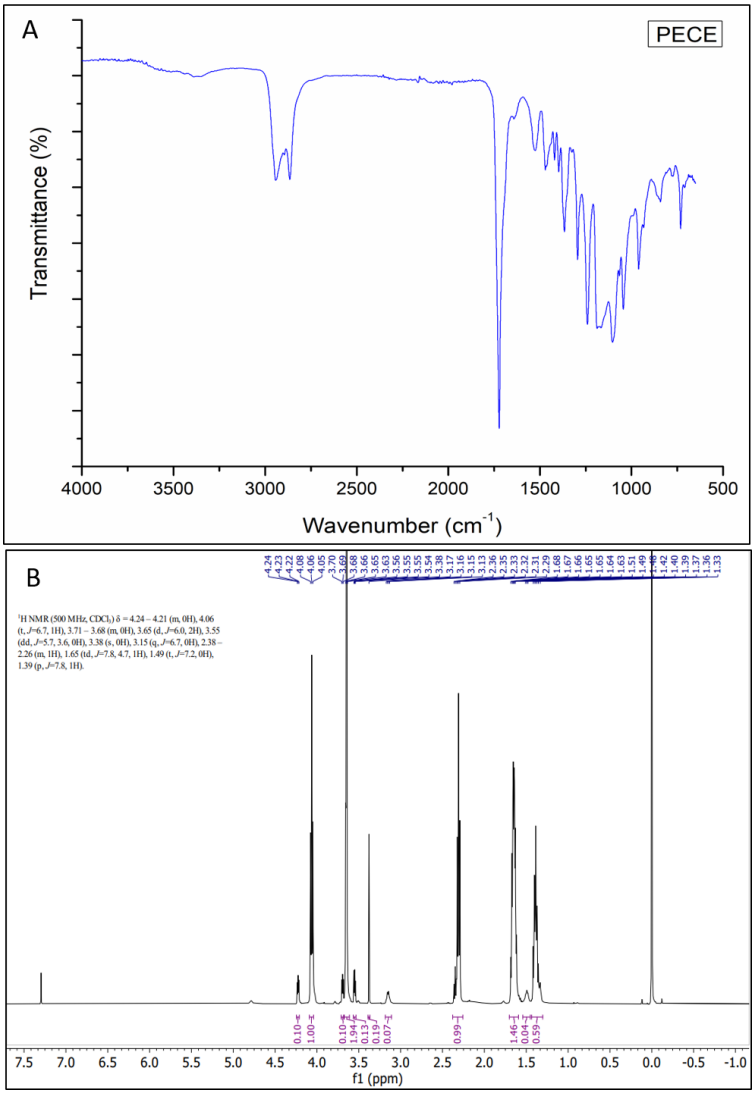


Figure 3.3 A) FTIR of PECE; B) H-NMR of PECE.

The chemical structure of the PECE copolymer and prepared hydrogels 25% $^{w}/_{v}$ PECE hydrogel (PECE-1), and nano-embedded 25% $^{w}/_{v}$ PECE hydrogel (PECE-2) showed no change in the characteristic bands indicating the change was only in the physical state of the matter from solid to hydrogel. From **Figure 3.4 A** the same characteristics peaks were detected in the hydrogel and NP-loaded hydrogel. Additionally, the crystal characteristics of the samples were evaluated using XRPD technique. This analysis was carried out for all samples (PECE copolymer, PECE-1, and PECE-2). As shown in **Figure 3.4 B**, the XRPD was analysed to ascertain the crystalline structure of the PECE copolymer. Two main diffraction peaks at ~2θ-21° and 23, were identified corresponding to PCL blocks and PEG blocks, respectively, indicating the crystalline nature of both. These peaks were also visible in the hydrogel and the NP-loaded PECE with a slight decrease in intensity. This observation suggested that the crystalline

structure of PCL is not affected, neither during the hydrogel formation nor upon the NPs loading. Meanwhile, the PEG diffraction peak intensity weakens upon hydrogel formation and loading of the NPs, suggesting that the crystallisation ability of PEG blocks decrease upon hydration. As reported in other studies, the formation of micelles by PEG copolymers in water is hindered due to the excessively long molecular chains and structural characteristics (Lee *et al.*, 2001; Wu *et al.*, 2020), resulting in the formation of a hydrogel with a core-shell structure that reduces direct exposure of the IFN-loaded NPs to the medium and prolongs IFN release acting as a shield and ultimately creating a sustained release platform.

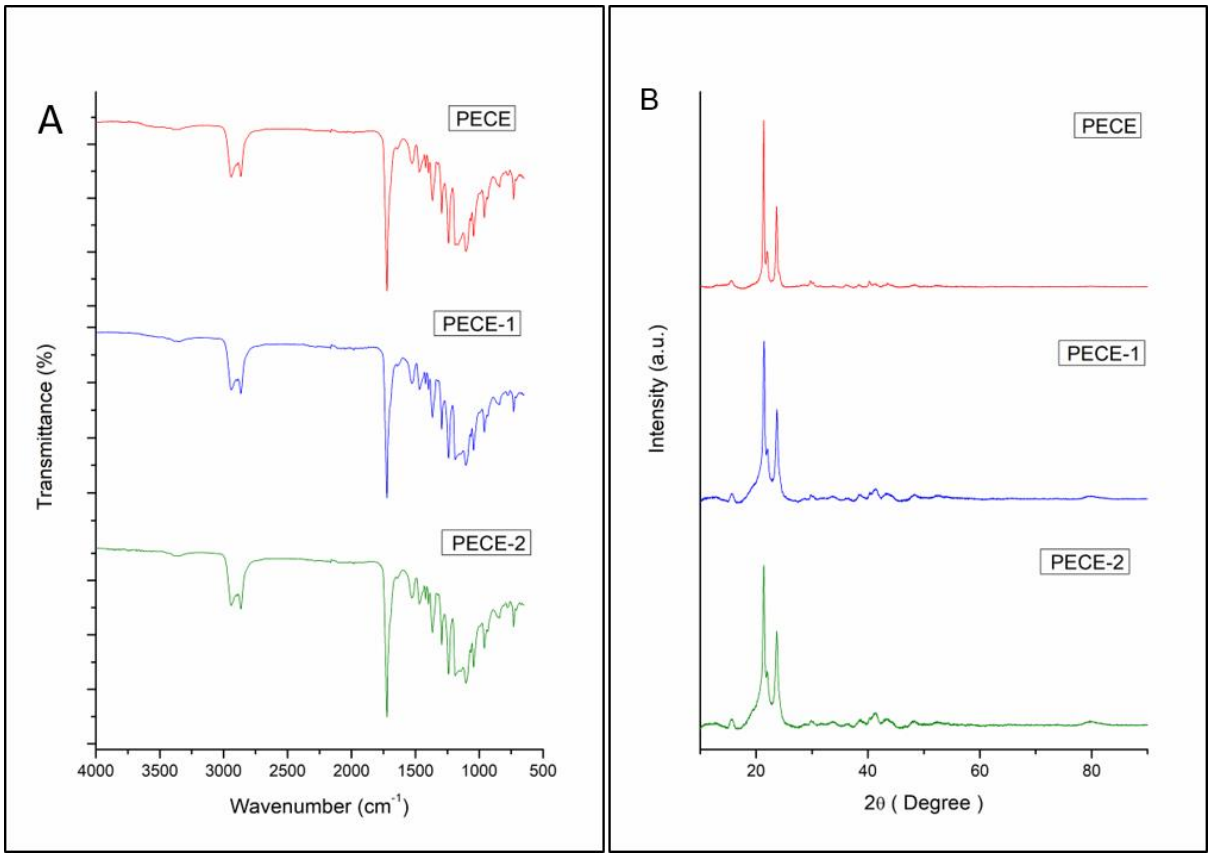


Figure 3.4 A) FTIR of PECE, PECE-1 and PECE-2; B) XRPD images of PECE, PECE-1 and PECE-2.

3.3.2. Evaluation of the thermal behaviour of the hydrogels

Differential scanning calorimetry (DSC) analysis was conducted to evaluate the transitions in the formulated hydrogels thermal behavior compared to the native components. **Figure 3.5** depicts the thermal curves of PECE copolymer, PECE-1 and PECE-2. Endothermic peaks were observed at 36°C and 48°C for the PECE

copolymer. The two endothermic peaks correspond to the melting of PEG and PCL, respectively, in the dry state. In the hydrated state of PECE-1 and PECE-2, a single endothermic peak was observed at ~48°C corresponding to the melting point of PCL. Meanwhile, endothermic peaks representative of the melting points of PEG and the NPs peaks were not evident due to their amorphous nature. The hydrophilic nature of PEG rendered it completely soluble in water at room temperature, hence no melting peak of PEG was evident in the hydrogel. **Figure 3.5** depicts the cooling process of all the samples from 70°C to 0°C; single exothermic peaks were observed for all the samples. The peaks indicate the crystallization of the samples occurring at ~18-20°C increased in the hydrogel state and slightly decreased upon the addition of the NPs. The decrease in the crystallization temperature upon addition of the NPs to the hydrogel is proposed to be due to disruptions of the PECE chain. Similar results have been reported, where addition of different concentrations of nano-hydroxyapatite powder to a PECE copolymer hydrogel resulted in a decrease in the crystallization temperature (Fu et al., 2009). Thermogravimetric analysis **Figure 3.6** was conducted to investigate the thermal stability of the PECE copolymer and hydrogels (PECE-1, PECE-2). The TGA thermogram demonstrates that the PECE copolymer commenced with decomposition at 290°C, PECE-1 at 282°C, and PECE-2 at 291°C. The decomposition curve of all three demonstrated a major weight loss (95%), in the temperature range from 280°C to 460°C. The similarity in decomposition profiles signifies that the hydrogel preparation would not affect the chemical composition of the PECE copolymer and that loading of NPs would not negatively affect the thermal stability.

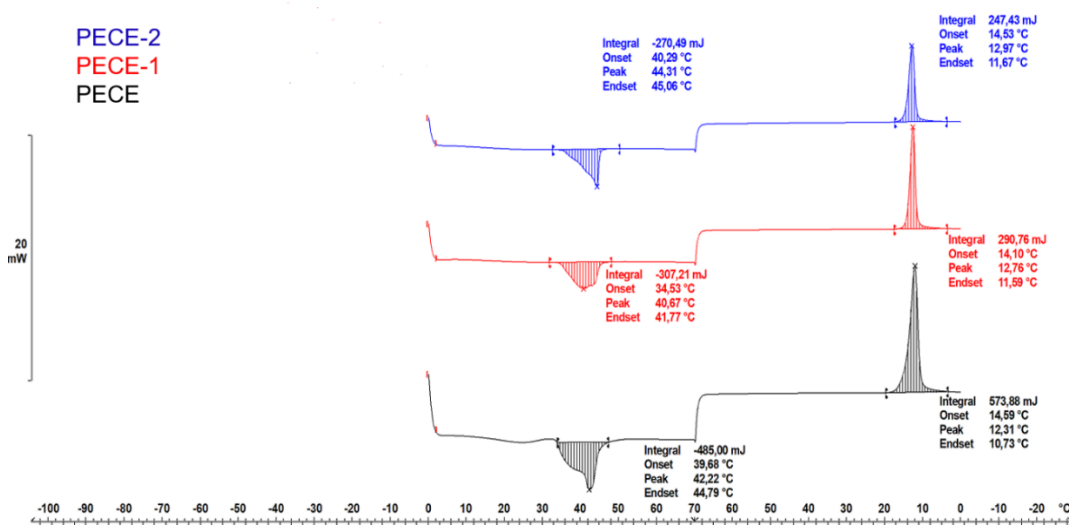


Figure 3.5 DSC thermograms of the PECE copolymer, PECE-1 and PECE-2.

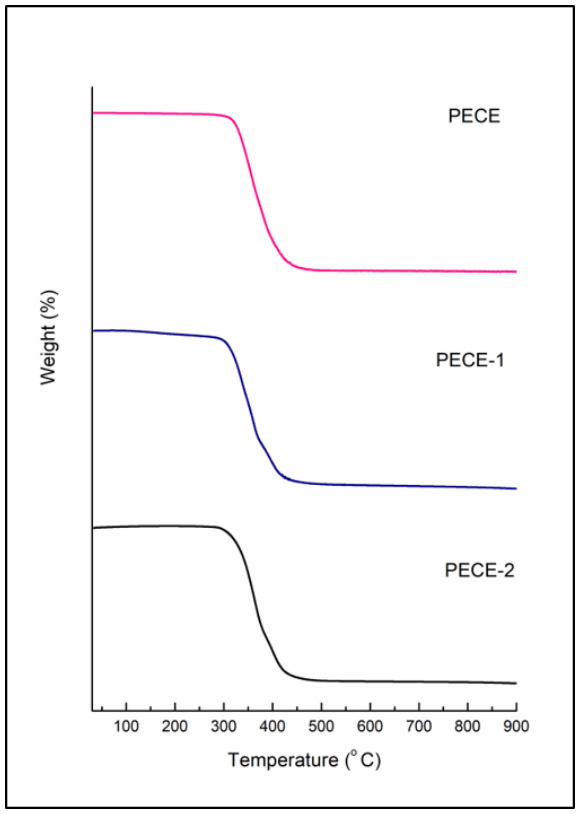


Figure 3.6 TGA thermograms of PECE, PECE-1 and PECE-2.

3.3.3. Particle size and distribution, zeta potential and entrapment efficiency of the nanoparticles

Table 3.1 displays the particle size of the NPs and IFN-α2b loaded PBAE-NPs (IFNPs) to be 137.1 and 151 nm, respectively, demonstrating that the size increased with IFN-α2b loading and that the prepared NPs are within a good particle size range. Additionally, the PDI of the nanoparticles was reported to be 0.270 and 0.148 for the NP and IFNPs, respectively. The low PDI is an indication of the acceptably narrow size range distribution of the NPs. The zeta potential indicates the stability of colloidal dispersions; the higher the zeta potential values (above +20 mV and below -20 mV), the more NPs would resist aggregation. The zeta potentials were -23.9 and -16.4 mV for the NPs and IFNPs, respectively. **Table 3.1** further shows the entrapment efficiency of the IFNPs. The NPs achieved a high entrapment efficiency of 89% for IFN-α2b.

The pH value of the media affected the size, PDI and zeta potential of the drug free NPs. As evident in **Table 3.2**, the size changed in response to the acidic environment. As the pH value was adjusted to a more acidic environment from pH 7.4 to a weakly acidic tumour pH of 6.6 the size increased from ~180 to 216 nm with a narrow size distribution, while the zeta potential became more positive, from -11.4mV at physiological pH to - 6mV at pH 6.6. The increase in size suggested the presence of a stable expanded core-shell structure that underwent protonation in the presence of an acidic environment. The TEM images of the NPs displayed a spherical morphology with an average size of ~100 nm as evident in **Figure 3.7**. The decrease in size in the microscopic analyses was attributed to differences in the measuring environment, whereby TEM measurements were in the dry state and DLS in the hydrated state.

Table 3.1 Particle size, PDI and zeta potential of unloaded and loaded nanoparticles and drug entrapment efficacy of loaded nanoparticles.

Sample	Size (nm)	PDI (a.u)	Zeta potential (mV)	% EE
NP	137.1 ± 0.47	0.270 ± 0.002	-23.9 ± 0.58	-
IFNP	151 ± 1.46	0.148 ± 0.03	-16.4 ± 0.25	89 ± 0.35

Note: Values are expressed as (n= 3, mean ± SD).

Table 3.2 Effect of pH of the medium on the size, PDI and zeta potential of the drug free NPs.

Formulation/ media	Size (nm)	PDI (a.u)	Zeta potential (mV)
NP/ H_2O	137.1 ± 0.47	0.270 ± 0.002	-23.9 ± 0.58
NP/ PBS 7.4	179.9 ± 1.72	0.115 ± 0.12	-11.4 ± 0.61
NP/ PBS 6.6	216.9 ± 4.70	0.079 ± 0.009	-6.12 ± 1.05
NP/ PBS 5.5	230.6 ± 5.62	0.137 ± 0.018	-3.36 ± 0.67

Note: Values are expressed as (n= 3, mean ± SD).

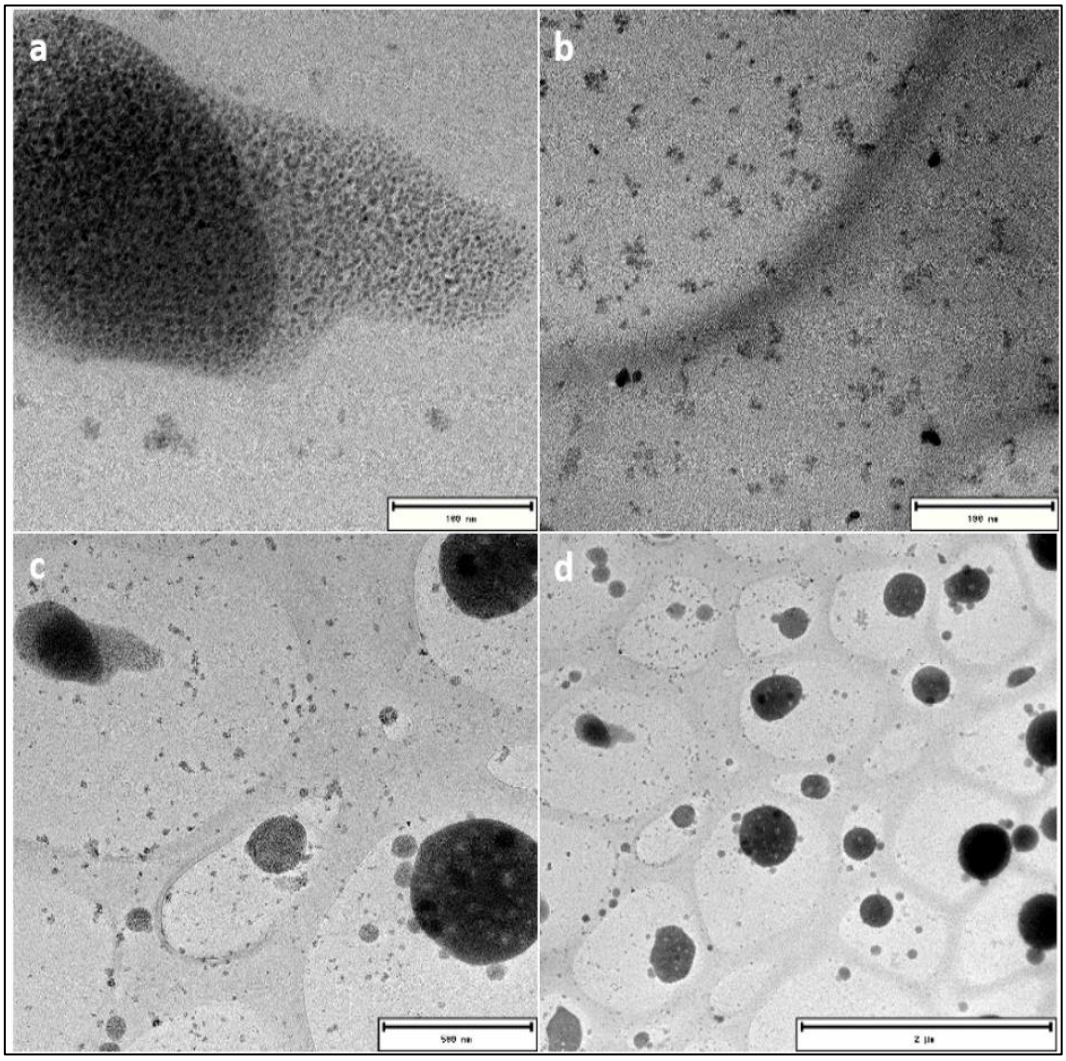


Figure 3.7 TEM images of PBAE nanoparticles. The scale bar for (a) and (b) is 100 nm, for (c) 500 nm and for (d) 2 µm of the drug free NPs.

3.3.4. Assessment of surface morphology of the hydrogels

The SEM images of the PECE hydrogel depicted in **Figure 3.8** indicate the presence of a porous structure, which acted as a matrix for the NPs. SEM has been the gold standard in the evaluation of surface topography. Nevertheless, comparison between data is difficult due to the qualitative nature of the results (Nguyen *et al.*, 2011). The porosity analysis discussed hereunder supported the SEM results, further confirming the matrix-like structure of the hydrogel and the IFNPH.

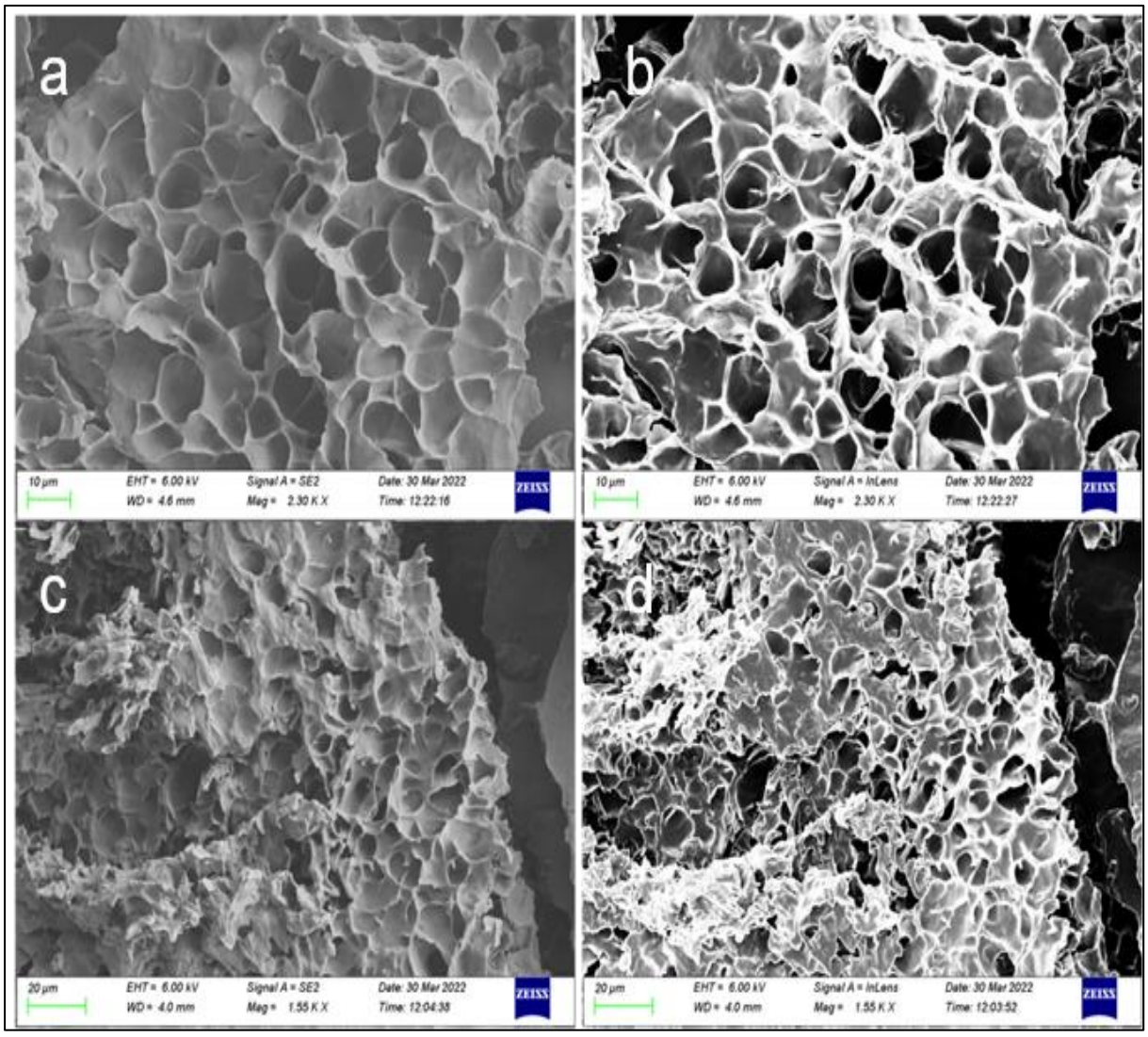


Figure 3.8 SEM images of PECE-1 (a) and (b) at 10 µm, PECE-2 (c) and (d) at 20 µm.

3.3.5. Assessment of the porosity profile of the hydrogels and NP-loaded hydrogels

The hydrogels' porositometric analysis indicated differences in surface area, pore volume, and pore size when generated with varied concentrations of PECE and constant NP loading. A degree of porosity is vital for the diffusion of the NPs from the hydrogel, and hence drug release. **Table 3.3** displays the results of porosimetric examination on hydrogels containing two concentrations of PECE: 25% $^{w}/_{v}$ and 30% $^{w}/_{v}$, as well as hydrogel samples loaded with PBAE NPs. The results listed display that PECE-1 exhibited a larger pore size and volume, but a smaller surface area compared to PECE-2. The presence of the NPs within PECE-2 decreased the pore size and increased the total surface area. The pore size and pore volume contributed to the cumulative surface area on the hydrogel surface pores whereby the increase in pore diameter and depth increases the pore surface area while decreasing the BET total surface area (Ramburrun *et al.*, 2015). However, the increase in PECE concentration to 30% $^{w}/_{v}$ for the PECE-3 resulted in a decline in pore size with a high BET surface area. PECE-4 exhibited a higher pore size and a smaller surface area as compared to the PECE-3 hydrogel. The lower BET surface area of the PECE-4 compared to that of the PECE-3, despite the formation of pores, may further suggest that the pore formation occurs only on the surface of the hydrogels and not throughout the entire hydrogel.

In the context of physisorption, pores expressed by materials can be categorised according to their size into macro- (>50 nm), meso- (2-50 nm) and micropores- (<2 nm). The adsorption isotherms provide insightful information regarding pore size distribution (Groen *et al.*, 2003; Sing, 1985). According to this classification, the pore size distribution for 30% hydrogels (PECE-3 and PECE-4) lies within the macropore range while the 25% hydrogels (PECE-1 and PECE-2) lies within the mesoporous range **Table 3.3**. The PECE-3 and PECE-4 hydrogels exhibited a Type II isotherm with a H3 hysteresis loop indicating a monolayer-multilayer adsorption of a macroporous material (Sing, 1985). The PECE-1 and PECE-2 hydrogels exhibited a Type III isotherm with a H3 hysteresis loop suggestive of the presence of a multilayer material with complete pore filling including capillary condensation that occurs in the presence of mesopores (Groen *et al.*, 2003; Sing, 1985). The presence of H3 hysteresis loop indicates the presence of an interconnected pore system of specialised

distribution within the hydrogel matrix (Groen *et al.*, 2003). Similar results were visualised on the SEM images. The interconnection of pores is vital for the diffusion of liquid within the hydrogel allowing the diffusion of the NPs out of the hydrogel, and subsequent drug release.

Table 3.3 Porositometric analysis of lyophilised PECE hydrogels and nanoparticulate-loaded PECE hydrogels.

Porositometric Parameters	**PECE-1**	**PECE-2**	**PECE-3**	**PECE-4**
Surface Area				
Single point surface area (m^2/g)	0.1637	0.2112	0.2330	0.2085
BET Surface Area (m^2/g)	0.1462	0.2088	0.4479	0.2398
BJH Adsorption cumulative surface area of pores between 17.000 Å and 3000.000 Å diameter (m^2/g)	0.032	0.084	0.272	0.355
BJH Desorption cumulative surface area of pores between 17.000 Å and 3000.000 Å diameter (m^2/g)		0.1172	0.2823	
Pore Volume				
Single point adsorption total pore volume of pores (cm^3/g)	0.001478	0.00032	0.00075	0.003647
BJH Adsorption cumulative volume of pores between 17.000 Å and 3000.000 Å diameter (cm^3/g)	0.002437	0.00222	0.00126	0.003468
BJH Desorption cumulative volume of pores between 17.000 Å and 3000.000 Å diameter (cm^3/g)	0.002500	0.00217	0.00125	
Pore Size				
Adsorption average pore width (4V/A by) (Å)	1916.746	61.5310	67.1867	608.3260

BJH Adsorption average pore diameter (4V/A) (Å)	98.191	1054.71	185.162	390.541
BJH Desorption average pore diameter (4V/A) (Å)	47.168	742.370	177.708	

Note: PECE-1 (25% $^{w}/_{v}$ hydrogel), PECE-2 (NP loaded into 25% $^{w}/_{v}$ hydrogel), PECE-3 (30% $^{w}/_{v}$ hydrogel) and PECE-4 (NPs loaded into 30% $^{w}/_{v}$ hydrogel).

3.3.6. Assessment of rheological properties of the hydrogels

The sol-gel transition of PECE hydrogels at different concentrations was studied to confirm the suitability of the system for application at body temperature. **Figure 3.9** visually presents the temperature-dependent sol-gel transition of the PECE hydrogel with PBAE NPs loading at a hydrogel concentration of 25% $^{w}/_{v}$ using the test-tube inversion method. The sol-gel transition of the PECE was concentration-dependent, below which the transition will not occur; this is referred to as the critical gelling concentration (CGC), which in this case is 15 % $^{w}/_{v}$. The sol-gel transition of 20% $^{w}/_{v}$ PECE was transient with a window i.e., between 26°C and 44°C. Further increasing the concentration broadened the sol-gel transition window with increasing temperature. As evident in **Figure 3.10 (b)**, the window shifted from 26°C to 24°C and from 44°C to 47°C at 20-25% $^{w}/_{v}$. The loading of the NPs into the hydrogel resulted in a slight decrease in the transition temperature from 26°C to 25°C. The 20% $^{w}/_{v}$ PECE had a transient sol-gel window between 26°C and 44°C. This concentration was selected as the preferred concentration based on the ease of preparation, ease of administration, and minimal discomfort upon the administration, which is discussed in further details in the section below.

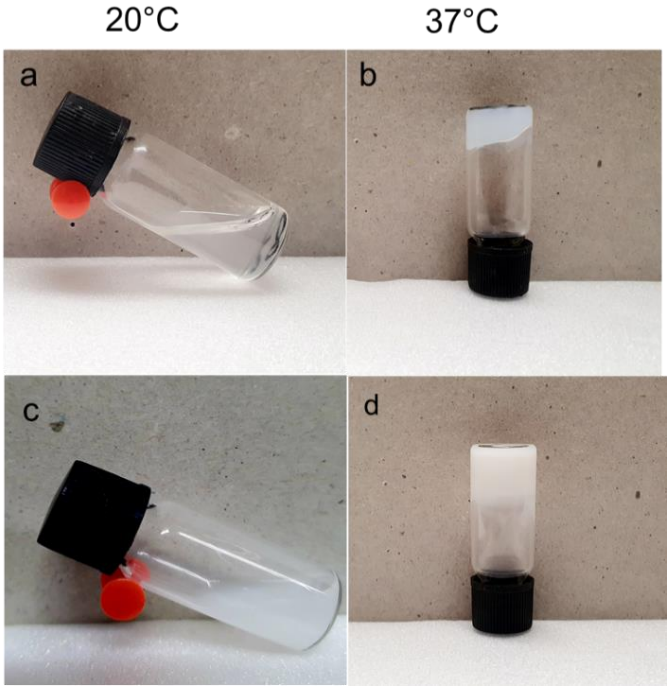


Figure 3.9 Photographic images of the sol-gel transition of hydrogels at room and body temperature (a) solution of PECE-1, (b) gel of PECE-1 and (c) solution of PECE-2, (d) gel of PECE-2.

Moreover, the storage modulus (G′) and the loss modulus (G″) signifying the elastic and viscous behaviour, respectively, were monitored as a function of temperature. In **Figure 3.10 (a, b)**, the G″ was higher than G′ at low temperature, corresponding to the sol state. As the temperature increases a crossover, around 24°C from sol state to gel state (lower transition), the G′ was equal to the G″. At the second crossover above 42°C (upper transition), the PECE transitioned from gel state to sol state.

The viscosity increased as the temperature increased, depicted in **Figure 3.10 (d)**, further confirming transition from sol state into gel state. Additionally, the viscosity demonstrated a concentration-dependent manner, as evident in **Figure 3.10 (e)**. The oscillatory stress sweep measurement on PECE-1 and PECE-2 further confirmed the hydrogel formation. The hydrogels, within their linear viscoelastic region approaching

100 Pa in terms of shear stress, demonstrated that the elastic modulus G′ dominated the viscous modulus G″ with a magnitude of 210 Pa, noted in **Figure 3.10 (c).**

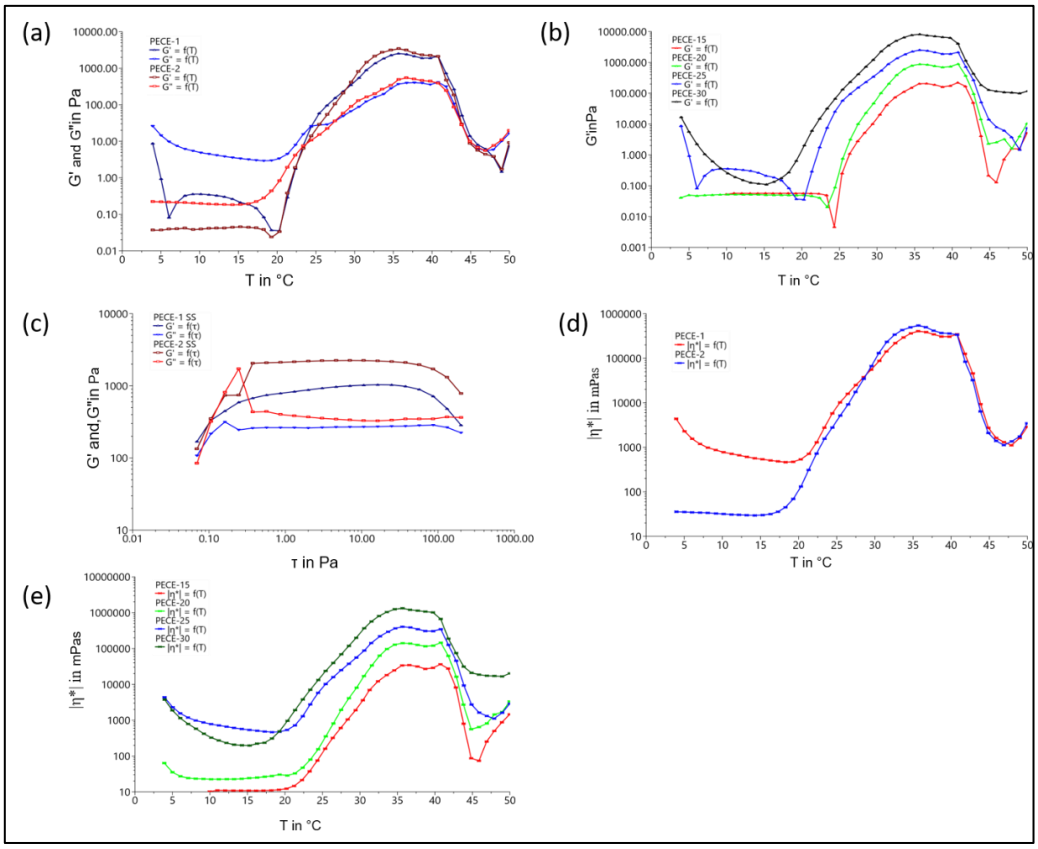


Figure 3.10 a) Temperature ramp of PECE-1 and PECE- 2; (b) Temperature ramp of PECE hydrogel at different concentrations (15%, 20%, 25% and 30% $^{w}/_{v}$); (c) Stress sweep of PECE-1 and PECE-2 at 25°C; (d) Viscosity of PECE-1 and PECE-2 and (e) Viscosity of PECE hydrogel.

3.3.7. Assessment of the syringeability of the hydrogels

Texture analysis was used to establish the maximum force required to inject hydrogels, and the findings are presented in **Figure 3.11**. The hydrogels and NPs loaded hydrogel syringeability experiments were carried out using 27-gauge needles. The texture analyser force required to inject the PECE hydrogels through a 1 mL syringe connected to 27G needles was used to assess syringeability. The injection force includes three elements: the force required to overcome syringe plunger resistance, delivering kinetic energy to the liquid under evaluation, and propelling the liquid through the needle (Allahham *et al.*, 2004). PECE hydrogels (20 and 25% $^{w}/_{v}$) required 8 N and 16.1 N, respectively, to inject them through 27G needles, whereas

nano-embedded PECE hydrogels (20 and 25% $^{w}/_{v}$) required 9 N and 16.5 N, respectively. The concentration of the hydrogel and the dispersion of NPs in the hydrogel were two factors that influenced the injection force, resulting in an increased maximum force required for injection as these factors increased. These results are within two-thirds of the maximum force recommended for a manual injection, which is 30 N. As a result, the nano-embedded hydrogel PECE is appropriate for injection via a variety of routes of administration.

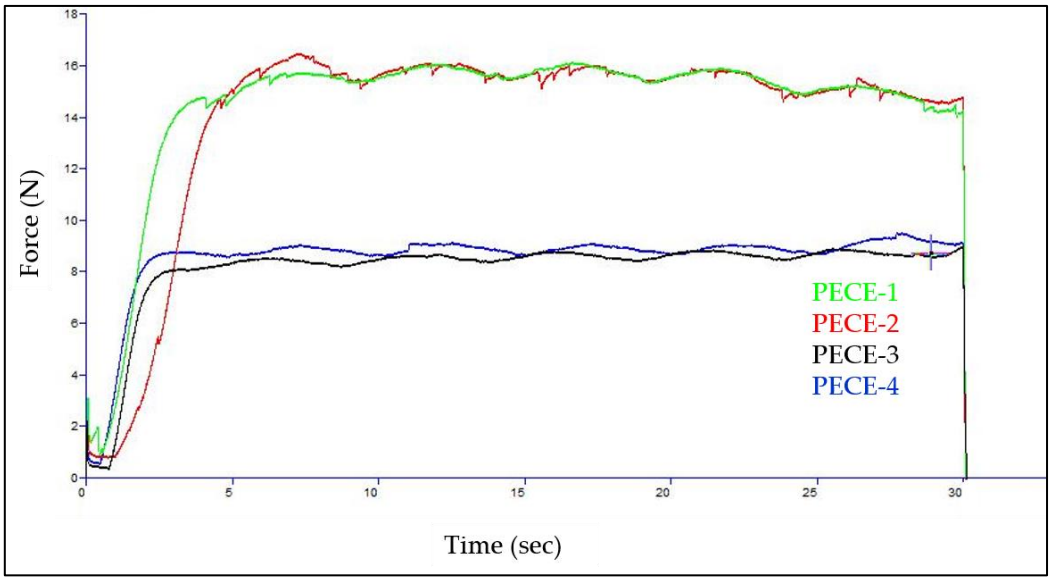


Figure 3.11 Required force to inject PECE hydrogel at different concentration from 1 mL syringes equipped with 27 G needle, PECE-1 (25% $^{w}/_{v}$ hydrogel), PECE-2 (25% $^{w}/_{v}$ NP-loaded hydrogel), PECE-3 (20% $^{w}/_{v}$ hydrogel) and PECE-4 (20% $^{w}/_{v}$ NP-loaded hydrogel).

3.3.8. *In vitro* release analysis of IFN-α2b from IFNPs and IFNPH

The *in vitro* release of IFN-α2b from the IFNPH and the IFNP was investigated in PBS at different pH values (7.4 and 6.6, at 37°C) for two weeks. PBS pH 6.6 was used to simulate pH conditions relevant to the extracellular tumour tissues, whereas PBS pH 7.4 was used to simulate the normal extracellular cells conditions. **Figure 3.12** and **Figure 3.13** depicts the release pattern of IFN-α2b, and the influence of the pH on the drug release. The release from the IFNPH revealed a biphasic release pattern, where an initial burst release was followed by sustained release. The cumulative percentage release from the IFNPH was 4.6% and 4.05% within the first 24 hrs at pH 7.4 and 6.6; respectively. The influence of the pH on the drug released from the IFNPH revealed

that the release was higher at the normal extracellular microenvironment contrarily to our initial hypothesis. Which was further explained by the degradation studies; the nano-embedded PECE hydrogel degraded in the acidic medium of pH 6.6 at a slightly higher rate due to the ionization of the PBAE-NPs. The presence of the IFN-α2b in the IFNPH formulation slowed the release and degradation of the formulation due to the aggregation and entanglement of the protein in the hydrogel matrix. The release from IFNP showed a cumulative percentage release of 4.9% and 3.9% following a 24 hrs at pH 7.4 and 6.6, respectively. The initial burst release of IFNPs was greater compared to that of IFNPH due to the release of surface-located IFN-α2b, which was accessible for immediate release. The limited release behaviour from the IFNP at both pH values was attributed to inactivation by long-term exposure to physiological temperature and acidification of the medium. The IFNPH thus shields the IFN-α2b from the cursive acid environment at the tumour site. The slow release of IFN-α2b from the IFNPH formulation is beneficial as it prevents chronic activation of type I IFN pathway, as evidence has reported that chronic exposure to IFN may result in the development of resistance (Budhwani *et al.*, 2018). A student paired t-test was used to compare the release from the IFNP after 24 hrs at the two different pH values; there was significant differences between the groups ($p=0.00$). For the release from the IFNPH after 14 days at both pH values, there was significance difference between the groups ($p= 0.044$). The comparison between the release from the IFNP and the IFNPH after 24 hrs at pH 7.4 was significantly ($p= 0.01$) as well as at pH 6.6 ($p= 0.034$).

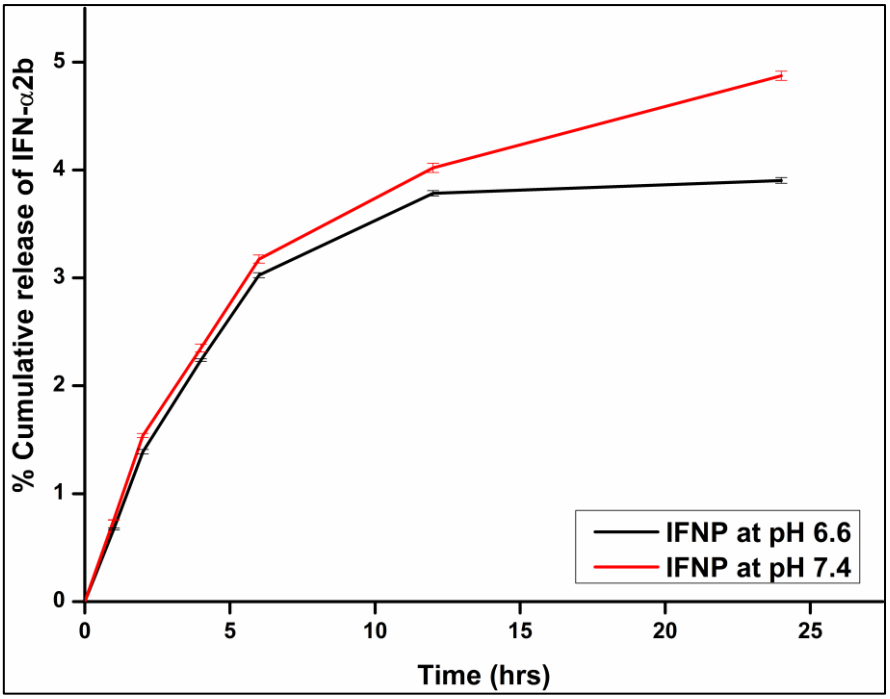


Figure 3.12 *In vitro* release profiles of immunoenzymatically detected IFN-α2b from IFNP at 37°C at different pH values the slow release is due to the aggregation and entanglement of the protein in the hydrogel matrix.

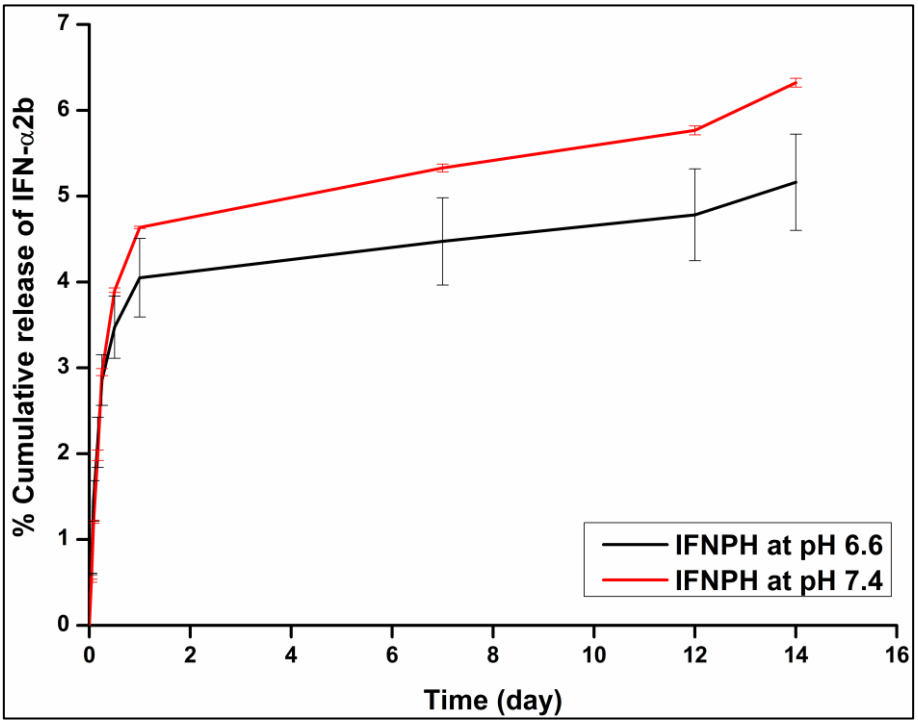


Figure 3.13 *In vitro* release profiles of immunoenzymatically detected IFN-α2b from IFNPH at 37°C at different pH values the low values were attributed to inactivation by long-term exposure to physiological temperature and acidification of the medium.

3.3.9. Degradation analysis of the formulations

Biodegradable hydrogels are of great importance in ocular disease as they would degrade slowly removing the need for frequent administration. The nano-embedded PECE hydrogel NPH showed inconsistency and slight degradation with 8% and 7.67% degradation on the 14th day at pH 6.6 and 7.4, respectively. This slow degradation might erase the need for multiple rounds of application. The degraded formulation showed no colour change, simultaneously the formulation displayed low water uptake indicating that upon subconjunctival administration the hydrogel will not swell extensively causing tissue damage. As evident in **Figure 3.14** the slow erosion of the hydrogel confirms that further release of the IFN-α2b from the IFNPH is possible as only 8% of the hydrogel has eroded after 14 days.

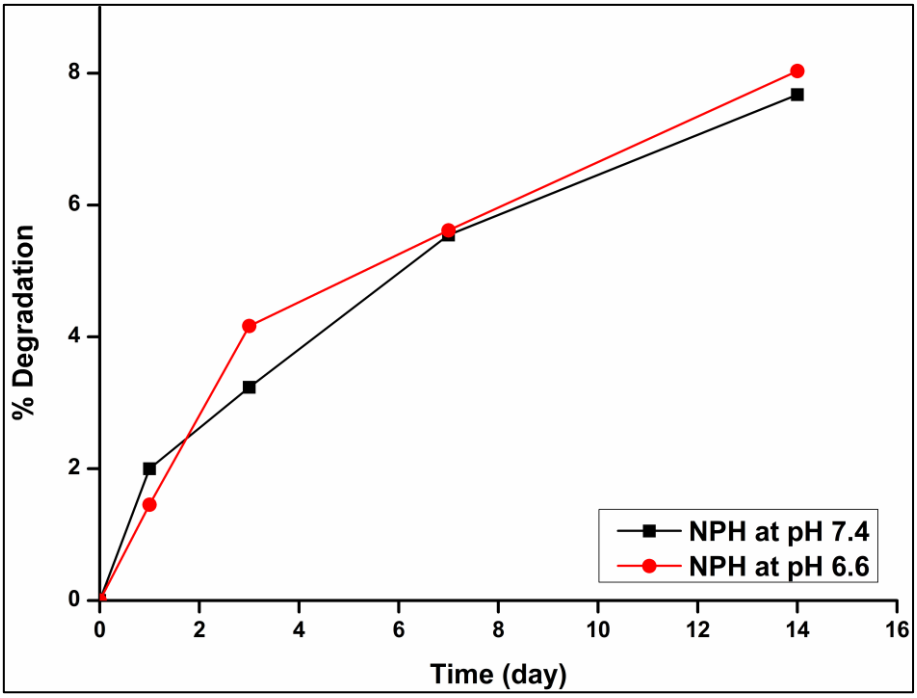
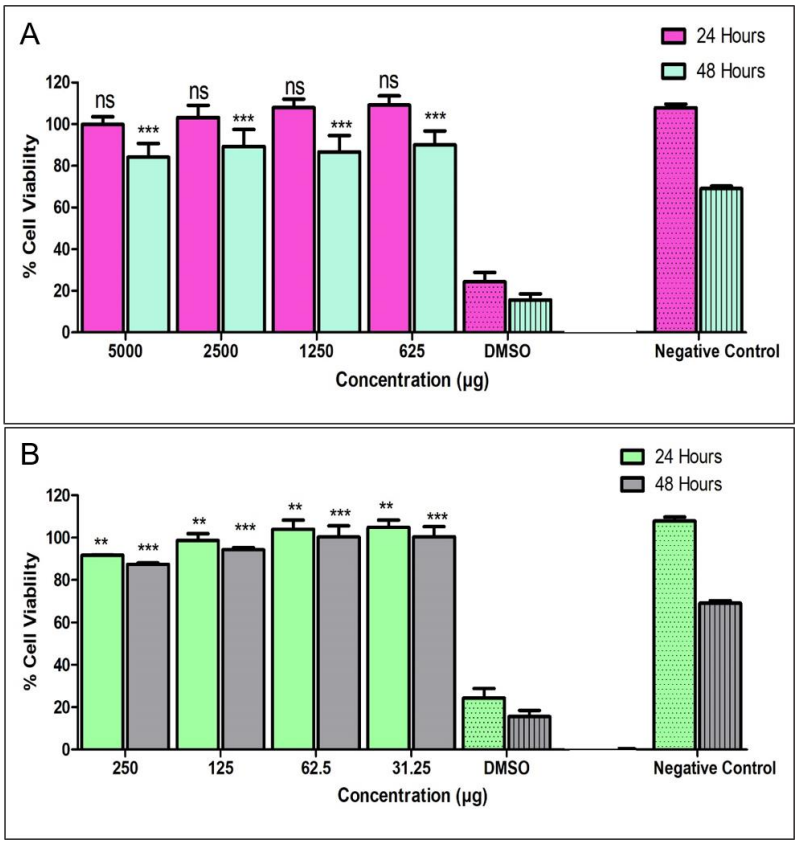


Figure 3.14. Biodegradation behaviour of the NPH in PBS solution (pH 6.6 and 7.4) at 37°C. The error bars were small, indicating that the data obtained did not differ among themselves the standard deviation ranged is (0-4.62×10^{-15}).

3.3.10. Biocompatibility evaluation of the formulations

The MTT assay was used to evaluate the cytotoxicity of the formulations on a HRPE cell line. The assay was employed to measure viability and cyto-compatibility with HRPE after 24 and 48 hrs treatment with PECE hydrogel, NPs, IFN-α2b, and the IFNPH at different concentrations. The results showed that the formulations displayed

acceptable levels of cell viability, with minimal cytotoxicity effects on HRPE after 24 and 48 hrs and the viability is dose-dependent as evident in **Figure 3.15**. Although the viability after 48 hrs was reduced, the percentage cell viability was greater than 70% (Standard, 2009), the substance is regarded as non-cytotoxic; thus, these findings indicate that the IFNPH is non-cytotoxic to HRPE cell lines. The cells' metabolic waste products may have accumulated after 48 hrs of treatment, resulting in increased cytotoxicity evident in the MTT assay results (Ghasemi *et al.*, 2021). A student's unpaired t-test was used to compare the cytotoxicity at 24 hrs vs 48 hrs. There was no statistical significance between the cytotoxicity after 24 hrs vs 48 hrs treatment ($p = 0.4727$) when comparing the PECE hydrogel concentrations from 5000 -625 µg/mL with the negative control at 24 hrs there is no significant differences. The results after 48hrs treatment compared to the negative control showed a significant difference ($p< 0.001$). The results of comparing the PBAE-NP with the negative control was not significant and significant ($p<0.01$ and $p<0.001$) after 24 hrs and 48 hrs, respectively. Comparison with IFN-α2b showed no significant difference at 24 hrs and a significant difference ($p<0.001$) after 48 hrs. The IFNPH showed a significant difference ($p<0.001$) after 24 hrs and 48 hrs when compared to the negative control.



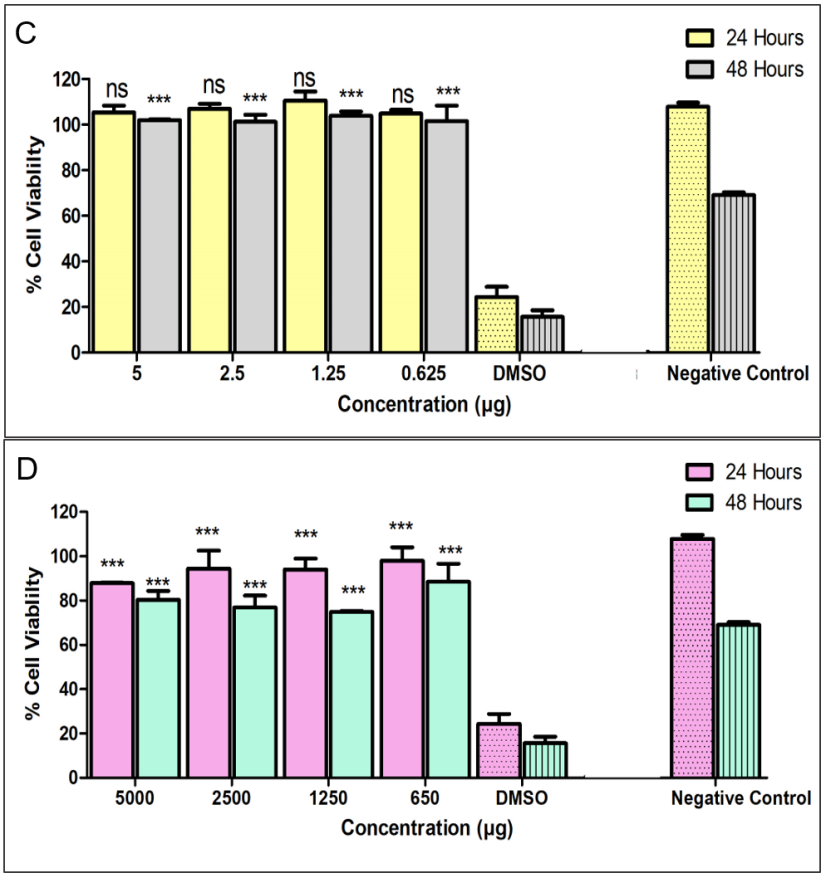


Figure 3.15. MTT assay measurement of viability of HRPE cells following 24 and 48 hrs treatment with A) PECE hydrogel, B) PBAE-NP, C) IFN-α2b, and D) IFNPH at different concentrations (Data represents n = 3, mean ± SD). ** Indicates $p<0.01$, *** indicates $p<0.001$, and (ns) indicates no significant difference when compared to negative control. 5% $^{v}/_{v}$ DMSO and culture medium were used as positive and negative controls, respectively, indicated by the patterned columns.

3.3.11. Assessment of the stability of the released IFN-α2b from the IFNPH

The biological activity of the released IFN-α2b was investigated as shown in **Figure 3.16**. The results show that the biological activity of the released IFN-α2b was maintained for the duration of the study. The structure integrity of IFN-α2b was maintained during the preparation and release from the IFNPH. A student's unpaired t-test was used to compare the released IFN-α2b at the different pH values with standard IFN-α2b. There was no significant difference after 24 and 48 hrs treatment. When compared to the negative control there was a significant difference after 24 hrs

at pH 7.4 was significant ($p < 0.01$) as well as at pH 5.5 ($p < 0.05$). After 48 hrs there was a significant difference at pH 7.4 and pH 5.5 ($p<0.001$).

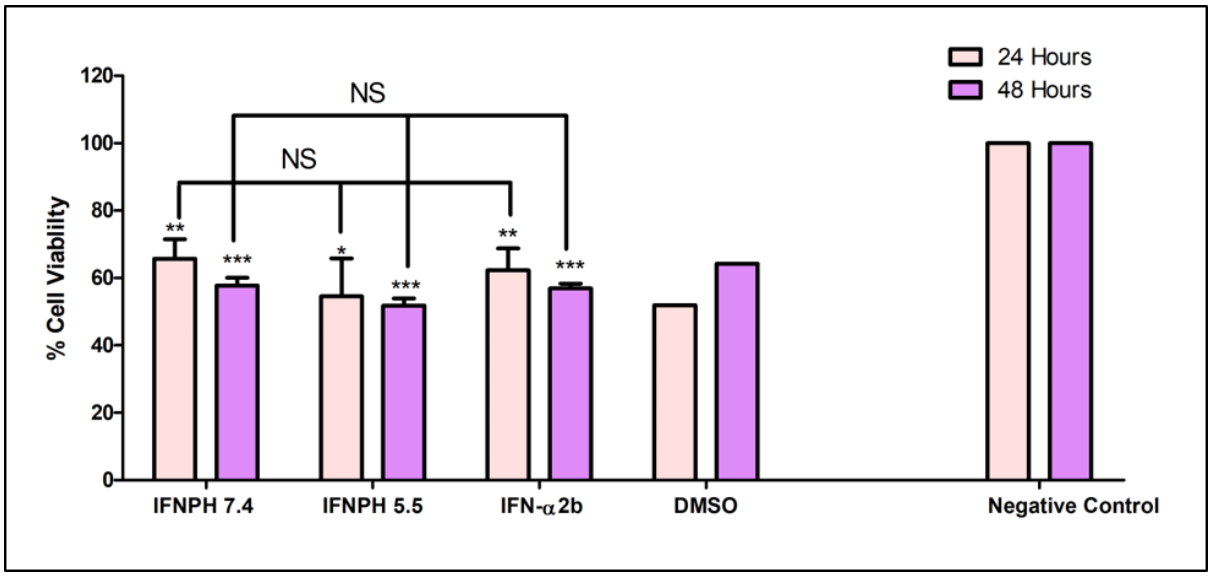


Figure 3.16. *In vitro* antiproliferative activity on A172 cells of IFN-α2b released from the IFNPH formulation at different pH values. 5% $^{v}/_{v}$ DMSO and culture medium were used as positive control and as negative control, respectively (Data represent n = 3, mean ± SD). * Indicates $p<0.05$, ** indicates $p<0.01$, *** indicates $p<0.001$ when compared to negative control. NS indicates no significant difference when compared to standard IFN-α2b.

3.4. Discussion

Interferons are glycosylated polypeptides produced in the body with antineoplastic, antiviral, and antibacterial properties (Bracarda *et al.*, 2010). The antitumor effect is achieved through a combination of antiangiogenic, antiproliferative, cytotoxic effects, as well as cytostatic effects and enhancement of cell lysis (Bracarda *et al.*, 2010). IFN-α2b has been used in management of different types of malignancies. The clinical efficiency of IFN-α2b is hindered due to the high sensitivity of IFN-α2b to degradation and clearance by the reticuloendothelial system (Feczkó *et al.*, 2016). Thus, this work employed a thermo-responsive hydrogel loaded with pH-responsive NPs to design and engineer a platform for site-specific delivery of IFN-α2b for ocular surface tumour therapy.

The PECE copolymer was synthesised successfully by ring opening polymerisation, and the FTIR spectra revealed the presence of the characteristic peaks of PECE

copolymer (Gong *et al.*, 2009a; Gong *et al.*, 2009b). The findings correlate to previous reports, and the ^{1}H-NMR confirmed the synthesis of the PECE copolymer (Gong *et al.*, 2007; Hwang *et al.*, 2005).

The PECE hydrogel possessed thermo-responsive and biodegradable properties, which have been reported previously, as well as functionality as *in situ*-forming depot for a sustained drug delivery system (Gong *et al.*, 2009a; Kissel *et al.*, 2002; Luo *et al.*, 2016). In this study, the sol-gel transition of the PECE copolymer was investigated employing the test tube-inversion method and rheological studies (Ni *et al.*, 2012). The amphiphilic nature of the PECE copolymer is owed to its hydrophilic PEG block and hydrophobic PCL block. The sol-gel transition is mainly due to micelle aggregation; the PECE copolymer tends to form micelles with a hydrophobic PCL core and a hydrophilic PEG shell, whereas the gel-sol transition is due to acceleration of the molecular motion of PCL resulting in the breakage of the micelle structure; the mechanism of hydrogel formation for PECE copolymer has been previously reported (Bae *et al.*, 2005).

The rheological parameters such as viscosity, loss modulus and storage modulus are important parameters to consider when administering the hydrogel through injection. The moduli measure the elasticity or rigidity of the hydrogel upon shear (i.e., injection), while the viscosity measures the ability of the material to resist deformation upon stress, during hydrogel formulation injection (Chen *et al.*, 2017; El Kechai *et al.*, 2015). The results indicated that higher PECE concentrations result in higher G′ values and viscosity, as a result, the maximum force necessary for injection was increased. Lower concentrations provide better injectable capabilities, but lower hydrogel strength, highlighting that the final copolymer solution concentration must balance the effects of numerous parameters. To minimize the discomfort and eye damage, 30 N is the recommended maximum force which means the lower the force, the better the treatment process (Wang *et al.*, 2018). In this study, 20% $^{w}/_{v}$ PECE was selected as the preferred concentration based on the ease of preparation and ease of administration, which is proposed to result in minimal discomfort to the patient.

The NPs synthesised were in the nanosize range with excellent polydispersity (low PDI) and zeta potential. The average particle size and PDI are essential physical properties to consider as they affect the encapsulation efficiency, stability,

biodistribution, drug release profile and cellular uptake (Ban *et al.*, 2017; Chaw *et al.*, 2021; Tseng *et al.*, 2013). The DLS studies show that the prepared IFNPs had an average size of 151 nm with an encapsulation efficiency of 89% with a narrow PDI. Furthermore, the TEM images generated revealed that the formulated NPs are uniform spherical shape with intact structure within the nanosize range and verified the DLS results. The pH-sensitive PBAE-NPs were developed and loaded into the PECE hydrogel to enable site-specific delivery of IFN-α2b to ocular surface tumour cells. IFN-α2b was released at a slower rate from PBAE-NPs in the acidic environment. The pH-protective NPs were stable with drug release minimised, indicating that this drug delivery system can reduce unwanted systemic side effects of anticancer drugs during cancer therapy by providing pH-sensitive drug release (Ko *et al.*, 2007). The PBAE-NPs would proposedly be stable following diffusion from the hydrogel matrix into the solid tumour microenvironment and degrade in the extracellular and late endosomes/lysosomes where the pH is approximately 5–6 and 4–5, respectively, rendering them suitable for extracellular and cytoplasmic drug delivery (Shen *et al.*, 2009).

du Toit et al. (2021) designed an injectable nano-enabled thermogel of PECE for controlled delivery of p11 anti-angiogenic peptide for the potential treatment of ocular angiogenic disorder. The release of the peptide from the nano-thermogel system was proposed to be due to diffusion mediated release through the gel matrix, with minimal swelling and ultimate erosion of the hydrogel (du Toit *et al.*, 2021). The release of IFN-α2b from the IFNPH was proposed to follow a similar release pattern. When evaluating the release kinetics of proteins from nanosystems embedded into hydrogels, it is essential to consider that with hydrogel systems, 100% protein release is hardly achieved. The protein might get physically entrapped in the highly entangled hydrogel network, limiting the diffusivity. The release kinetics proposed that the size of the protein plays the primary role in its diffusivity, in addition to the density of the hydrogel (Koutsopoulos *et al.*, 2009). Furthermore, the low release levels of protein may be due not only to protein denaturing during processing, but also due to the experimental conditions (by medium acidification, destabilizing release medium, etc.). The pH of the medium plays an important role in the release kinetics, affecting both the protein stability and polymer degradation. Firstly, the pH influences the protein conformation, whereby acidity might either denature a protein or might cause aggregation. Secondly,

the alkaline or acidic medium are known to accelerate polymer degradation (Giteau *et al.*, 2008). Fador-Kardos et al. (2020) reported the effect of pH on the release profile of IFN-β, the protein was loaded into nanoparticles with high encapsulation efficiency (>95%) for the management of multiple sclerosis. The *in vitro* release of IFN-β revealed a decline in the release profile by the end of the two-week study; the proposed explanation was that the pH caused aggregation of the protein (Fodor-Kardos *et al.*, 2020). The limited release behaviour reported previously for IFNP at both pH values was attributed to inactivation by long-term exposure to physiological temperature and acidification of the medium. Determining IFN-α2b levels via ELISA provides an indicator of its stability (Sanchez *et al.*, 2003), which was further confirmed by assessing the antiproliferative activity on the A172 cells. *In vitro* experiments in this investigation demonstrated the stability of the released IFN-α2b from IFNPH for the duration of the study; thus, the IFNPH exhibits pH- and temperature-protective properties.

Safety assessment of the formulations *in vitro* revealed that at concentrations ranging from 5000 to 0.625 µg/mL employed in the study, were within acceptable levels of cell viability, with no significant cytotoxicity effects on HRPE cells. Similar results were reported in other studies, confirming the biocompatibility of the PECE hydrogel (du Toit *et al.*, 2021). Furthermore, concentration influences the percentage of cell viability, as higher concentrations are associated with lower viability. The difference in cell viability was statistical significant between the varied concentrations at the two different time points ($p < 0.001$) in all the formulations.

3.5. Conclusions

In this work, PBAE-NPs and PECE copolymer were successfully synthesised. The triblock copolymer PECE was loaded with PBAE-NPs to prepare a nano-embedded pH-protective-thermo-responsive hydrogel formulation. Rheological measurements showed that the gelation points of the PECE hydrogel composites were adequate for subconjunctival injection. The gelation temperature could be adjusted by adding PBAE-NPs into the PECE matrix. The pH-protectiveness of the IFNPH hydrogel composites demonstrated that they could be employed for protecting the IFN from high levels of degradation and providing controlled release of IFN at tumour sites. Therefore, the IFNPH hydrogel nanocomposite is a prospective candidate as an

injectable biomaterial for ocular drug delivery to tumour sites. Although the concept of injectable and pH thermo-responsive hydrogel nanocomposites has been introduced in this study, further research is required to validate the application of such systems in tumour delivery via preclinical investigation in an appropriate animal model, as reported in the subsequent chapter.

3.6. References

1. Allahham, A., Mainwaring, D., Stewart, P. & Marriott, J. 2004. Development and application of a micro-capillary rheometer for in-vitro evaluation of parenteral injectability. *Journal of pharmacy and pharmacology,* 56**,** 709-716.
2. An, T., Zhang, C., Han, X., Wan, G., Wang, D., Yang, Z., Wang, Y., Zhang, L. & Wang, Y. 2016. Hyaluronic acid-coated poly (β-amino) ester nanoparticles as carrier of doxorubicin for overcoming drug resistance in breast cancer cells. *Royal Society of Chemistry Advances,* 6**,** 38624-38636.
3. Asmana Ningrum, R. 2014. Human interferon alpha-2b: a therapeutic protein for cancer treatment. *Scientifica (Cairo),* 2014**,** 970315.
4. Bae, S. J., Suh, J. M., Sohn, Y. S., Bae, Y. H., Kim, S. W. & Jeong, B. 2005. Thermogelling poly (caprolactone-b-ethylene glycol-b-caprolactone) aqueous solutions. *Macromolecules,* 38**,** 5260-5265.
5. Ban, J., Zhang, Y., Huang, X., Deng, G., Hou, D., Chen, Y. & Lu, Z. 2017. Corneal permeation properties of a charged lipid nanoparticle carrier containing dexamethasone. *International Journal of Nanomedicine,* 12**,** 1329.
6. Beilharz, M. W., Cummins, M. J., Bennett, A. L. & Cummins, J. M. 2010. Oromucosal Administration of Interferon to Humans. *Pharmaceuticals,* 3**,** 323-344.
7. Bracarda, S., Eggermont, A. M. & Samuelsson, J. 2010. Redefining the role of interferon in the treatment of malignant diseases. *European Journal of Cancer,* 46**,** 284-297.
8. Budhwani, M., Mazzieri, R. & Dolcetti, R. 2018. Plasticity of type I interferon-mediated responses in cancer therapy: from anti-tumor immunity to resistance. *Frontiers in oncology,* 8**,** 322.
9. Chaw, S. Y., Novera, W., Chacko, A.-M., Wong, T. T. L. & Venkatraman, S. 2021. In vivo fate of liposomes after subconjunctival ocular delivery. *Journal of Controlled Release,* 329**,** 162-174.

10. Chen, M. H., Wang, L. L., Chung, J. J., Kim, Y.-H., Atluri, P. & Burdick, J. A. 2017. Methods to assess shear-thinning hydrogels for application as injectable biomaterials. *ACS biomaterials science & engineering,* 3**,** 3146-3160.
11. Cilurzo, F., Selmin, F., Minghetti, P., Adami, M., Bertoni, E., Lauria, S. & Montanari, L. 2011. Injectability evaluation: an open issue. *AAPS PharmSciTech,* 12**,** 604-609.
12. Dai, Y., Xu, C., Sun, X. & Chen, X. 2017. Nanoparticle design strategies for enhanced anticancer therapy by exploiting the tumour microenvironment. *Chemical Society Reviews,* 46**,** 3830-3852.
13. du Toit, L. C., Choonara, Y. E. & Pillay, V. 2021. An injectable nano-enabled thermogel to attain controlled delivery of p11 peptide for the potential treatment of ocular angiogenic disorders of the posterior segment. *Pharmaceutics,* 13**,** 176.
14. El Kechai, N., Bochot, A., Huang, N., Nguyen, Y., Ferrary, E. & Agnely, F. 2015. Effect of liposomes on rheological and syringeability properties of hyaluronic acid hydrogels intended for local injection of drugs. *International journal of pharmaceutics,* 487**,** 187-196.
15. Feczkó, T., Fodor-Kardos, A., Sivakumaran, M. & Shubhra, Q. T. H. 2016. In vitro IFN-α release from lFN-α- and pegylated IFN-α-loaded poly(lactic-co-glycolic acid) and pegylated poly(lactic-co-glycolic acid) nanoparticles. *Nanomedicine,* 11**,** 2029-2034.
16. Fodor-Kardos, A., Kiss, Á. F., Monostory, K. & Feczkó, T. 2020. Sustained in vitro interferon-beta release and in vivo toxicity of PLGA and PEG-PLGA nanoparticles. *Royal Society of Chemistry Advances,* 10**,** 15893-15900.
17. Galor, A., Karp, C. L., Chhabra, S., Barnes, S. & Alfonso, E. C. 2010. Topical interferon alpha 2b eye-drops for treatment of ocular surface squamous neoplasia: a dose comparison study. *British journal of ophthalmology,* 94**,** 551-554.
18. Ghasemi, M., Turnbull, T., Sebastian, S. & Kempson, I. 2021. The MTT Assay: Utility, Limitations, Pitfalls, and Interpretation in Bulk and Single-Cell Analysis. *International Journal of Molecular Sciences,* 22**,** 12827.
19. Giteau, A., Venier-Julienne, M.-C., Aubert-Pouëssel, A. & Benoit, J.-P. 2008. How to achieve sustained and complete protein release from PLGA-based microparticles? *International journal of pharmaceutics,* 350**,** 14-26.

20. Gong, C., Qian, Z., Liu, C., Huang, M., Gu, Y., Wen, Y., Kan, B., Wang, K., Dai, M. & Li, X. 2007. A thermosensitive hydrogel based on biodegradable amphiphilic poly (ethylene glycol)–polycaprolactone–poly (ethylene glycol) block copolymers. *Smart materials and structures,* 16**,** 927.
21. Gong, C., Shi, S., Dong, P., Kan, B., Gou, M., Wang, X., Li, X., Luo, F., Zhao, X. & Wei, Y. 2009a. Synthesis and characterization of PEG-PCL-PEG thermosensitive hydrogel. *International journal of pharmaceutics,* 365**,** 89-99.
22. Gong, C. Y., Dong, P. W., Shi, S., Fu, S. Z., Yang, J. L., Guo, G., Zhao, X., Wei, Y. Q. & Qian, Z. Y. 2009b. Thermosensitive PEG–PCL–PEG hydrogel controlled drug delivery system: sol–gel–sol transition and in vitro drug release study. *Journal of pharmaceutical sciences,* 98**,** 3707-3717.
23. Groen, J. C., Peffer, L. A. & Pérez-Ramírez, J. 2003. Pore size determination in modified micro-and mesoporous materials. Pitfalls and limitations in gas adsorption data analysis. *Microporous and mesoporous materials,* 60**,** 1-17.
24. Gulia, M., Rai, S., Jain, U. K., Katare, O. P., Katyal, A. & Madan, J. 2014. Sustained-release protamine sulphate-impregnated microspheres may reduce the frequent administration of recombinant interferon α-2b in ovarian cancer: in-vitro characterization. *Anti-Cancer Drugs,* 25**,** 63-71.
25. Gupta, P., Authimoolam, S. P., Hilt, J. Z. & Dziubla, T. D. 2015. Quercetin conjugated poly (β-amino esters) nanogels for the treatment of cellular oxidative stress. *Acta biomaterialia,* 27**,** 194-204.
26. Hwang, M. J., Suh, J. M., Bae, Y. H., Kim, S. W. & Jeong, B. 2005. Caprolactonic poloxamer analog: pEG-PCL-PEG. *Biomacromolecules,* 6**,** 885-890.
27. Kakde, D., Jain, D., Shrivastava, V., Kakde, R. & Patil, A. 2011. Cancer therapeutics-opportunities, challenges and advances in drug delivery. *Journal of Applied Pharmaceutical Science***,** 01-10.
28. Karp, C. L., Galor, A., Chhabra, S., Barnes, S. D. & Alfonso, E. C. 2010. Subconjunctival/perilesional recombinant interferon α2b for ocular surface squamous neoplasia: a 10-year review. *Ophthalmology,* 117**,** 2241-2246.
29. Kissel, T., Li, Y. & Unger, F. 2002. ABA-triblock copolymers from biodegradable polyester A-blocks and hydrophilic poly (ethylene oxide) B-blocks as a candidate for in situ forming hydrogel delivery systems for proteins. *Advanced drug delivery reviews,* 54**,** 99-134.

30. Ko, J., Park, K., Kim, Y.-S., Kim, M. S., Han, J. K., Kim, K., Park, R.-W., Kim, I.-S., Song, H. K. & Lee, D. S. 2007. Tumoral acidic extracellular pH targeting of pH-responsive MPEG-poly (β-amino ester) block copolymer micelles for cancer therapy. *Journal of Controlled Release,* 123**,** 109-115.
31. Koutsopoulos, S., Unsworth, L. D., Nagai, Y. & Zhang, S. 2009. Controlled release of functional proteins through designer self-assembling peptide nanofiber hydrogel scaffold. *Proceedings of the National Academy of Sciences,* 106**,** 4623-4628.
32. Kristó, K., Szekeres, M., Makai, Z., Márki, Á., Kelemen, A., Bali, L., Pallai, Z., Dékány, I. & Csóka, I. 2020. Preparation and investigation of core-shell nanoparticles containing human interferon-α. *International Journal of Pharmaceutics,* 573**,** 118825.
33. Lee, J. W., Hua, F.-j. & Lee, D. S. 2001. Thermoreversible gelation of biodegradable poly (ε-caprolactone) and poly (ethylene glycol) multiblock copolymers in aqueous solutions. *Journal of Controlled Release,* 73**,** 315-327.
34. Liu, Y., Li, Y., Keskin, D. & Shi, L. 2019. Poly (β-Amino Esters): synthesis, formulations, and their biomedical applications. *Advanced healthcare materials,* 8**,** 1801359.
35. Luo, Z., Jin, L., Xu, L., Zhang, Z. L., Yu, J., Shi, S., Li, X. & Chen, H. 2016. Thermosensitive PEG–PCL–PEG (PECE) hydrogel as an in situ gelling system for ocular drug delivery of diclofenac sodium. *Drug delivery,* 23**,** 63-68.
36. Lynn, D. M. & Langer, R. 2000. Degradable poly (β-amino esters): synthesis, characterization, and self-assembly with plasmid DNA. *Journal of the American Chemical Society,* 122**,** 10761-10768.
37. Mehvar, R. 2000. Modulation of the pharmacokinetics and pharmacodynamics of proteins by polyethylene glycol conjugation. *Journal of pharmacy & pharmaceutical sciences: a publication of the Canadian Society for Pharmaceutical Sciences, Societe canadienne des sciences pharmaceutiques,* 3**,** 125-136.
38. Nanji, A. A., Sayyad, F. E. & Karp, C. L. 2013. Topical chemotherapy for ocular surface squamous neoplasia. *Current opinion in ophthalmology,* 24**,** 336-342.
39. Navya, P., Kaphle, A., Srinivas, S., Bhargava, S. K., Rotello, V. M. & Daima, H. K. 2019. Current trends and challenges in cancer management and therapy using designer nanomaterials. *Nano convergence,* 6**,** 1-30.

40. Nguyen, T. T., Miller, A. & Orellana, M. F. 2011. Characterization of the porosity of human dental enamel and shear bond strength in vitro after variable etch times: initial findings using the BET method. *The Angle Orthodontist,* 81**,** 707-715.
41. Ni, P. Y., Fan, M., Qian, Z. Y., Luo, J. C., Gong, C. Y., Fu, S. Z., Shi, S., Luo, F. & Yang, Z. M. 2012. Synthesis and characterization of injectable, thermosensitive, and biocompatible acellular bone matrix/poly (ethylene glycol)-poly (ε-caprolactone)-poly (ethylene glycol) hydrogel composite. *Journal of Biomedical Materials Research Part A,* 100**,** 171-179.
42. Park, J., Han, J., Chung, T.-Y., Lim, D. H. & Choi, C. Y. 2022. Pegylated Interferon Alpha 2a for the Treatment of Ocular Surface Squamous Neoplasia. *Cornea,* 41**,** 1271-1275.
43. Pe'er, J. 2015. Ocular surface squamous neoplasia: evidence for topical chemotherapy. *International ophthalmology clinics,* 55**,** 9-21.
44. Pestka, S., Krause, C. D. & Walter, M. R. 2004. Interferons, interferon-like cytokines, and their receptors. *Immunological reviews,* 202**,** 8-32.
45. Ramburrun, P., Choonara, Y. E., Kumar, P., du Toit, L. C. & Pillay, V. 2015. Design of chitospheres loaded with pristine polymer particles for extended drug delivery via polyelectrolyte complexation and particulate leaching. *International Journal of Pharmaceutics,* 479**,** 189-206.
46. Sanchez, A., Tobío, M. a., González, L., Fabra, A. & Alonso, M. a. J. 2003. Biodegradable micro-and nanoparticles as long-term delivery vehicles for interferon-alpha. *European journal of pharmaceutical sciences,* 18**,** 221-229.
47. Shen, Y., Tang, H., Zhan, Y., Van Kirk, E. A. & Murdoch, W. J. 2009. Degradable poly (β-amino ester) nanoparticles for cancer cytoplasmic drug delivery. *Nanomedicine: nanotechnology, biology and medicine,* 5**,** 192-201.
48. Sing, K. S. 1985. Reporting physisorption data for gas/solid systems with special reference to the determination of surface area and porosity (Recommendations 1984). *Pure and applied chemistry,* 57**,** 603-619.
49. Song, W., Tang, Z., Li, M., Lv, S., Yu, H., Ma, L., Zhuang, X., Huang, Y. & Chen, X. 2012. Tunable pH-sensitive poly (β-amino ester) s synthesized from primary amines and diacrylates for intracellular drug delivery. *Macromolecular bioscience,* 12**,** 1375-1383.

50. Standard, I. 2009. Biological evaluation of medical devices—Part 5: Tests for in vitro cytotoxicity. *Geneve, Switzerland: International Organization for Standardization*.

51. Tseng, C.-L., Chen, K.-H., Su, W.-Y., Lee, Y.-H., Wu, C.-C. & Lin, F.-H. 2013. Cationic gelatin nanoparticles for drug delivery to the ocular surface: in vitro and in vivo evaluation. *Journal of Nanomaterials,* 2013.

52. Venkateswaran, N., Mercado, C., Galor, A. & Karp, C. L. 2019. Comparison of topical 5-fluorouracil and interferon alfa-2b as primary treatment modalities for ocular surface squamous neoplasia. *American journal of ophthalmology,* 199**,** 216-222.

53. Wang, Q., Sun, C., Xu, B., Tu, J. & Shen, Y. 2018. Synthesis, physicochemical properties and ocular pharmacokinetics of thermosensitive in situ hydrogels for ganciclovir in cytomegalovirus retinitis treatment. *Drug delivery,* 25**,** 59-69.

54. Wu, Y., Li, L., Chen, S., Qin, J., Chen, X., Zhou, D. & Wu, H. 2020. Synthesis, characterization, and crystallization behaviors of poly (D-lactic acid)-based triblock copolymer. *Scientific reports,* 10**,** 1-12.

55. Zhang, Q., Fassihi, M. A. & Fassihi, R. 2018. Delivery considerations of highly viscous polymeric fluids mimicking concentrated biopharmaceuticals: Assessment of injectability via measurement of total work done “WT”. *AAPS PharmSciTech,* 19**,** 1520-1528.

Chapter Four

Ocular pharmacokinetics of IFN-α2b from a single subconjunctival administration of IFN-α2b nanoparticles-loaded thermo-responsive hydrogel

4.1. Introduction

Ocular drug delivery poses a significant challenge in the field of ophthalmic pharmaceuticals due to several constraints that hinder administered drugs from reaching the ocular surface. The ocular anatomy and physiology render it impermeable to foreign objects, including therapeutics. The anterior and posterior segments include obstacles that slow therapeutic agent absorption and consequently reduce ocular bioavailability. These obstacles are static and dynamic barriers, with static barriers composed of tissues and limiting membranes and dynamic barriers including drug clearance systems (Gaudana *et al.*, 2010; Urtti, 2006). These barriers pose a challenge to the efficient delivery of therapeutics to the targeted ocular tissue. The corneal epithelium allows the diffusion of hydrophobic drugs but prevents the absorption of hydrophilic drugs and macromolecules of topically applied drugs (Gote *et al.*, 2019). Amongst the therapeutics currently in use for management of ocular disease is IFN-α2b that has been used to treat a variety of cancers (Ferrantini *et al.*, 2007). IFN-α2b are natural leukocytes, with anti-neoplastic, and anti-viral properties (Nava-Castañeda *et al.*, 2018). The anti-neoplastic properties results from the ability to suppress angiogenesis, anti-proliferative capabilities, the initiation of antibodies against tumour cells, and cytotoxicity (Fernandes *et al.*, 2014). Several studies have shown the efficiency of IFN-α2b in the management of ocular malignancies, with a high rate of resolution and a minimal risk of side effects (Galor *et al.*, 2012; Shah *et al.*, 2012; Sripawadkul *et al.*, 2023). IFN-α2b is applied via subconjunctival injections and/or eye drops utilized as primary or adjuvant therapy in the management of ocular tumors (Galor *et al.*, 2010){Lewczuk, 2019 #601}. Topical ocular therapies such as eye drops are the most prevalent in ocular applications. Unfortunately, because eye drops are rapidly drained from the ocular surface (via lacrimation, reflux blinking, or nasolacrimal drainage), and the medication absorption requires a few minutes, the dose/response profiles (bioavailability) are often quite poor (Ahmed, 2003; Gote *et al.*, 2019; Urtti, 2006). The IFN-α2b eye drop dosage is 1 million IU/mL, which is frequently administered four times a day until complete clinical resolution, which may take up to three months (Boehm and Huang, 2004; Galor *et al.*, 2010).

The downside of utilizing topical IFN-α2b is that the medication must be refrigerated, requires extemporaneous compounding, and is expensive, with frequent application resulting in reduced patient complaints (Al Bayyat *et al.*, 2019; Sayed-Ahmed *et al.*, 2017). The subconjunctival injection is administered 1-3 times weekly, in a single or multiple locations depending on the extent of tumour diffusion (Al Bayyat *et al.*, 2019; Karp *et al.*, 2010). Subconjunctival injection may be a beneficial choice for patients with superior tumours where drops are less likely to reach, individuals who struggle to adhere to a treatment routine, and those able to commit to regular clinic visits (Monroy *et al.*, 2023). While subconjunctival injections are generally well tolerated, they are associated with transient systemic flu-like symptoms, which can be easily treated with an oral antipyretic such as acetaminophen (Antonietta Blasi *et al.*, 2018; Kaliki *et al.*, 2016; Kim *et al.*, 2012).

To circumvent the limitations of the available ocular delivery systems, ophthalmic formulations such as in situ hydrogels, contact lenses, ocular implants, and physical devices have been developed (Bourges *et al.*, 2006; Sapino *et al.*, 2019). Among these formulations, stimuli-responsive hydrogels which are liquid at room temperature and transition to a gel upon instillation as a result of stimuli such as pH, temperature, etc. are taking center stage (Wu *et al.*, 2019). In situ gel formulations increases pre-corneal residence duration and improve medication bioavailability, and the loading of nanosystems into the hydrogel enhances the permeability across corneal barriers (Cholkar *et al.*, 2012; Makwana *et al.*, 2016). Poly(beta-amino esters) nanoparticles (PBAE-NPs) are prepared from PBAE polymers synthesised via Michael addition polymerisation of acrylates and amines that have been employed for protein, gene, anticancer, and antimicrobial delivery (Green *et al.*, 2008; Liu *et al.*, 2019). Under acidic conditions, these polymers undergo a hydrophobic-hydrophilic phase transition. As a result, the PBAE nanoparticles are biodegradable in the acidic microenvironment, resulting in the controlled release of their contents (Fang *et al.*, 2012; Song *et al.*, 2013).

The goal of this research was to design a pH-protective nano-embedded thermo-responsive hydrogel for subconjunctival delivery of IFN-α2b, referred to as IFNPH. The triblock copolymer of poly(ethylene glycol)-poly(caprolactone)-poly(ethylene glycol) (PEG-PCL-PEGE) was synthesized via ring-opening polymerization and employed to

prepare the hydrogel. In this chapter, this systems' *ex vivo* and *in vivo* ocular pharmacokinetics as a controlled release dosage form was subsequently investigated.

4.2. Materials and Methods

4.2.1. Materials

PEG-PCL-PEG triblock copolymer and poly (beta amino ester) nanoparticles (PBAE-NPs) were synthesised as described in chapter 3. IFN-α2b, Fluorescein isothiocyanate (FITC), Dulbecco's modified Eagle medium (DMEM) were purchased from Sigma Aldrich (St Louis, MO, USA). The ELISA kits were purchased from Thermofisher (Vienna, Austria). Rhodamine phalloidin (RP) and DAPI stain were purchased from Thermofisher (Vienna, Austria). All of the extra chemicals and solvents were of analytical grade and were used exactly as received.

4.2.2. Methods

4.2.2.1. Preparation of the IFNα nano-embedded PECE hydrogels

The IFNPH was prepared in two steps. The first step involved the preparation and characterisation of the PBAE-NPs and loading of the IFN-α2b, while in the second step, the IFN-α2b loaded nanoparticles were dispersed in the PECE aqueous solution yielding the IFNPH, as illustrated in **Figure 4.1**. The prepared system underwent rheological characterisation using a rheometer (Haake Modular Advanced Rheometer System, Thermo Fisher Scientific, Germany). As demonstrated in the previous chapter, the 20%w/v system displayed a sol-gel transition of 27-45°C and was liquid at room temperature and transition to gel upon administration to an environment simulating body temperature. Ease of preparation and syringeability strengthen the system's potential for ocular application. The loaded PBAE-NPs had a particle size of 151 nm and polydispersity index of 0.148 with an encapsulation efficiency of 89%.

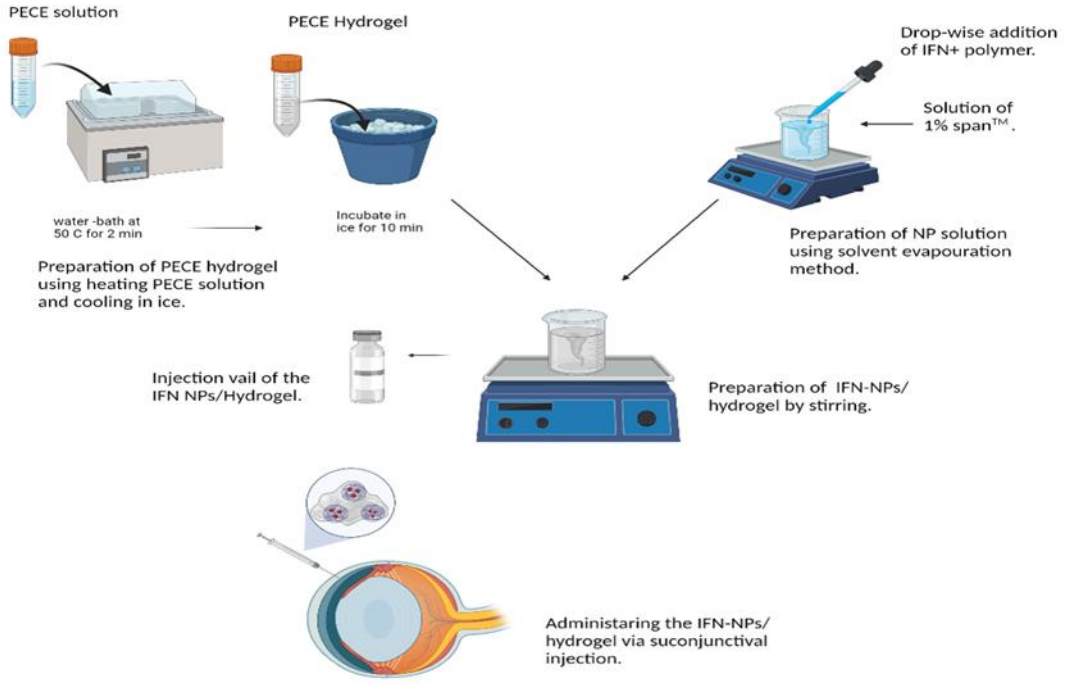


Figure 4.1 Schematic illustration of IFNPH formulation process from IFN- α2b loaded NPs and PECE precursor solution.

4.2.2.2. Transcorneal permeability of IFNPH

The corneal permeability was evaluated using the corneas of New Zealand albino rabbits on a Franz diffusion cell (PermeGear Inc., Bethlehem, PA, USA) with an effective diffusion area of 1.7 cm^2. Three eyes were enucleated, and the cornea and approximately 3 mm of scleral tissue were removed. To avoid dehydration, these were rinsed with artificial tear fluid (ATF), wrapped in film, and refrigerated until used within 4 hrs of collection (Bierbrauer *et al.*, 2023; Uwaezuoke *et al.*, 2022). The cornea was placed between the donor and receiving chambers with the endothelium facing downward towards the receiving chambers. The receiving chamber was filled with 12 mL of ATF (pH 7.4), and the system temperature was maintained at 37°C using a circulating water bath. The IFNPH dispersion in ATF was introduced into the donor chamber. Aliquots (0.2 mL) were taken from the receiving chamber and replenished with ATF at various time points. Using an ELISA kit, the samples were analysed at 450 nm with a multimode microplate reader (Filter MaxTM F5, Molecular Devices, CA,

USA). The quantity of IFN-α2b released was determined using a typical linear IFN-α2b curve in PBS (pH 7.4) refer to Appendix A.

4.2.2.3. Cellular uptake and internalization

The human immortalized keratinocytes HaCaT cells were used to overcome the issues of the short culture lifespan experienced with HRPE. The HaCaT cells are used for their great capacity to differentiate and proliferate *in vitro*. The HaCaT were cultured, until the cells reached ~80-90% confluence the cells were seeded at a density of 10^5 cells/mL and cultured on coverslips in 6-well plates. The cells were maintained in culture medium containing advance DMEM supplemented with 10% FBS and 1% penicillin–streptomycin and incubated for 24 hrs in 95% humidity, 5% CO_2 at 37°C. After 24 hrs, the adhered cells were treated with 90 μg/mL FITC loaded PBAE-NPs. Subsequently, the cells were incubated for 24 hrs after treatment. Thereafter, the cells were first spiked with 500 μL of 4% paraformaldehyde to avoid damaging the cells by the abrupt change in osmolarity between the fixation solution and culture medium osmolarity. Thereafter, the media was aspirated after 2 min, and the cells were covered with 1 mL of 4% paraformaldehyde for about 20 min. After 20 min of fixation, the cells were gently washed with 2 mL PBS four times to remove any unbound fixation agent. Thereafter, the cells were stained with 20 μL of a 66 μM Rhodamine phalloidin (RP) solution for 20 min at room temperature in the dark. After 20 min, the cells were washed four times with PBS to remove the unbound stain. Subsequently the cells were stained with 500 μL of 500 nM DAPI at room temperature for 5 min in the dark. After incubation the cells were rinsed twice with PBS to remove the unbound DAPI stain. The cover slips were mounted on glass slides and viewed under the compound fluorescent microscope (Olympus IX51, Olympus Corporation, Tokyo, Japan).

4.2.2.4. Animal experiments

The *in vivo* evaluation was undertaken in twenty New Zealand albino rabbits (average weight 2.5 - 3.5 kg) at the Wits Research Animal Facility (WRAF), treated according to the procedure approved and monitored by the animal Research Ethics Committee (AREC) at the University of the Witwatersrand. Before application, all rabbit's eyes were evaluated to rule out any ocular abnormalities by a trained ophthalmologist. The overall health, body mass index, and other physiological indicators of the animals were

monitored constantly following injection. The Animal Research Ethics Committee (AREC) at the Faculty of Health Sciences the University of the Witwatersrand authorised the study's procedure with ethics certificate number, 2021/03/07/C. The protocol followed international ethical requirements.

4.2.2.5. Pharmacokinetics studies

PECE aqueous solution (0.2 mL of 20% $^{w}/_{v}$) loaded with IFN-α2b (3 µg/mL) was administered to the rabbits through a subconjunctival injection by the ophthalmologist. The aqueous solution was injected subconjunctivally in the left eye using a 27G needle while the right eye served as a control. Five rabbits were terminated at specified time points which were 1, 3, 5, and 14 days. Their eyes were enucleated, and their aqueous humour and vitreous humour were collected for the quantification of IFN-α2b. The animals were allocated to four groups named (I–IV) in accordance with the termination times, which were 1, 3, 5, and 14 days, respectively. The samples were collected and analysed using an ELISA kit according to the manufacturer's protocol. The quantity of IFN-α2b released was determined using the standard curve of IFN-α2b in PBS pH 7.4 (refer to **Appendix A)**.

4.2.2.6. *In vivo* toxicity and histopathological examination

The toxicity of the IFNPH to the ocular tissues was evaluated on the rabbit eyes at pre-determined time points (1, 3, 7, and 14 days). Histological analysis was conducted on enucleated eyes to evaluate tissue response and histopathological changes. Following fixation of the samples in 10% neutral buffered formalin, the samples were cut according to standard procedure (idexxSA-AP-SOP-26). The biopsies were processed in an automated tissue processor (idexxSA-AP-SOP-27). Following tissue processing, sections of 5-6 µm (idexxSA-AP-SOP-30), the tissues were subsequently stained in an automated haematoxylin and eosin tissue strainer (idexxSA-AP-SOP-205). The toxicity of the injected IFNPH on the ocular tissues and histopathological changes were observed under the microscopic.

4.3. Results

4.3.1. Transcorneal permeability of IFNPH across rabbit cornea

Generally, delivery of therapeutics to the eye, specifically the ocular surface, is challenged by the anatomical and physiological barriers of the eye. These ocular barriers protect the eyes from invasion by foreign substances; namely the static and dynamic barriers, and efflux pump in ocular tissue. The diffusion and permeability of therapeutics (that are also seen as foreign by the eye) to the ocular tissue are therefore hindered, resulting in reduced bioavailability (Huang *et al.*, 2018). The static barriers include the cornea, sclera and the retinal pigment epithelia (including the blood-aqueous barrier and the blood retinal barrier). The lymphatic flow in the choroid and conjunctiva blood flow represents the dynamic barriers (Gaudana *et al.*, 2010; Patel *et al.*, 2013).

Following topical application, a drug molecule would need to cross several ocular barriers to deliver to the targeted site, represented in **Figure 4.2**. For the IFNPH developed herein, the therapeutic efficiency is dependent on the drug-loaded NPs release from the hydrogel, their penetration or permeation across the ocular layers namely (the tear film, and the corneal barriers) and their effective delivery to the target region the conjunctival epithelium.

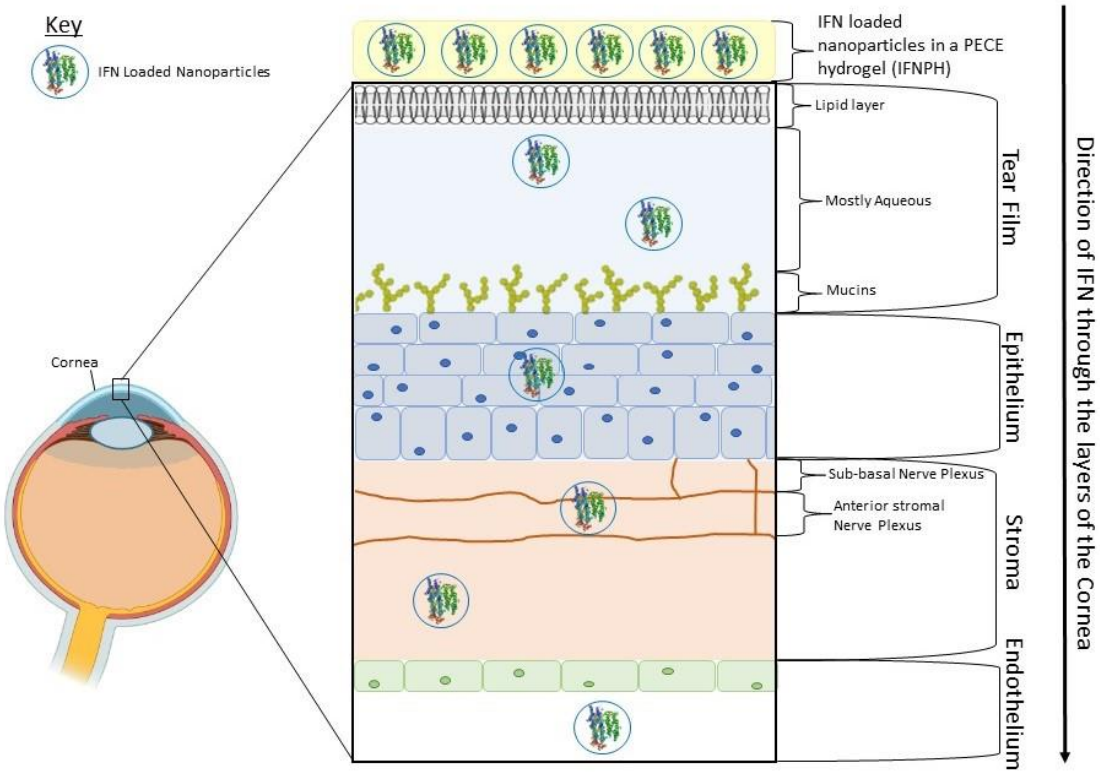


Figure 4.2 The barriers encountered by drug carriers following topical application onto the ocular surface.

Figure 4.3 depicts the amount of IFN-α2b permeated per unit area. During the 6hrs examination period, the amount of IFN-α2b that penetrated the tissue per unit area increased. The maximum cumulative permeated amount was 1528 pg/cm^2 at a flux of 440.6 pg/cm^2 /hrs, and coefficient of permeability (1.1 × 10^{-2} cm/hrs). The IFNPH enabled a cumulative IFN-α2b percent permeation of 0.45% after 6 hrs. The IFN-α2b permeation from the IFNPH was fitted into different mathematical models, including the zero-order, first-order, Higuch, and Korsmeyer-Peppas models. Mathematical models are applied for defining and clarifying release mechanisms. The regression coefficient values for IFN-α2b in the selected models were: 0.9845, 0.9680, 0.8112, and 0.9985; for zero-order, first-order, Higuchi, and Korsmeyer-Peppas, respectively. The Korsmeyer-Peppas model is the most suitable fit for describing the IFNα permeation with an R^2 of 0.9985. The release exponent (n) was 1.24 indicating that the release mechanism was super case II transport also known as super diffusion.

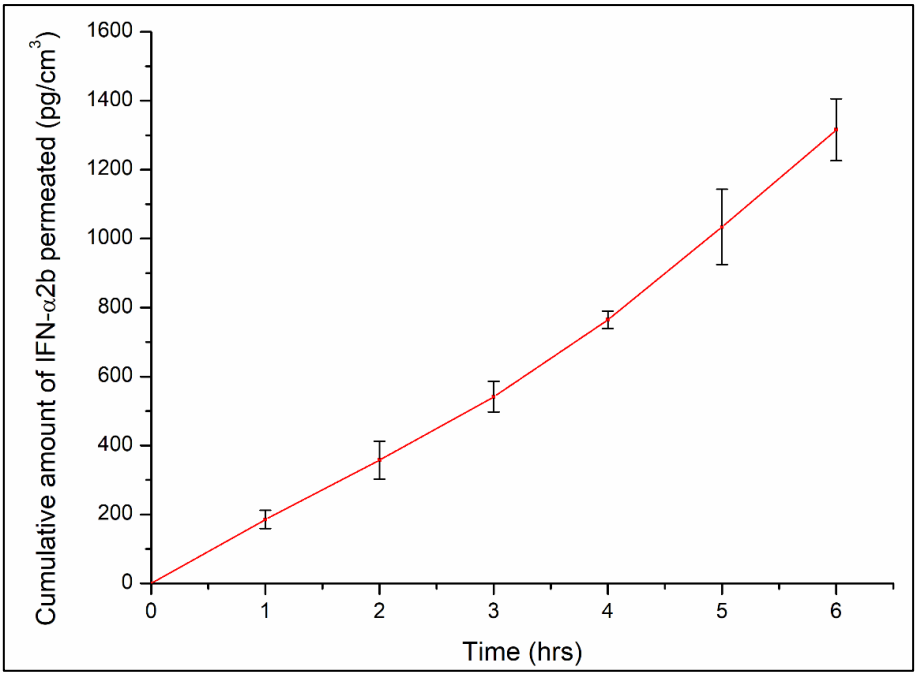


Figure 4.3 Corneal permeability of the IFNPH across the rabbit's cornea.

4.3.2. Assessment of the cellular uptake of the IFNPs

Nanoparticles' safe cellular uptake is crucial to their intended function of delivering their payload (drugs, proteins, genes, etc.) to the nucleus, cytoplasm, or other specific intracellular region (Behzadi *et al.*, 2017; Donahue *et al.*, 2019). The physiochemical characteristics of nanoparticles, as well as variations in cell-membrane properties, govern nanoparticle cellular internalisation. Nanoparticle interaction with cells influences intracellular trafficking, sorting into separate cellular compartments, and release, all of which influence toxicity, pharmacokinetics, and therapeutic efficacy (Adjei *et al.*, 2014; Donahue *et al.*, 2019; Rees *et al.*, 2019). The intended site for delivering IFN-α2b is the cell surface, where it binds to specific receptors. The PBAE-NP protects IFN-α2b from degradation by the low pH at the tumour site and removal by the reticular endothelial system. The cellular uptake behaviour of the PBAE-NPs was evaluated qualitatively using fluorescence microscope. DAPI was used to stain the nucleus. Its blue fluorescence contrasts with the green, yellow, or red fluorescent probes seen in other structures (Tarnowski *et al.*, 1991). Following incubation for 24hrs FITC-loaded NPs were evident as specks of green fluorescence in the cytoplasm (H), whereas the control group (G) displayed no signs of florescence as shown in **Figure 4.4**. The results indicate that the PBAE-NPs were internalised by the cells, as indicated by the arrows in image (H).

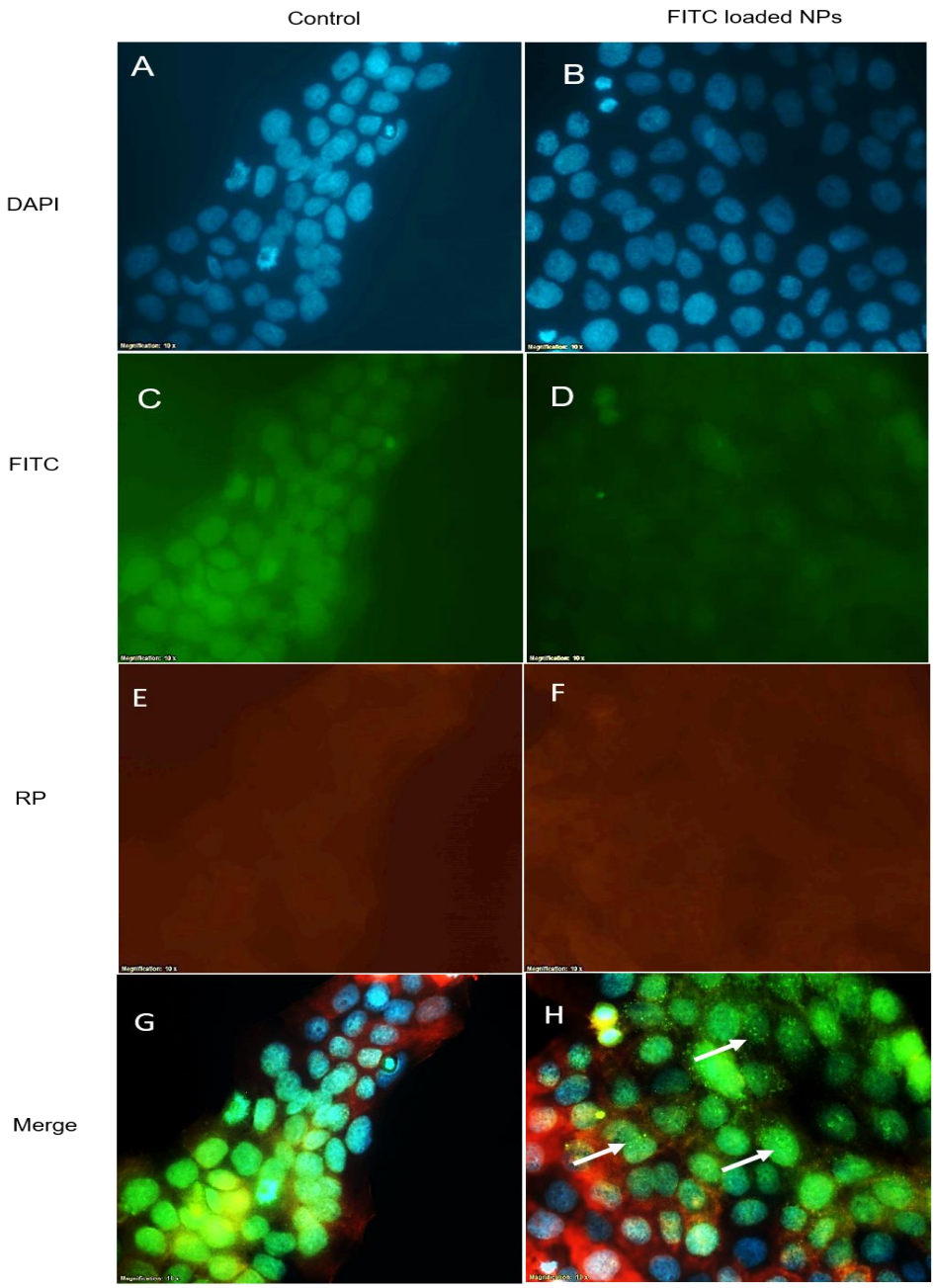


Figure 4.4 Fluorescence microscope images of cellular uptake of NP (control) and FITC-loaded NP at (10X magnification). Where ;(A, B) are the DAPI stained cells, (C, D) are the FITC stained cells, (E, F) are the RP-stained cells, and (G, H) are the merged images of all.

4.3.3. *In vivo* toxicity analysis

Prior to treatment, all rabbit eyes were evaluated to rule out any ocular abnormalities. Throughout the investigation, there were no fatalities or complications from the injection, and the hydrogel remained in the subconjunctival space. **Figure 4.5** shows

images of the rabbit eyes captured at the beginning and end of the study, after subconjunctival administration, to demonstrate the IFNPH features at the injection site. The IFNPH aqueous solution produced a matrix in the subconjunctival space proving the thermo-responsive behaviour of the system. The images reveal the presence of IFNPH after the termination at 14 days, as indicated by the arrow in **Figure 4.5 (b)**. The amount of IFNPH has decreased due to the release of the drug from the system and the degradation of the hydrogel. Furthermore, the presence of the residues indicate that the system would further release the remainder of the loaded IFN-α2b from the IFNPH.

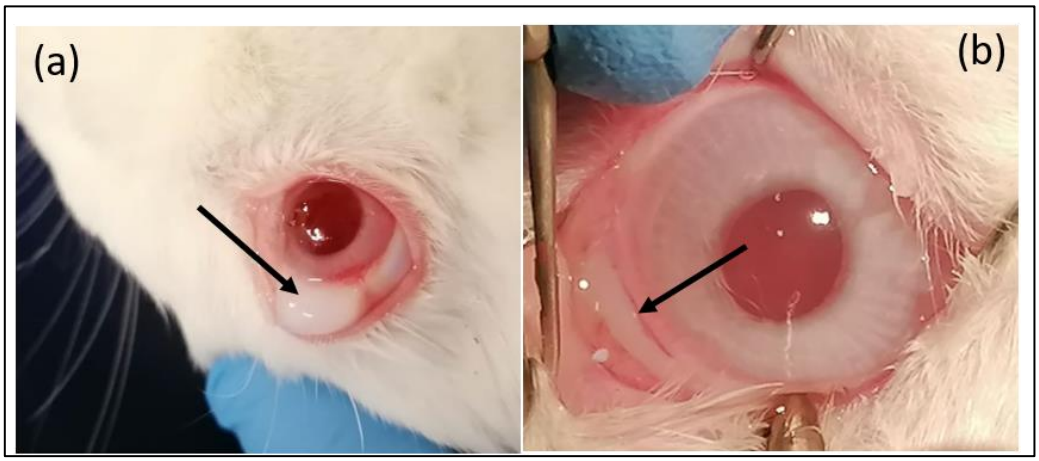


Figure 4.5 IFNPH formation in vivo following subconjunctival injection in a rabbit eye model: (a) at 0 days and (b) at 14 days post application.

4.3.4. Histopathological analysis

The biocompatibility of IFNPH was evaluated in rabbit eyes. After subconjunctival injection, haematoxylin-eosin tissue slices of the eyes were studied for the 14 days investigation period. **Figure 4.6** depicts the histopathological examination images of untreated control and the groups from of the rabbit's eyes. For Group I and Group II, there was inflammation in the periocular connective tissue, which is linked to the injection site. The inflammation is limited to a small area, though it extended into the adjacent muscle in some animals. The inflammatory response is primarily composed of heterophils, with lymphoplasmacytic cells present in some animals ranging from minimal to mild and with associated to haemorrhage and oedema. Group III presented with periocular connective tissue granulomas, which appear as well-demarcated nodular masses composed of foamy macrophages, lymphocytes, and plasma cells

appearing in some samples. One sample in Group III had a cystic formation with no evidence of inflammation which is thought to be residue of the IFNPH. Group IV; samples had elongated granulomas either in the bulbar conjunctival deep submucosa or the periocular connective tissue as well as cyst formation (i.e., enclosing the residue of IFNPH).

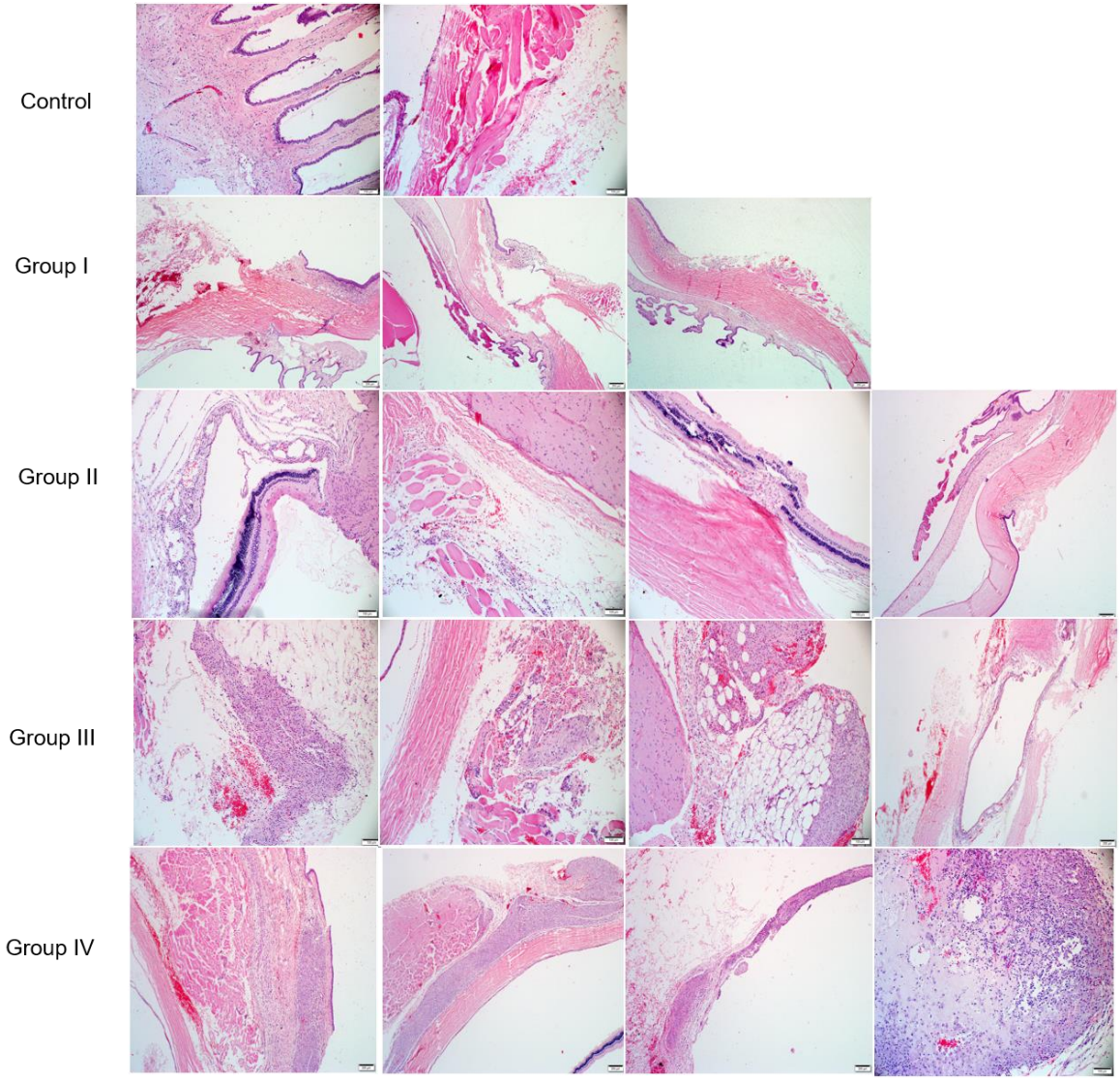


Figure 4.6 Histopathological sections of eyes following subconjunctival application. Control; untreated eyes, Group I; termination after one day, Group II; termination after 3 days, Group III; termination after 7days, and Group IV; termination after 14 days.

4.3.5. Intraocular pharmacokinetics

The pharmacokinetic parameters are listed in **Table 4.1**, and PKsolver 2.0 software was utilized for analysing the data using a non-compartmental model (Zhang *et al.*, 2010). **Figure 4.7** depicts the concentration of IFN-α2b in ocular tissues after

subconjunctival administration of 0.2 mL IFNPH at a concentration of 3 µg/mL. The maximum concentration (C_{max}) in the vitreous and aqueous humours were 129.7 ± 0.01 and 88.7 ± 0.01 pg/mL, respectively, achieved after 24 hrs (t_{max}) following application. The T½ in the vitreous and aqueous humour was 55 and 105 days, respectively. The area under the curve ($AUC_{0\text{-}14}$ days) was 1637 and 1150.8 pg/mL.days, respectively, in the vitreous and aqueous humour. The subconjunctival pathway avoids the cornea-conjunctiva barrier, which prevents macromolecules from passing through the sclera to the anterior chamber. The drug diffuses to the cornea and intraocular tissue or is eliminated via conjunctival blood and lymphatic flow. Consequently, drug clearance from the subconjunctival area becomes a key indicator of vitreous drug levels after subconjunctival delivery. The drug molecule passes through the conjunctiva, permeates the sclera and choroid, and reaches the retinal pigmented epithelia (Gaudana *et al.*, 2010; Nomoto *et al.*, 2009). As a result, subconjunctival injection is a viable route for the delivery of macromolecules to the anterior and posterior regions.

Table 4.1 Pharmacokinetic parameters of IFN-α2b (0.125 MIU, 0.6 µg per rabbit eye) following subconjunctival injection of IFNPH.

Tissue Sample	Aqueous humour	Vitreous humour
Cmax(pg/ml)	88.7	129.7
Tmax (days)	1	1
T½ (days)	105.8	55.6
AUC0-14 (pg/ml .days)	1150.8	1637
AUC0-∞ (pg/ml .days)	13075	9780.9

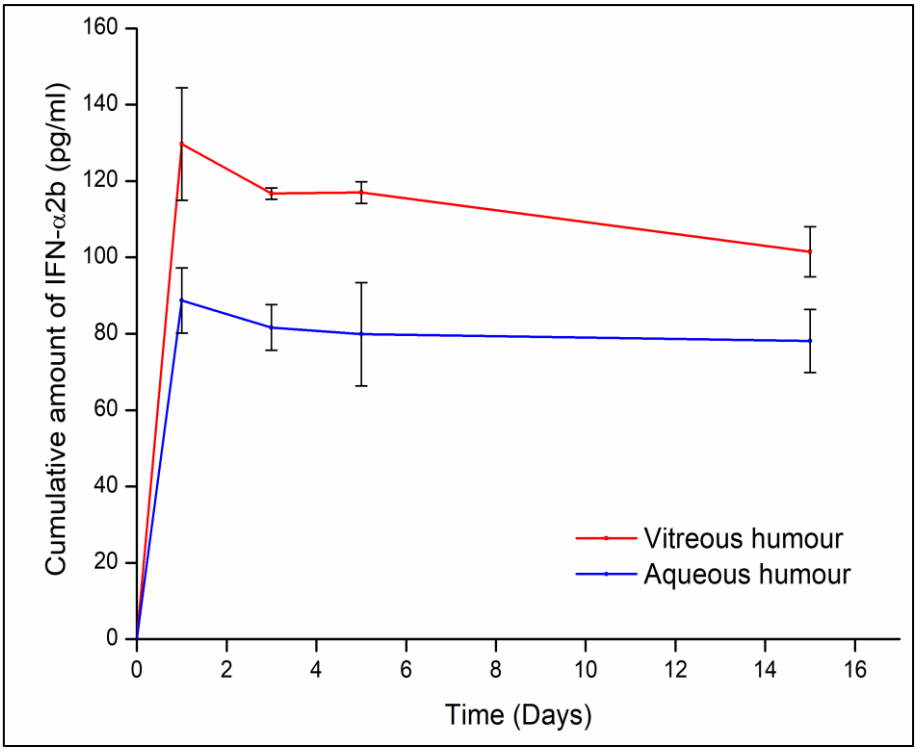


Figure 4.7 The intraocular pharmacokinetic profile of IFN-α2b following subconjunctival application of IFNPH in rabbits (n =5, mean± SD).

4.4. Discussion

Interferon alpha's susceptibility to degradation, the very short half-life of 2-3 hrs, and quick clearance by the reticuloendothelial system (RES) have all hampered its use in the treatment of ocular cancers (Beilharz *et al.*, 2010; Bonetti and Kim, 1993; Lewczuk *et al.*, 2019). The available subconjunctival injections and eye drops of interferon require multiple rounds of application (Meel *et al.*, 2021). Hence, the need to develop advanced delivery systems to address these constraints in clinical use has arisen. Researchers have been investigating the possibility for improving the bioavailability of IFN-α2b while reducing the side effects (Castro *et al.*, 2021). Delivering IFN-α2b locally to the ocular surface would be a promising approach in the management of ocular tumors, providing a high concentration at the tumour site with reduced systemic side effects.

The PECE hydrogel was previously recognized for its thermo-responsiveness and biodegradability and has received substantial attention as a potential controlled delivery system (du Toit *et al.*, 2021; Gong *et al.*, 2009c; Luo *et al.*, 2016). According to earlier research, the micelle packing, and aggregation processes may be

responsible for the temperature-dependent change of PECE aqueous solution to gel (Gong *et al.*, 2009a; Gong *et al.*, 2009b). At body temperature, the 20% w/v PECE hydrogel developed quickly. Furthermore, incorporating IFNα-loaded nanoparticles into the PECE solution had no effect on the sol-gel transition window. Thermo-responsive hydrogels are potential candidates to deliver the IFN-α2b macromolecule to the intraocular tissues. In a previous study, Xu *et al*. (2018) investigated the delivery of the full-length humanized monoclonal antibody Bevacizumab (Avastin®) loaded into PFCE hydrogel. Following a single subconjunctival injection in an animal model; the concluding results where that the Avastin®-hydrogel might be a promising choice for the prevention of corneal neovascularization (Xu *et al.*, 2018). The findings in our study correlates to Xu's results; as the IFN-α2b concentration was maintained throughout the investigation in the aqueous humour due to the physical entrapment of the protein in the highly entangled hydrogel micro-porous structure causing sustained diffusion (Bawa *et al.*, 2009). Furthermore, the IFN-α2b reached the vitreous via sclera diffusion, and the hydrogel protected the IFN-α2b from degradation.

Several studies have demonstrated the application of nanoparticles in the delivery of IFN-α, but none for ocular delivery. In one such study conducted by, Cánepa *et al*. (2017) IFNα-loaded chitosan nanoparticles with high encapsulation efficiency for oral delivery were synthesised. Following oral administration, a preliminary *in vivo* study on CF-1 mice demonstrated that IFNα was detectable in the plasma after one hour; however, free IFNα was not detected in the plasma at the same time point (Cánepa *et al.*, 2017). Imperiale *et al*. (2019) arrived at the same conclusion, stating that the mucoadhesive characteristics of chitosan improved oral bioavailability to levels comparable to intravenous dosing (Imperiale *et al.*, 2019). Giri *et al*. (2011) created cationic PLGA nanoparticles that were coated with hepatitis B surface antigens. The particle size of 174 nm and surface characteristics of the nanoparticles influenced their distribution and opsonization. The study concluded that IFNα remained stable within the cationic nanoparticles, with 91% of IFNα retrieved from nanoparticles containing trehalose (Giri *et al.*, 2011). In this study, the corneal permeability demonstrated that the PBAE nanoparticles penetrated through the cornea with a flux of 440.6 pg/cm^2 /hrs. The corneal epithelium and stroma are constraints that prevent hydrophilic, macromolecules and hydrophobic medications from penetrating the eye (Hegde *et al.*, 2013). The particle size of the prepared PBAE nanoparticles was 151 nm, which is

within the nano-size range allowing the permeability across the corneal barriers (Cholkar *et al.*, 2012). These findings imply that PBAE-NPs have a high potential for sustained *in vivo* protein delivery. The results obtained in this study suggests that the IFNPH enhanced the permeability by two mechanisms that act concordantly. The first proposed mechanism is that the hydrogel acts as a depot from which the nanoparticles are released in a sustained manner, the viscosity of the hydrogel enhanced the residence time of system. The second mechanism proposed is that transcellular transport of IFNα-loaded NP across the ocular barriers into the receiving compartment is achieved by the properties of the cationic PBAE and the coupled PEG molecule. The PEGylated PBAE form core-shell nanoparticles, the PEG corona has excellent stealth properties capable of bypassing major biological barriers (Mastorakos *et al.*, 2015a; Mastorakos *et al.*, 2015b; Schopf *et al.*, 2015). The PBAE nanoparticles enhanced the permeation through ocular barriers which was further confirmed by the cellular uptake studies of FITC-loaded nanoparticles. The fluorescent microscope was utilised to assess NPs cellular uptake; FITC-loaded PBAE-NPs were synthesised and used as a model. To examine the NP-cell interaction, human immortalised keratinocytes HaCaT cells were used as an *in vitro* model. Images of cells cultured with FITC-loaded NPs exhibit an unspecific amount of green fluorescence. Following a 24 hrs incubation period, FITC-loaded NPs showed specks of green fluorescence in the cytoplasm. Some NPs remained outside the cells, visualised as a spherical structure. These findings support the ability of PBAE-NPs to transport IFN-α2b or other encapsulated medications to the cellular milieu. The intended site for delivering IFN-α2b is the cell surface, where it binds to specific receptors and activates the Janus-activated kinase and signal transduction pathways. The encapsulation of IFN-α2b in nanoparticles protects the protein from degradation during transport or at the delivery site, thus enhancing therapeutic efficacy and reducing toxicity (Ye and Chi, 2018). The design of nanocarriers with the ability to be efficiently internalised by cells increases the likelihood of success for many treatments (Ramsay *et al.*, 2018).

The subconjunctival route circumvents the cornea-conjunctival barrier, which hinders hydrophilic molecules from permeating through (Gaudana *et al.*, 2010). Following subconjunctival injection, the drug molecule must pass through the sclera, which has a large and permeable surface area as well as a high degree of hydration, rendering

it accessible to the hydrophilic molecules (Kim *et al.*, 2002; Ranta and Urtti, 2006). One study that evaluated the subconjunctival route for the delivery of dexamethasone showed that the route proved effective in delivering the drug to the anterior and posterior ocular segments (Weijtens *et al.*, 1999). In the current study, the *in vivo* pharmacokinetic parameters revealed that IFN-α2b concentration in ocular humours peaked on the first day, followed by a gradual release over a 14 day period. It is therefore expected that the dosing frequency will be decreased with reference to a study in patients with ocular tumours treated with subconjunctival IFN-α2b injections. In the referenced study, the patients were administered IFN-α2b (3 MIU/0.5 mL) three times a week, and the median resolution time was 1.4 months (Karp *et al.*, 2010). The extended half-life is representative of improved retention; it is known that the elimination from the posterior segment involves permeation across the blood-retinal barrier, either through passive permeability of small molecules or active transport of macromolecules. Hence, the half-life of macromolecules in the vitreous is prolonged (Urtti, 2006). The AUC0-∞ in this study injection of IFN-α2b (0.125 MIU), was 13075 and 9780.9 pg*d /mL in the aqueous and vitreous humour, respectively, compared to a study conducted on healthy volunteers (Radwanski *et al.*, 1987), which demonstrated an AUC0-∞ and Cmax after intravenous administration of IFNα (5 MIU) were 994 pg*h/mL and 853 pg/mL, respectively (Radwanski *et al.*, 1987). Considering the dose difference, the values reported in this investigation are in good agreement with those obtained from human volunteers. These results highlight the potential of the IFNPH formulation for the improved controlled ocular delivery of IFN-α2b, with a potential for a reduction in dosing frequency.

4.5. Conclusion

In this work, the concentration of IFN-α2b in ocular humours following a single subconjunctival injection of the synthesised IFNPH in rabbits is reported. The IFNPH was loaded with 3 µg/mL IFN-α2b, and rapidly formed a gel at body temperature. *In vivo* examination revealed no significant inflammatory response in the conjunctivae or sclera. The intraocular pharmacokinetic results demonstrated the sustained release of the loaded IFN-α2b. The corneal permeability and cellular uptake studies suggested that the system is a possible candidate for site-specific treatment of ocular surface tumours. Further assessment for the *in vivo* performance in a preclinical tumour model is proposed.

4.6. References

1. Adjei, I. M., Sharma, B. & Labhasetwar, V. 2014. Nanoparticles: cellular uptake and cytotoxicity. *Nanomaterial: impacts on cell biology and medicine*, 73-91.
2. Ahmed, I. 2003. The noncorneal route in ocular drug delivery. *Drugs and the pharmaceutical sciences,* 130, 335-364.
3. Al Bayyat, G., Arreaza-Kaufman, D., Venkateswaran, N., Galor, A. & Karp, C. L. 2019. Update on pharmacotherapy for ocular surface squamous neoplasia. *Eye and Vision,* 6, 1-12.
4. Antonietta Blasi, M., Maceroni, M., Grazia Sammarco, M. & Pagliara, M. M. 2018. Mitomycin C or interferon as adjuvant therapy to surgery for ocular surface squamous neoplasia: comparative study. *European journal of ophthalmology,* 28, 204-209.
5. Bawa, P., Pillay, V., Choonara, Y. E. & Du Toit, L. C. 2009. Stimuli-responsive polymers and their applications in drug delivery. *Biomedical materials,* 4, 022001.
6. Behzadi, S., Serpooshan, V., Tao, W., Hamaly, M. A., Alkawareek, M. Y., Dreaden, E. C., Brown, D., Alkilany, A. M., Farokhzad, O. C. & Mahmoudi, M. 2017. Cellular uptake of nanoparticles: journey inside the cell. *Chemical society reviews,* 46, 4218-4244.
7. Beilharz, M. W., Cummins, M. J., Bennett, A. L. & Cummins, J. M. 2010. Oromucosal Administration of Interferon to Humans. *Pharmaceuticals,* 3, 323-344.
8. Bierbrauer, K. L., Comini, L. R., Leonhard, V., Escobar Manzanelli, M. A., Castelli, G., Farfán, S., Alasino, R. V. & Beltramo, D. M. 2023. Eudragit Films as Carriers of Lipoic Acid for Transcorneal Permeability. *Polymers,* 15, 1793.
9. Boehm, M. D. & Huang, A. J. 2004. Treatment of recurrent corneal and conjunctival intraepithelial neoplasia with topical interferon alfa 2b. *Ophthalmology,* 111, 1755-1761.
10. Bonetti, A. & Kim, S. 1993. Pharmacokinetics of an extended-release human interferon alpha-2b formulation. *Cancer chemotherapy and pharmacology,* 33, 258-261.
11. Bourges, J., Bloquel, C., Thomas, A., Froussart, F., Bochot, A., Azan, F., Gurny, R., BenEzra, D. & Behar-Cohen, F. 2006. Intraocular implants for extended

drug delivery: therapeutic applications. *Advanced drug delivery reviews,* 58**,** 1182-1202.

12. Cánepa, C., Imperiale, J. C., Berini, C. A., Lewicki, M., Sosnik, A. & Biglione, M. M. 2017. Development of a drug delivery system based on chitosan nanoparticles for oral administration of interferon-α. *Biomacromolecules,* 18**,** 3302-3309.
13. Castro, L. S., Lobo, G. S., Pereira, P., Freire, M. G., Neves, M. C. & Pedro, A. Q. 2021. Interferon-Based Biopharmaceuticals: Overview on the Production, Purification, and Formulation. *Vaccines,* 9**,** 328.
14. Cholkar, K., Patel, A., Dutt Vadlapudi, A. & K Mitra, A. 2012. Novel nanomicellar formulation approaches for anterior and posterior segment ocular drug delivery. *Recent patents on nanomedicine,* 2**,** 82-95.
15. Donahue, N. D., Acar, H. & Wilhelm, S. 2019. Concepts of nanoparticle cellular uptake, intracellular trafficking, and kinetics in nanomedicine. *Advanced Drug Delivery Reviews,* 143**,** 68-96.
16. du Toit, L. C., Choonara, Y. E. & Pillay, V. 2021. An injectable nano-enabled thermogel to attain controlled delivery of p11 peptide for the potential treatment of ocular angiogenic disorders of the posterior segment. *Pharmaceutics,* 13**,** 176.
17. Fang, C., Kievit, F. M., Veiseh, O., Stephen, Z. R., Wang, T., Lee, D., Ellenbogen, R. G. & Zhang, M. 2012. Fabrication of magnetic nanoparticles with controllable drug loading and release through a simple assembly approach. *Journal of controlled release,* 162**,** 233-241.
18. Fernandes, B. F., Nikolitch, K., Coates, J., Novais, G., Odashiro, A., Odashiro, P. P., Belfort, R. N. & Burnier Jr, M. N. 2014. Local chemotherapeutic agents for the treatment of ocular malignancies. *survey of ophthalmology,* 59**,** 97-114.
19. Ferrantini, M., Capone, I. & Belardelli, F. 2007. Interferon-α and cancer: Mechanisms of action and new perspectives of clinical use. *Biochimie,* 89**,** 884-893.
20. Galor, A., Karp, C. L., Chhabra, S., Barnes, S. & Alfonso, E. C. 2010. Topical interferon alpha 2b eye-drops for treatment of ocular surface squamous neoplasia: a dose comparison study. *British journal of ophthalmology,* 94**,** 551-554.

21. Galor, A., Karp, C. L., Oellers, P., Kao, A. A., Abdelaziz, A., Feuer, W. & Dubovy, S. R. 2012. Predictors of ocular surface squamous neoplasia recurrence after excisional surgery. *Ophthalmology,* 119**,** 1974-1981.
22. Gaudana, R., Ananthula, H. K., Parenky, A. & Mitra, A. K. 2010. Ocular drug delivery. *The AAPS journal,* 12**,** 348-360.
23. Giri, N., Tomar, P., Karwasara, V. S., Pandey, R. S. & Dixit, V. K. 2011. Targeted novel surface-modified nanoparticles for interferon delivery for the treatment of hepatitis B. *Acta Biochimica et Biophysica Sinica,* 43**,** 877-883.
24. Gong, C., Shi, S., Dong, P., Kan, B., Gou, M., Wang, X., Li, X., Luo, F., Zhao, X. & Wei, Y. 2009a. Synthesis and characterization of PEG-PCL-PEG thermosensitive hydrogel. *International journal of pharmaceutics,* 365**,** 89-99.
25. Gong, C., Shi, S., Wu, L., Gou, M., Yin, Q., Guo, Q., Dong, P., Zhang, F., Luo, F. & Zhao, X. 2009b. Biodegradable in situ gel-forming controlled drug delivery system based on thermosensitive PCL–PEG–PCL hydrogel. Part 2: Sol–gel–sol transition and drug delivery behavior. *Acta biomaterialia,* 5**,** 3358-3370.
26. Gong, C. Y., Dong, P. W., Shi, S., Fu, S. Z., Yang, J. L., Guo, G., Zhao, X., Wei, Y. Q. & Qian, Z. Y. 2009c. Thermosensitive PEG–PCL–PEG hydrogel controlled drug delivery system: sol–gel–sol transition and in vitro drug release study. *Journal of pharmaceutical sciences,* 98**,** 3707-3717.
27. Gote, V., Sikder, S., Sicotte, J. & Pal, D. 2019. Ocular drug delivery: Present innovations and future challenges. *Journal of Pharmacology and Experimental Therapeutics,* 370**,** 602-624.
28. Green, J. J., Langer, R. & Anderson, D. G. 2008. A combinatorial polymer library approach yields insight into nonviral gene delivery. *Accounts of chemical research,* 41**,** 749-759.
29. Hegde, R. R., Verma, A. & Ghosh, A. 2013. Microemulsion: new insights into the ocular drug delivery. *International Scholarly Research Notices,* 2013.
30. Huang, D., Chen, Y.-S. & Rupenthal, I. D. 2018. Overcoming ocular drug delivery barriers through the use of physical forces. *Advanced drug delivery reviews,* 126**,** 96-112.
31. Imperiale, J. C., Schlachet, I., Lewicki, M., Sosnik, A. & Biglione, M. M. 2019. Oral Pharmacokinetics of a Chitosan-Based Nano- Drug Delivery System of Interferon Alpha. *Polymers,* 11**,** 1862.

32. Kaliki, S., Singh, S., Iram, S. & Tripuraneni, D. 2016. Recombinant interferon alpha 2b for ocular surface squamous neoplasia: an efficient and cost-effective treatment modality in Asian Indian patients. *Indian Journal of Ophthalmology,* 64**,** 702.
33. Karp, C. L., Galor, A., Chhabra, S., Barnes, S. D. & Alfonso, E. C. 2010. Subconjunctival/perilesional recombinant interferon α2b for ocular surface squamous neoplasia: a 10-year review. *Ophthalmology,* 117**,** 2241-2246.
34. Kim, H. J., Shields, C. L., Shah, S. U., Kaliki, S. & Lally, S. E. 2012. Giant ocular surface squamous neoplasia managed with interferon alpha-2b as immunotherapy or immunoreduction. *Ophthalmology,* 119**,** 938-944.
35. Kim, T. W., Lindsey, J. D., Aihara, M., Anthony, T. L. & Weinreb, R. N. 2002. Intraocular Distribution of 70-kDa Dextran after Subconjunctival Injection in Mice. *Investigative Ophthalmology & Visual Science,* 43**,** 1809-1816.
36. Lewczuk, N., Zdebik, A. & Bogusławska, J. 2019. Interferon alpha 2a and 2b in ophthalmology: a review. *Journal of Interferon & Cytokine Research,* 39**,** 259-272.
37. Liu, Y., Li, Y., Keskin, D. & Shi, L. 2019. Poly (β-Amino Esters): synthesis, formulations, and their biomedical applications. *Advanced healthcare materials,* 8**,** 1801359.
38. Luo, Z., Jin, L., Xu, L., Zhang, Z. L., Yu, J., Shi, S., Li, X. & Chen, H. 2016. Thermosensitive PEG–PCL–PEG (PECE) hydrogel as an in situ gelling system for ocular drug delivery of diclofenac sodium. *Drug delivery,* 23**,** 63-68.
39. Makwana, S., Patel, V. & Parmar, S. 2016. Development and characterization of in-situ gel for ophthalmic formulation containing ciprofloxacin hydrochloride. *Results in pharma sciences,* 6**,** 1-6.
40. Mastorakos, P., da Silva, A. L., Chisholm, J., Song, E., Choi, W. K., Boyle, M. P., Morales, M. M., Hanes, J. & Suk, J. S. 2015a. Highly compacted biodegradable DNA nanoparticles capable of overcoming the mucus barrier for inhaled lung gene therapy. *Proceedings of the National Academy of Sciences,* 112**,** 8720-8725.
41. Mastorakos, P., Zhang, C., Berry, S., Oh, Y., Lee, S., Eberhart, C. G., Woodworth, G. F., Suk, J. S. & Hanes, J. 2015b. Highly PEGylated DNA Nanoparticles Provide Uniform and Widespread Gene Transfer in the Brain. *Advanced Healthcare Materials,* 4**,** 1023-1033.

42. Meel, R., Dhiman, R., Vanathi, M., Sen, S., Gupta, N. & Tandon, R. 2021. Treatment outcome with interferon alpha 2b in ocular surface squamous neoplasia: Recommendation as primary treatment by peripheral ophthalmologists. *Oman Journal of Ophthalmology,* 14**,** 27.
43. Monroy, D., Serrano, A., Galor, A. & Karp, C. L. 2023. Medical treatment for ocular surface squamous neoplasia. *Eye,* 37**,** 885-893.
44. Nava-Castañeda, Á., Hernández-Orgaz, J., Garnica-Hayashi, L., Ansart, A., Matus, G., Tovilla-Canales, J. L. & Zuazo, F. 2018. Management of ocular surface squamous neoplasia with topical and intralesional interferon alpha 2B in Mexicans. *Nepalese Journal of Ophthalmology,* 10**,** 143-150.
45. Nomoto, H., Shiraga, F., Kuno, N., Kimura, E., Fujii, S., Shinomiya, K., Nugent, A. K., Hirooka, K. & Baba, T. 2009. Pharmacokinetics of Bevacizumab after Topical, Subconjunctival, and Intravitreal Administration in Rabbits. *Investigative Ophthalmology & Visual Science,* 50**,** 4807-4813.
46. Patel, A., Cholkar, K., Agrahari, V. & Mitra, A. K. 2013. Ocular drug delivery systems: An overview. *World journal of pharmacology,* 2**,** 47.
47. Radwanski, E., Perentesis, G., Jacobs, S., Oden, E., Affrime, M., Symchowicz, S. & Zampaglione, N. 1987. Pharmacokinetics of Interferon α-2b in Healthy Volunteers. *The Journal of Clinical Pharmacology,* 27**,** 432-435.
48. Ramsay, E., Del Amo, E. M., Toropainen, E., Tengvall-Unadike, U., Ranta, V.-P., Urtti, A. & Ruponen, M. 2018. Corneal and conjunctival drug permeability: Systematic comparison and pharmacokinetic impact in the eye. *European Journal of Pharmaceutical Sciences,* 119**,** 83-89.
49. Ranta, V.-P. & Urtti, A. 2006. Transscleral drug delivery to the posterior eye: prospects of pharmacokinetic modeling. *Advanced drug delivery reviews,* 58**,** 1164-1181.
50. Rees, P., Wills, J. W., Brown, M. R., Barnes, C. M. & Summers, H. D. 2019. The origin of heterogeneous nanoparticle uptake by cells. *Nature Communications,* 10**,** 2341.
51. Sapino, S., Chirio, D., Peira, E., Abellán Rubio, E., Brunella, V., Jadhav, S. A., Chindamo, G. & Gallarate, M. 2019. Ocular Drug Delivery: A Special Focus on the Thermosensitive Approach. *Nanomaterials,* 9**,** 884.

52. Sayed-Ahmed, I. O., Palioura, S., Galor, A. & Karp, C. L. 2017. Diagnosis and medical management of ocular surface squamous neoplasia. *Expert review of ophthalmology,* 12**,** 11-19.
53. Schopf, L. R., Popov, A. M., Enlow, E. M., Bourassa, J. L., Ong, W. Z., Nowak, P. & Chen, H. 2015. Topical ocular drug delivery to the back of the eye by mucus-penetrating particles. *Translational vision science & technology,* 4**,** 11-11.
54. Shah, S. U., Kaliki, S., Kim, H. J., Lally, S. E., Shields, J. A. & Shields, C. L. 2012. Topical interferon alfa-2b for management of ocular surface squamous neoplasia in 23 cases: outcomes based on American Joint Committee on Cancer classification. *Archives of Ophthalmology,* 130**,** 159-164.
55. Song, L., Ho, V. H. B., Chen, C., Yang, Z., Liu, D., Chen, R. & Zhou, D. 2013. Efficient, pH-Triggered Drug Delivery Using a pH-Responsive DNA-Conjugated Gold Nanoparticle. *Advanced Healthcare Materials,* 2**,** 275-280.
56. Sripawadkul, W., Reyes-Capo, D., Zein, M., Wylegala, A., Albayyat, G., Galor, A. & Karp, C. L. 2023. Long term study of topical interferon α-2b eye drops as primary treatment of ocular surface squamous neoplasia. *The Ocular Surface,* 28**,** 108-114.
57. Tarnowski, B. I., Spinale, F. G. & Nicholson, J. H. 1991. DAPI as a useful stain for nuclear quantitation. *Biotechnic & histochemistry,* 66**,** 296-302.
58. Urtti, A. 2006. Challenges and obstacles of ocular pharmacokinetics and drug delivery. *Advanced drug delivery reviews,* 58**,** 1131-1135.
59. Uwaezuoke, O., Du Toit, L. C., Kumar, P., Ally, N. & Choonara, Y. E. 2022. Linoleic Acid-Based Transferosomes for Topical Ocular Delivery of Cyclosporine A. *Pharmaceutics,* 14**,** 1695.
60. Weijtens, O., Feron, E. J., Schoemaker, R. C., Cohen, A. F., Lentjes, E. G. W. M., Romijn, F. P. H. T. M. & van Meurs, J. C. 1999. High concentration of dexamethasone in aqueous and vitreous after subconjunctival injection. *American Journal of Ophthalmology,* 128**,** 192-197.
61. Wu, Y., Liu, Y., Li, X., Kebebe, D., Zhang, B., Ren, J., Lu, J., Li, J., Du, S. & Liu, Z. 2019. Research progress of in-situ gelling ophthalmic drug delivery system. *Asian journal of pharmaceutical sciences,* 14**,** 1-15.
62. Xu, X., Yu, J., Shi, H., Zhang, J. & Li, X. 2018. Prevention of corneal neovascularization by subconjunctival injection of avastin® loaded

thermosensitive hydrogels in rabbit model. *International Journal of Pharmaceutics,* 552**,** 164-170.

63. Ye, C. & Chi, H. 2018. A review of recent progress in drug and protein encapsulation: Approaches, applications and challenges. *Materials Science and Engineering: C,* 83**,** 233-246.

64. Zhang, Y., Huo, M., Zhou, J. & Xie, S. 2010. PKSolver: An add-in program for pharmacokinetic and pharmacodynamic data analysis in Microsoft Excel. *Computer methods and programs in biomedicine,* 99**,** 306-314.

Chapter Five

Conclusions, recommendations, and future prospects

5.1. Conclusions

Several ocular illnesses that lead to blindness could benefit from effective treatment delivery to the site of action. Efficacy, however, remains restricted due to the multiple static and dynamic obstacles present in the eye, despite substantial study into administration procedures and delivery vehicle. Delivering drugs to the ocular anterior segment is a significant challenge in the field of ophthalmic pharmaceuticals. Several constraints obstruct medicine supply to this area. Topical ocular therapies and systemic administrations are the most popular routes for delivering medications to the anterior region. The most commonly utilised dose type in ocular medication delivery is topical ocular eye drops. Unfortunately, because eye drops are rapidly drained from the ocular surface and medication absorption require a few minutes, the dose/response profiles are often quite poor. Biodegradable polymers can be employed to create solid or injectable matrixes, as well as to encapsulate specific systems like nano and microparticles. Polymers can be engineered as viscous or semi-solid materials that can be localised within the eye and employed as a slow-release intraocular implant following a simple injection, delivering drugs locally for an extended period. *In situ* hydrogels are an example of these biodegradable polymer that have a three-dimensional structure and the ability to retain water. Additionally, loading of nanoparticles into the hydrogel protects the loaded drug and provides sustained release. Delivering IFN-α2b locally to the tumour site would be a promising approach in the management of ocular tumours. Providing a high concentration at the tumour site with reduced systemic side effects.

In this study two systems for employment in combination, namely the PECE hydrogel and the PBAE-NPs, were prepared. It was demonstrated in this study that the IFNHP can be utilized to enhance IFN-α2b delivery to the anterior and posterior segment of the eye. The IFNPH was designed by combining the IFNα-loaded NPs with the aqueous solution of PECE at low temperature. At room temperature, the mixture was a solution that transitioned into a gel at body temperature. The storage modulus (G′) and loss modulus (G″) as a function of temperature were used to monitor the mechanical characteristics and gel formation kinetics of the hydrogel. The PECE

hydrogel demonstrated a sol-gel transition as the temperature increased. The sol-gel transition behaviour was not affected by the addition of nanoparticles to the PECE aqueous solution; however, it did shift the sol-gel transition to a lower gelation temperature. The drug release rate was affected by the porosity and pore size of the hydrogel. SEM and porosity analysis revealed a three-dimensional structure with a pore size of 61.5310 A, allowing the diffusion of the release medium into the hydrogel as well as the diffusion of the IFN-α2b loaded NP. The PBAE nanoparticles prepared are in the nanosize range with spherical shape and good polydispersity and zeta potential, as confirmed by the TEM and DLS results. The PBAE nanoparticles are pH-responsive, controlling the release of the drug in the acidic tumour microenvironment, as confirmed by the particle size, zeta potential and polydispersity results. Furthermore, the physiochemical parameters (FTIR, DSC, XPDR and TGA) demonstrated the synthesis and stability of the system, and the entrapment of the IFN-α2b nanoparticles in the PECE hydrogel. The system exhibited sustained release profile, with a slower release rate in a more acidic pH.

The *in vitro* cytotoxicity investigation found that cell viability on exposure to the IFNPH was acceptable at the dosages ranging from 5 to 0.625 mg/mL used in the study, with no notable cytotoxicity effects on cell line. The biocompatibility of the nano-embedded hydrogel was further validated by an *in vivo* toxicity study, which showed that the prepared IFNPH presented no, or minimal signs of inflammation as revealed by the histopathological examination. Overall, the designed IFNPH is expected to demonstrate notable efficiency in the quantity of the doses and the frequency of administration as compared to eye drops and subconjunctival injection of the commercially available IFN-α2b solution, hence, highlighting its potential as a promising candidate for ocular application in the treatment of ocular tumours.

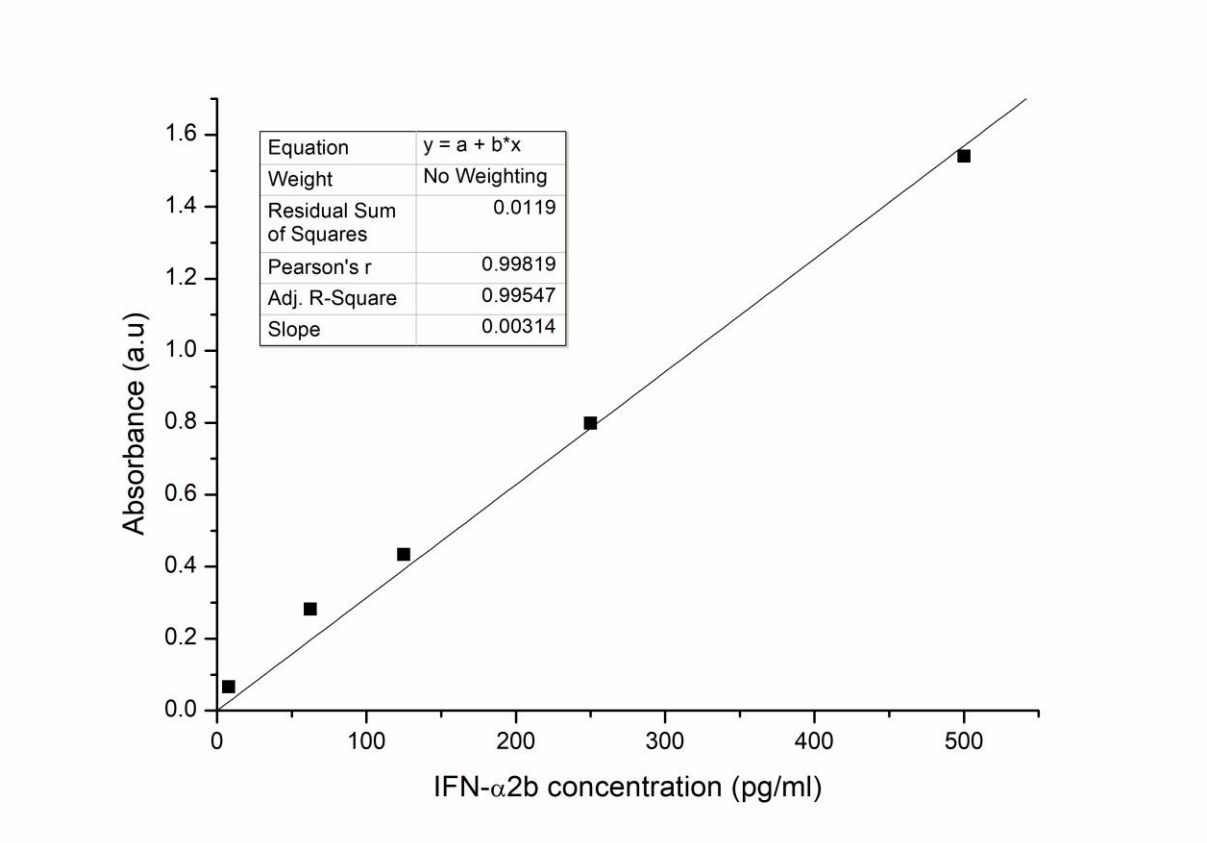
5.2. Recommendation and future perspective

The designed IFNPH yielded a system that met the study's requirements and objectives. The *in vitro* and *in vivo* evaluation of the system produced high-quality outcomes releasing in a sustain manner for 14 days and no cytotoxicity effect on the HRPE nor the rabbit eyes. Further research is required to validate the application of such systems in tumour delivery via preclinical investigation in an appropriate ocular

tumour animal model. Allograft models may be an appropriate method for assessing efficacy.

The IFNPH formulation is a potential site-specific delivery system for both ocular segments and can be applied for other ocular diseases and malignancies. The possibility for modification of the PBAE-NPs with ligands for active targeting to ocular sites would be a possible enhancement of the described delivery system.

Appendix A


Equation
y = a + b*x
Weight
No Weighting
Residual Sum of Squares
0.0119
Pearson's r
0.99819
Adj. R-Square
0.99547
Slope
0.00314
Absorbance (a.u)
IFN-α2b concentration (pg/ml)
0.0
0.2
0.4
0.6
0.8
1.0
1.2
1.4
1.6
0
100
200
300
400
500

Appendix B

ANIMALS RESEARCH ETHICS COMMITTEE (AREC)

UNIVERSITY OF THE WITWATERSRAND, JOHANNESBURG

STRICTLY CONFIDENTIAL

CLEARANCE CERTIFICATE NUMBER: 2021/03/07/C

APPLICANT: Ms OJ Owaezuoke
School: School of Therapeutic Sciences; Department: N/A; Location: WRAF

PROJECT TITLE: In vivo evaluation of a bioinspired protein resistant ocular biomaterial (BioPROT) in Albino New Zealand rabbits
Category: C; Species and Numbers involved: *70X 2.5 - 3.5 kg male or female, Albino New Zealand rabbits*

Approval is hereby given for the use of animals for the research project named above and described in the application reviewed by a quorate meeting of the AREC held on 30 Mar 2021. This approval remains valid until 20 May 2021 and is conditional to the following (if blank there are no special conditions):

Condition 1	Condition 2	Condition 3	Condition 4
Liaise with the WRAF staff about the feasibility of using an Elizabethan collar if irritation of the eyes			

All material changes to the approved research must be reported to the AREC before they are implemented. Failure to do so will invalidate this clearance certificate.

An annual progress report must be provided to the AREC.

The use of these animals is subject to AREC guidelines on the use and care of laboratory animals, is limited to the procedures described in the application and is subject to additional conditions listed below:

I, the Chair of the AREC (or my designated representative) am satisfied that the proposed research is ethical as judged by local law, international standards and University policy.

Signed: _____ _____ Date: __21/05/2021_____

(Chairperson of the AREC)

I am satisfied that the persons listed in this application are competent to perform the procedures described in the application, in the context of Section 23 (1) (c) of the veterinary and Para-veterinary Professions Act (19 of 1982).

CC: Student supervisor: «Title1» «Initials1» «Supervisor_surname»
Director Wits Research Animal Facility (WRAF): Dr Kim Jardine

Appendix C

AESC 2012 M&E

Please note that only typewritten applications will be accepted.

UNIVERSITY OF THE WITWATERSRAND

ANIMAL ETHICS SCREENING COMMITTEE
MODIFICATIONS AND EXTENSIONS TO EXPERIMENTS

a. Name: Onyinye J. Uwaezuoke

b. Department: Pharmacy and Pharmacology

c. Experiment to be modified / extended

			AESC NO
Original AESC number	**AESC21**	**02**	**003**
Other M&Es :			nil

d. Project Title: IN vivo evaluation of a bioinspired protein resistant ocular biomaterial (BioPROT) in Albino New Zealand white rabbits

		No.	Species
e.	Number and species of animals originally approved:	70	*Rabbits*
f.	Number of additional animals previously allocated on M&Es:	nil	
g.	Total number of animals allocated to the experiment to date:	5	Rabbits
h.	Number of animals used to date:	nil	

i. Specific modification / extension requested: Addition of a co-worker.

Name: Yosra Abdalla.

Phone number: +27719664801.

Email: 2359317@students.wits.ac.za.

Qualification: PhD student in Pharmacy and Pharmacology currently developing nanoplatforms for ocular drug delivery.

j. Motivation for modification / extension: I will be working with so many rabbits and hence will be needing assistance often. Yosra understands the focus of my research and will be of immense assistance.

Date: Signature:

RECOMMENDATIONS

Approval for the addition of Y. Abdalla a as co-worker to the project. Co-workers must ensure that they attend the WRAF orientation course, if already not done so. Please contact Dr K. Jardine for details (Kimberly.Jardine@wits.ac.za).

Date:3 November 2021 Signature:

Deputy-Chair, AESC

DEVELOPMENT OF AN INJECTABLE THERMO-RESPONSIVE PEG-PCL-PEG HYDROGEL FOR OCULAR DRUG DELIVERY

Yosra Abdalla1, Lisa Du Toit1, Naseer Ally2 and Yahya E. Choonara *

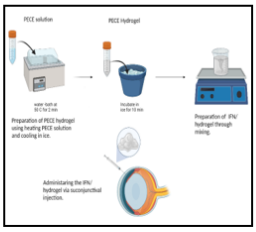
[1] Wits Advanced Drug Delivery Platform Research Unit, Department of Pharmacy and Pharmacology, School of Therapeutic Sciences, Faculty of Health Sciences, University of the Witwatersrand, Johannesburg, 7 York Road, Parktown, 2193, South Africa

[2]Department of Neurosciences, Division of Ophthalmology, St John Eye Hospital, University of the Witwatersrand, Johannesburg, South Africa.

Introduction

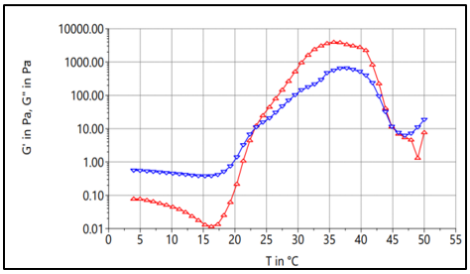
- Ocular drug delivery is hindered by the anatomical and physiological barriers of the eye (rapid reflux blinking, rate of tear turnover and the nasolacrimal drainage etc).
- These limit ocular bioavailability from the most commercially available ocular products such as eye drops (90%).
- There is therefore a need to design and develop a thermo-responsive hydrogel for sustain ocular delivery (TSD).

Methods and Materials

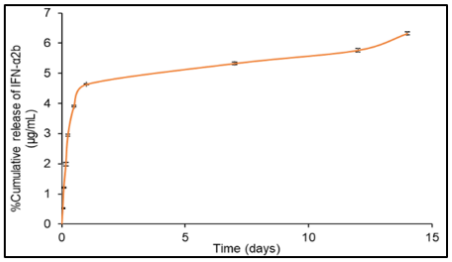


- The synthesis of the copolymer was through ring opening polymerisation of ε caprolactone in the presence of polyethyleneglycol methylether (MPEG) (Gong et al. 2009).
- Physiochemical properties of the TSD were evaluated (rheology etc).
- *In vitro* cytotoxicity of optimized hydrogel was evaluated in Human Retinal Epithelial cells.
- The release profile of interferon alpha nanoparticles from the gel was evaluated *in vitro*

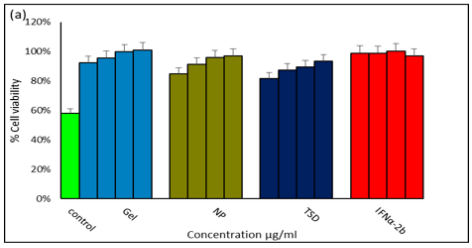
Results and Discussion







- Thermal transition of the hydrogel occurred at Tsol 22 °C and Tgel 45 °C with a high storage modulus G' indicating the suitability for sustained release from the gel (Hwang et al. 2005)
- Over 6% of IFN was released in the 14 days studied. The gel was nontoxic to primary Human retinal epithelial cells displaying above 70% viability (du Toit et al. 2021).



Conclusion

- The hydrogel was successfully synthesised and all the physiochemical characteristic of the hydrogel evaluated..
- The optimized formulation demonstrated favourable rheological parameters with a promising drug release pattern and no cytotoxicity effects on human retinal epithelial

References

1. Gong, C., et al., *Synthesis and characterization of PEG-PCL-PEG thermosensitive hydrogel.* International journal of pharmaceutics, 2009.**365**(1-2): p. 89-99.
2. Hwang, M.J., et al., *Caprolactonic poloxamer analog: pEG-PCL-PEG.* Biomacromolecules, 2005. **6**(2): p. 885-890.
3. 2. du Toit, L.C., Y.E. Choonara, and V. Pillay, *An injectable nano-enabled thermogel to attain controlled delivery of p11 peptide for the potential treatment of ocular angiogenic disorders of the posterior segment.* Pharmaceutics, 2021. **13**(2): p. 176.

Appendix E

UNIVERSITY OF THE WITWATERSRAND, JOHANNESBURG

FACULTY OF HEALTH SCIENCES

PLAGIARISM DECLARATION TO BE SIGNED BY ALL HIGHER DEGREE STUDENTS

SENATE PLAGIARISM POLICY: APPENDIX ONE

I Yosra Mahjoub Ahmed Abdalla (Student number: 2359317) am a student registered for the degree of PhD in Pharmacy in the academic year 2023

I hereby declare the following:

- I am aware that plagiarism (the use of someone else's work without their permission and/or without acknowledging the original source) is wrong.
- I confirm that the work submitted for assessment for the above degree is my own unaided work except where I have explicitly indicated otherwise.
- I have followed the required conventions in referencing the thoughts and ideas of others.
- I understand that the University of the Witwatersrand may take disciplinary action against me if there is a belief that this is not my own unaided work or that I have failed to acknowledge the source of the ideas or words in my writing.
- I have included as an appendix a report from "Turnitin" (or other approved plagiarism detection) software indicating the level of plagiarism in my research document.

Signature: [signature] Date: 13 November 2023

1

Appendix F

Yosra MA. Abdalla PhD Thesis

ORIGINALITY REPORT

14%	%	14%	%
SIMILARITY INDEX	INTERNET SOURCES	PUBLICATIONS	STUDENT PAPERS

PRIMARY SOURCES

1	Poornima Ramburrun, Yahya E. Choonara, Pradeep Kumar, Lisa C. du Toit, Viness Pillay. "Design of chitospheres loaded with pristine polymer particles for extended drug delivery via polyelectrolyte complexation and particulate leaching", International Journal of Pharmaceutics, 2015 Publication	1%
2	Hillary Mndlovu, Lisa C. du Toit, Pradeep Kumar, Thashree Marimuthu, Pierre P.D. Kondiah, Yahya E. Choonara, Viness Pillay. "Development of a fluid-absorptive alginate-chitosan bioplatform for potential application as a wound dressing", Carbohydrate Polymers, 2019 Publication	1%
3	Lisa Claire du Toit, Yahya Essop Choonara, Viness Pillay. "An Injectable Nano-Enabled Thermogel to Attain Controlled Delivery of p11 Peptide for the Potential Treatment of Ocular Angiogenic Disorders of the Posterior Segment", Pharmaceutics, 2021	1%

turnitin

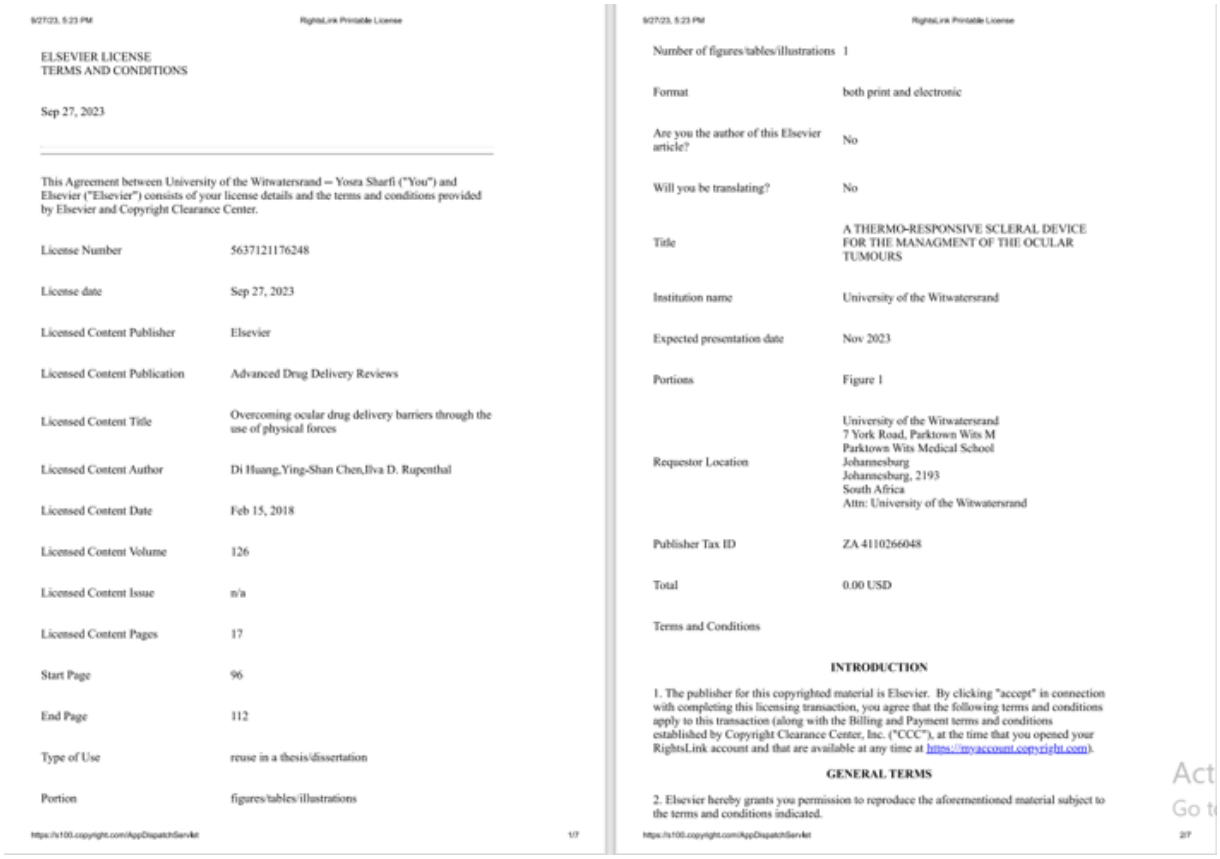
Digital Receipt

This receipt acknowledges that Turnitin received your paper. Below you will find the receipt information regarding your submission.

The first page of your submissions is displayed below.

Submission author:	yosra abdalla
Assignment title:	Lindo_review
Submission title:	Yosra MA. Abdalla PhD Thesis
File name:	Yosra_MA._Abdalla_PhD_Thesis.txt
File size:	191.01K
Page count:	119
Word count:	28,892
Character count:	165,414
Submission date:	24-Nov-2023 03:39AM (UTC+0200)
Submission ID:	2237146816

Appendix G



9/27/23, 5:23 PM RightsLink Printable License

ELSEVIER LICENSE
TERMS AND CONDITIONS

Sep 27, 2023

This Agreement between University of the Witwatersrand -- Yosra Sharfi ("You") and Elsevier ("Elsevier") consists of your license details and the terms and conditions provided by Elsevier and Copyright Clearance Center.

License Number	5637121176248
License date	Sep 27, 2023
Licensed Content Publisher	Elsevier
Licensed Content Publication	Advanced Drug Delivery Reviews
Licensed Content Title	Overcoming ocular drug delivery barriers through the use of physical forces
Licensed Content Author	Di Huang,Ying-Shan Chen,Ilva D. Rupenthal
Licensed Content Date	Feb 15, 2018
Licensed Content Volume	126
Licensed Content Issue	n/a
Licensed Content Pages	17
Start Page	96
End Page	112
Type of Use	reuse in a thesis/dissertation
Portion	figures/tables/illustrations

https://s100.copyright.com/AppDispatchServlet 1/7

9/27/23, 5:23 PM RightsLink Printable License

Number of figures/tables/illustrations	1
Format	both print and electronic
Are you the author of this Elsevier article?	No
Will you be translating?	No
Title	A THERMO-RESPONSIVE SCLERAL DEVICE FOR THE MANAGMENT OF THE OCULAR TUMOURS
Institution name	University of the Witwatersrand
Expected presentation date	Nov 2023
Portions	Figure 1
Requestor Location	University of the Witwatersrand 7 York Road, Parktown Wits M Parktown Wits Medical School Johannesburg Johannesburg, 2193 South Africa Attn: University of the Witwatersrand
Publisher Tax ID	ZA 4110266048
Total	0.00 USD

Terms and Conditions

INTRODUCTION

1. The publisher for this copyrighted material is Elsevier. By clicking "accept" in connection with completing this licensing transaction, you agree that the following terms and conditions apply to this transaction (along with the Billing and Payment terms and conditions established by Copyright Clearance Center, Inc. ("CCC"), at the time that you opened your RightsLink account and that are available at any time at https://myaccount.copyright.com).

GENERAL TERMS

2. Elsevier hereby grants you permission to reproduce the aforementioned material subject to the terms and conditions indicated.

https://s100.copyright.com/AppDispatchServlet 2/7



ROYAL SOCIETY OF CHEMISTRY

View PDF Version | Previous Article | Next Article

Check for updates

Open Access Article

This Open Access Article is licensed under a Creative Commons Attribution-Non Commercial 3.0 Unported Licence

DOI: 10.1039/D0RA04971A (Review Article) *RSC Adv.*, 2020, **10**, 27835-27855

Nanocarriers for ocular drug delivery: current status and translational opportunity

Srividya Gorantla[†a], Vamshi Krishna Rapalli[a], Tejashree Waghule[a], Prem Prakash Singh[b], Sunil Kumar Dubey[a], Ranendra N. Saha[ac] and Gautam Singhvi[†a]*

Rights and permissions

Open Access This article is distributed under the terms of the Creative Commons Attribution 4.0 International License (http://creativecommons.org/licenses/by/4.0/), which permits unrestricted use, distribution, and reproduction in any medium, provided you give appropriate credit to the original author(s) and the source, provide a link to the Creative Commons license, and indicate if changes were made.

Reprints and Permissions

ELSEVIER LICENSE
TERMS AND CONDITIONS
Sep 30, 2023

This Agreement between University of the Witwatersrand -- Yosra Sharfi ("You") and Elsevier ("Elsevier") consists of your license details and the terms and conditions provided by Elsevier and Copyright Clearance Center.

License Number	5637140390228
License date	Sep 27, 2023
Licensed Content Publisher	Elsevier
Licensed Content Publication	European Journal of Pharmaceutical Sciences
Licensed Content Title	Chitosan coated sodium alginate–chitosan nanoparticles loaded with 5-FU for ocular delivery: In vitro characterization and in vivo study in rabbit eye
Licensed Content Author	Ramesh C. Nagarwal,Rakesh Kumar,J.K. Pandit
Licensed Content Date	Nov 20, 2012
Licensed Content Volume	47
Licensed Content Issue	4
Licensed Content Pages	8
Start Page	678
End Page	685
Type of Use	reuse in a thesis/dissertation
Portion	figures/tables/illustrations
Number of figures/tables/illustrations	1
Format	both print and electronic
Are you the author of this Elsevier article?	No
Will you be translating?	No
Title	A THERMO-RESPONSIVE SCLERAL DEVICE FOR THE MANAGMENT OF THE OCULAR TUMOURS
Institution name	University of the Witwatersrand
Expected presentation date	Nov 2023
Portions	Figure 6
Requestor Location	University of the Witwatersrand 7 York Road, Parktown Wits M Parktown Wits Medical School Johannesburg Johannesburg, 2193 South Africa Attn: University of the Witwatersrand
Publisher Tax ID	ZA 4110266048
Total	0.00 USD
Terms and Conditions	

INTRODUCTION

1. The publisher for this copyrighted material is Elsevier. By clicking "accept" in connection with completing this licensing transaction, you agree that the following terms and conditions apply to this transaction (along with the Billing and Payment terms and conditions

ELSEVIER LICENSE
TERMS AND CONDITIONS

Sep 27, 2023

This Agreement between University of the Witwatersrand -- Yosra Sharfi ("You") and Elsevier ("Elsevier") consists of your license details and the terms and conditions provided by Elsevier and Copyright Clearance Center.

License Number	5637140066217
License date	Sep 27, 2023
Licensed Content Publisher	Elsevier
Licensed Content Publication	Colloids and Surfaces B: Biointerfaces
Licensed Content Title	Modified PLA nano in situ gel: A potential ophthalmic drug delivery system
Licensed Content Author	Ramesh C. Nagarwal,Rakesh Kumar,M. Dhanawat,J.K. Pandit
Licensed Content Date	Aug 1, 2011
Licensed Content Volume	86
Licensed Content Issue	1
Licensed Content Pages	7
Start Page	28
End Page	34
Type of Use	reuse in a thesis/dissertation
Portion	figures/tables/illustrations

Number of figures/tables/illustrations	1
Format	both print and electronic
Are you the author of this Elsevier article?	No
Will you be translating?	No
Title	A THERMO-RESPONSIVE SCLERAL DEVICE FOR THE MANAGMENT OF THE OCULAR TUMOURS
Institution name	University of the Witwatersrand
Expected presentation date	Nov 2023
Portions	figure 10
Requestor Location	University of the Witwatersrand 7 York Road, Parktown Wits M Parktown Wits Medical School Johannesburg Johannesburg, 2193 South Africa Attn: University of the Witwatersrand
Publisher Tax ID	ZA 4110266048
Total	0.00 USD
Terms and Conditions	

INTRODUCTION

1. The publisher for this copyrighted material is Elsevier. By clicking "accept" in connection with completing this licensing transaction, you agree that the following terms and conditions apply to this transaction (along with the Billing and Payment terms and conditions established by Copyright Clearance Center, Inc. ("CCC"), at the time that you opened your RightsLink account and that are available at any time at https://myaccount.copyright.com).

GENERAL TERMS

2. Elsevier hereby grants you permission to reproduce the aforementioned material subject to the terms and conditions indicated.

Act
Go t